STATISTICAL CLASSIFICATION
OF
BRAINSTEM AUDITORY EVOKED POTENTIALS

AND

THE EFFECTS OF LOCAL COOLING
ON CANINE
SPINAL CORD BLOOD FLOW

By

© MARKAD VENKATRAYA KAMATH, Ph.D.

A Thesis

Submitted to the School of Graduate Studies

in Partial Fulfilment of the Requirements

for the Degree

Doctor of Philosophy

McMaster University

July 1987

CLASSIFICATION OE BAEPS AND SPINAL CORD BLOOD FLOW

DOCTOR OF PHILOSOPHY (1987) McMASTER UNIVERSITY

(Neuro Sciences) Hamilton, Ontario

TITLE: Statistical Classification of
Brainstem Auditory Evoked Potentials
and
The Effects of Local Cooling on
Canine Spinal Cord Blood Flow

AUTHOR: Markad Venkatraya Kamath,
B.E.(University of Mysore)
M.S. (Indian Institute of Technology, Madras)
Ph.D. (Indian Institute of Technology, Madras)

SUPERVISOR: Professor Dhanjoo N. Ghista, Ph.D.

Number of Pages: xvii, 210

ABSTRACT

Brainstem auditory evoked potentials (BAEPs), the time locked scalp recorded electrical responses to auditory stimuli, are clinically useful for diagnosing and monitoring the disorders of neurological system. The first part of the thesis presents the development and evaluation of computer based statistical classifiers to recognize normal and patients' BAEPs. The classifiers using time domain features, namely, latencies of peaks V, IV and III of BAEPs, gave the optimal performance as measured by accuracy (85.3%), sensitivity (80%) among other indices. Power spectra of BAEPs in normals show three main frequency bands. In a second formulation of classifiers, three features, each feature representing the total power in each of the three frequency bands were used. The classifiers designed with these frequency domain features yielded a performance with accuracies upto 77%. Both of these classifiers may be used to assist the clinician while assessing the BAEPs.

The second part of the thesis examines the effects of

cooling on canine spinal cord blood flow (SCBF). The SCBF is an important physiological variable altered during spinal cord injury (SCI). Localized cooling of the spinal cord improves functional recovery after SCI. Hence, the effects of cooling on SCBF in normal canine cord were studied. A computerized system to measure the SCBF using hydrogen polarography at two control sites and two cooled sites was developed. In five dogs, SCBF decreased to 50% of the normothermic values during cooling of the cord to a temperature of 16 degrees Celsius. The SCBF did not change at control sites. It is postulated that following SCI, decreased SCBF due to localized cooling tends to prevent the outpouring of edema fluid and other toxic factors from the injured vessels, preserving the cord function. Thus, the finding of decreased SCBF during spinal cord cooling is clinically relevant.

ACKNOWLEDGEMENTS

I wish to thank Professor Dhanjoo N. Ghista for his inspiring guidance and advice during the course of this work. I am also grateful to Professor Robert R. Hansebout, member of the supervisory committee, who provided me the direction, and facilities for performing this research. I appreciate the critical comments and helpful suggestions given by other member of the supervisory committee, Dr. John Rowe.

There are several people who provided timely input and were involved in certain parts of the work. I thank Drs. R.N.Lamont and S.N.Reddy for their help. I am very grateful to Professor M.E.Jernigan, Univ. of Waterloo, who taught me pattern recognition. Assistance provided by Dr.A.Talalla is also much appreciated. I wish to ackowledge the cooperation and assistance provided by Dr.A.R.M Upton and Dr.R.M.Duke in making the data available to me so generously, as well as for giving helpful suggestions. I am very grateful to Mr. W.Salterelli and Ms.J.Randall, who recorded the clinical BAEP data.

Finally, I acknowledge the assistance provided by my wife Padma, my parents and my teachers during the course of this work. I am very grateful to them for nurturing my interest in research.

TABLE OF CONTENTS

LIST OF ILLUSTRATIONS

PART I

PART II

LIST OF TABLES

CHAPTER 1

SCALP RECORDED EVOKED POTENTIALS IN MAN

1.1 Introduction:

Ever since Dr.Hans Berger recorded electroencephalogram in 1920s, scalp recorded electrical activity in man has been useful during diagnosis in clinical medicine. However, it was only in 1947, when Dawson ushered in the first averager to record the evoked electrical response on the scalp, that the concept of selective stimulation of a receptor or end-organ in order to test a sensory modality noninvasively, was realized in practice [Dawson, 1947]. Since the advent of integrated electronic circuits in 1960s, appropriate instrumentation for recording evoked responses/ or evoked potentials (EPs), in clinical setting has become readily available.

In humans, the recording of pattern-shift visual, brainstem auditory and short latency somatosensory evoked potentials yields reproducible results under controlled conditions. The EPs provide the physician with objective

data to assess a sensory organ and its related sensory pathways and/or structures. The presence of lesions along the path of transmission of a sensory signal can be usually recognized as delays in the signal or changes in its amplitude. Gross changes in the waveform morphology are evident in seriously diseased states. The EPs also aid the monitoring of patient status following an injury or during specific therapeutic interventions. Although recent in origin, the EPs have been accepted in clinical practice rather quickly as evidenced by many documented studies, text books and monographs on the subject [Callaway, 1978; Kiloh et al. 1981; Courjon et al., 1982; Halliday, 1982; Chiappa, 1983].

The neurophysician uses the evoked potential characteristics such as latency and amplitudes as the indices during diagnosis of disorders related to the central nervous system. The waveform morphology also provides important diagnostic information, albeit qualitative in nature but nevertheless useful, and is usually scrutinized by the physician. In order to improve the quality of objective information obtained from the evoked potential waveform, it is desirable that operator independent indices be extracted. There has been significant research effort in the recent past, to provide both manually and with the aid

of computers, reliable and quantitative measures derived from all modalities of evoked potential waveforms [Morley and Liedtke, 1977; Aunon and McGillem, 1982; Madhavan et al., 1986]. In addition, appropriate mathematical techniques have been employed to identify normal and pathological waveforms and tag them for easier identification during diagnosis [McGillem et al., 1981]. The problem of suitably quantifying evoked potential waveform for automatic classification is an interesting one, in that, one may examine the indices employed emperically by the physician for use in automatic recognition systems and extract other useful parameters for defining the evoked potential waveform both uniquely and parsimoniously.

1.2 Brainstem Auditory Evoked Potentials:

This thesis addresses the brainstem auditory evoked potentials and presents an attempt towards automatic classification of human brainstem auditory evoked potentials (BAEPs). The BAEPs recorded from scalp in humans are a sequence of seven peaks each less than a microvolt in amplitude and appear within ten milliseconds following the delivery of an auditory stimulus. Figure 1.1 shows a typical idealized BAEP [Stockard et al., 1977a]. In general, each peak is also called a "wave".

In order to understand the origin of different components of the BAEP in man, a number of clinical studies have been undertaken [Chiappa, 1983]. Since, the BAEPs that are generated in feline and other animal species closely resemble the human BAEP, investigations have been attempted in such animal models [Jewett et al., 1970a and 1970b; Wada and Starr, 1983]. The effects of different pharmacological agents and experimentally induced lesions have been documented to give an insight into the generation and transmission of the BAEPs in humans, in healthy and in diseased conditions [Starr, 1975; Stockard et al., 1977b; Desmedt, 1977; Desmedt, 1980]. These investigations suggest that wave I is generated in the VIII nerve, wave II in the cochlear nucleus, wave III in superior olivary complex, wave IV in the lateral lemniscus and wave V in the inferior colliculus. It has been also observed that waves VI and VII are not found in all human subjects. However, the generators responsible for them are presumed to lie in thalamic and/or cortical locations.

1.3 Objectives:

Research conducted in several laboratories during the last decade suggests that the latencies of initial five

waves in human BAEPs have been found to be the most stable indices that can be derived from the waveform [Rowe, 1978]. Consequently, most clinics establish a set of mean (and s.d.) basal values for these latencies and any variations from them by two or three standard deviations are suggestive of possible pathological state. The work reported in this thesis was started with the goal of answering the following questions:

i) What indices are used to identify normal and pathological BAEP waveforms uniquely in a clinical setting?

ii) What are the best features which describe a BAEP for computer based classification of waveforms of normal subjects and patients?

iii) Can the frequency analysis of the BAEP aid the clinician in discriminating between the normal and pathological waveforms? Further, can the frequency domain features provide information for automatic classification?

iv) What types of classifiers can yield clinically useful classification of BAEP indices, based upon measures such as their sensitivity, specificity, positive predictive value and negative predictive value?

It was perceived, when the work for this thesis was initiated, that the BAEPs hold clues to unravelling several important aspects of the brainstem function which can not be studied by any other non-invasive technique and that research in classification and quantification of BAEPs would contribute towards furthering the knowledge on BAEPs. The wealth of research on BAEPs that has been reported in several important journals and conferences and their increased use in clinical practice has vindicated this initial assumption, which motivated the work presented in this thesis.

Chapters 2 through 6 present the results of the investigations undertaken to answer the above questions. In chapter 2, current methods of recording BAEPs are delineated and a summary of clinical applications of BAEPs is presented. Chapter 3 deals with the pattern recognition techniques used for this work. The results of pattern recognition of BAEPs, using time domain features, are presented in chapter 4. The power spectra of normal and patients' BAEPs are examined to evluate their frequency content and as likely cadidates for obtaining frequency domain features to perform pattern classification. Chapter 6 summarizes the work presented in the chapters 2 through 5,

and points out to possible avenues for future work.

1.4 Summary:

Evoked potentials provide a means of testing the response of a receptor or an organ to a specific input and transmission of the generated electrical signal in the nervous system. The brainstem auditory evoked potentials (BAEPs) have evolved as a non-invasive probe for assessing the brainstem function. Their utility has been well established as an aid during diagnosis of disorders related to central nervous system.

The work reported in this thesis examines the quantitative indices useful for automatic recognition and classification of normal and pathological BAEPs. Pattern classifiers have been developed to carry out classification of normal and pathological BAEPs. Frequency analysis of BAEPs has been performed to evaluate the nature of their power spectra and the suitability of power spectra for pattern classification.

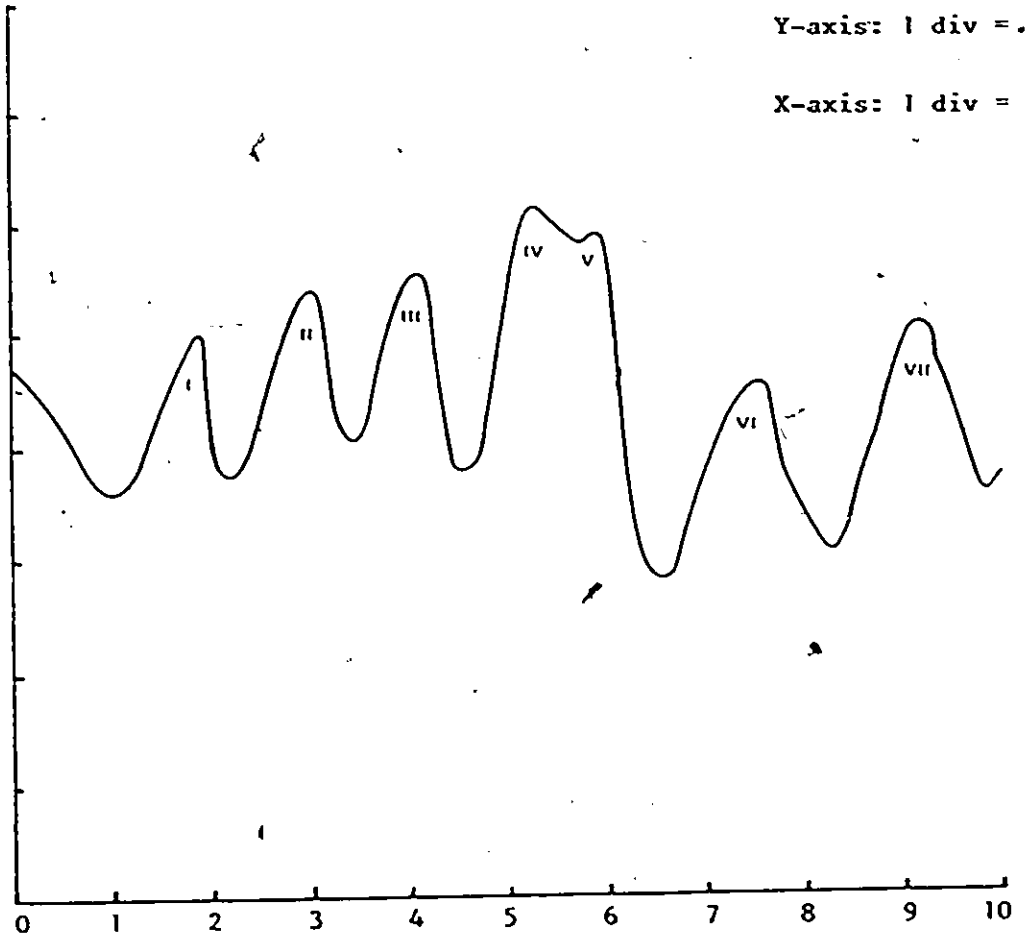

Figure 1.1 Hypothetical idealized brainstem auditory evoked potential.

CHAPTER 2

THE BRAINSTEM AUDITORY EVOKED POTENTIALS AND THEIR APPLICATIONS

2.1 Introduction:

In this chapter, the brainstem auditory evoked potentials (BAEPs) introduced in the previous chapter are examined more closely. The recording conditions and the methods used for obtaining clinically reproducible waveform are described. The applications of BAEPs are studied and clinical parameters used for evaluating the BAEPs in normals and patients are identified.

2.2 Recording:

The BAEPs were first recorded by Jewett and his colleagues in humans [Jewett, 1970b]. The BAEPs represent volume conducted events recorded on the scalp due to activation of auditory brainstem nuclei and pathways [Jewett, 1970a; Jewett and Williston, 1971].

In clinical practice, the BAEPs are usually recorded from scalp, in response to monoaural stimulation, ipsilateral to the ear being stimulated. A normal hearing is assumed, unless indicated otherwise, during interpretation of the BAEPs. A click of 100 microseconds width applied to the head phones is used as the auditory stimulus. The clicks are set at 60-65 dBs above the hearing threshold. A masking white noise is fed to the unstimulated ear to minimize cross-stimulation via bone and air conduction. The clicks are applied at the rate of 10 times a second. The ambient noise is kept low. The differential amplifier inputs are taken from vertex-right mastoid and vertex-left mastoid on the scalp and amplified in the frequency range of 100 - 3000 Hz [Rowe, 1978].

The EEG signal along with the BAEP is averaged for roughly 2000 clicks and displayed on a monitor. Such continuous display of the BAEP (on the monitor) during recording provides a feedback to the technician regarding the quality of the waveform. The recording trial is repeated twice for each ear, to ensure waveform reproducibility and fidelity. A hardcopy of the waveform is obtained on a X-Y recorder. These stimulus and recording parameters have been generally agreed upon by various laboratories [Rowe, 1978: Scherg and Speulda, 1982].

The evoked potential recording system performs the averaging of the BAEPs under the following assumptions:

a) The repeated stimuli elicit the same response, time locked to the stimuli.

b) Bioelectric events, other than those due to the stimuli, are statistically independent of the response.

c) The background bioelectric events have the same statistical characteristics from one stimulus epoch to the other.

Whereas the first assumption is not always valid especially while recording certain types of evoked potentials (such as visual evoked response) all the assumptions are necessary for practical recording of the evoked potentials. Averaging of N applied stimuli leads to the enhancement of the BAEP signal over the background EEG, $N^{1/2}$ times. A time locked signal when summated N times results in.

$$\text{Signal} = S_1 + S_2 + \ldots\ldots + S_N \qquad (2.1)$$

$$\text{Signal} = NS \qquad (2.1a)$$

where $S_1, S_2 \ldots \ldots \ldots S_N$ are individual responses and,

$$S_1 = S_2 = \ldots\ldots = S_N = S.$$

As the background EEG is assumed to be random with respect to the signal, it summates in the root mean square sense and is termed as noise.

$$(\text{Noise})^2 = A_1^2 + A_2^2 + \quad + A_N^2 \qquad (2.2)$$

where $A_1, A_2 \ldots A_N$ are the background EEG for individual epochs.

By assumption (c), $A_1 = A_2 = \ldots\ldots = A_N = A$

$$\text{Noise} = N^{1/2} A \qquad (2.3)$$

From (2.1a) and (2.3),

$$\text{Signal/Noise} = N^{1/2} S/A \qquad (2.4)$$

Equation (2.4) implies that if averages of evoked respsonses to N stimuli are performed, the signal-to-noise ratio improves $N^{1/2}$ times.

Whereas the averaging technique described above has been used in some rorm or the other, in recent years there

is a strong trend towards finding better methods for recording evoked potentials [McGillem et al., 1985; Madhavan, 1985; Boston, 1985]. Specifically, in the case of BAEPs, evoked responses to a few stimuli (as few as 256 or less) are being obtained using adaptive filters. [Thakor, 1987]. It is envisaged that evoked potential recording systems providing such responses would be available in clinical practice shortly. Of significance would be their applications to head injury and in operating theatre where the status of the subject changes rapidly and the averaging method may be taking too long a time.

2.3 Normative Data:

In normal adults, latencies of initial five peaks have been found to be the most stable measures derivable from BAEPs. It has been observed that latencies for normal subjects are statistically stable within individuals, between individuals and between different laboratories under similar recording conditions [Chiappa, 1979; Rowe, 1978]. A variation of more than three standard deviations from the normative mean values indicates a high probability of disorder in the nervous system [Chiappa, 1983]. Thus, accurate identification of peaks is crucial for BAEPs to be of clinical utility. Figure 2.1 shows the BAEPs of a normal

subject recorded in the neurology clinic of McMaster University Medical Centre. The stimulus was delivered at 9.8 times per second 60 dB above the threshold to the ipsilateral ear. Two trials of 2000 averages were conducted for each side.

The mean latency values (in milliseconds) for normal subjects from different laboratories are [Chiappa, 1983]: wave I : 1.7±0.15, wave II : 2.8±0.17, wave III : 3.9±0.19, wave IV : 5.1±0.24 and wave V : 5.7±0.25.

The absolute values of amplitudes show standard deviations of more than 50% of their mean values. Similar observations have been made on the amplitude ratios of different peaks. Hence these two indices of BAEPs are used less often in clinical context.

The effects of variations in recording parameters have been investigated by several workers and are summarized by Rowe [1978]. A stimulus rate of 10 clicks/second gives better waveform reproducibility and smaller variance of conduction times than a stimulus rate of 30 clicks/second. There is a progressive loss of amplitude and hence recognizability of the peaks, as the frequency of stimulation increases. The temperature of recording should

be kept constant. In patients with no hearing loss, a change of temperature from 27 degrees Celsius to 37 degrees Celsius produced an average increase of 1.4 milliseconds in I-V interpeak interval [Stockard, 1978]. The interpeak latency (IPL) of peaks I-V has been reported to be 0.3 mseconds less in females than in males [Beagley and Sheldrake, 1978]. The I-V IPL decreases during the first year of life, and there is an increase of the I-V IPL during the fifth decade of life, which is likely to be related to peripheral hearing deficits that develop later in life [Robinson and Rudge, 1982a].

2.4 Clinical Applications of the BAEPS:

The BAEPs have found extensive clinical use as evident from the literature reported during the past decade. Salient references related to the applications in diagnosis, prognosis and intraoperative monitoring are reviewed below.

The BAEPs are formed due to the transmission of the sound in the auditory afferent system and the passage of the electrical voltage generated thereby, through the brainstem structures. These events are volume conducted to the scalp where they are recorded. A damage to the brainstem

by means of tumors, loss of circulation or demyelination can result in loss of amplitude or increased delays in various components of BAEPs. A delay in the interpeak interval of I-III waves would indicate a lesion in the pontine-medullary region and an increase in the III-V interval may be due to dysfunction in the midbrain-pontine region [Chiappa, 1983].

Some specific etiologies wherein BAEPs have contributed to diagnosis of lesions in the Central Nervous System (CNS) are reported below in section 2.4.1. Section 2.4.2 examines how BAEPs are used to evaluate the head injury. Section 2.4.3 describes the utility of BAEPs recorded during intraoperative monitoring.

2.4.1 Clinical applications of BAEPs in the diagnosis of CNS disorders:

Multiple Sclerosis:

In demyelinating disease such as Multiple Sclerosis (MS), BAEPs are useful to detect the presence of unsuspected lesions, for confirmation of the diagnosis and for monitoring the treatments of the patients. There have been a number of studies on the application of BAEPs in patients with MS [Stockard, 1977b; Chiappa, 1980; Kjaer,

1980a and 1980b; Green and Walcoff, 1982]. The results of major studies of BAEPs in patients with MS have been reviewed by Chiappa [1983] where it is reported that the BAEP waveforms were abnormal in 38% - 46% of patients. The IPL of III-V, which corresponds to the white matter segment ofthe neural tissue between the superior olivary complex and inferior colliculus, increases in 28% of the MS patients with abnormal BAEPs. Figure 2.2 shows BAEPs recorded from a patient diagnosed to have multiple sclerosis. It can be observed that the latencies of the peaks have increased and consequently, inter-peak intervals have also increased. This increase has been attributed to the fact that the demyelinating process slows the transmission time of the signal, thus resulting in the increased latencies. In many instances the definition of peaks is poor [Chiappa, 1980 and 1984].

Birth Trauma:

In infants, the BAEPs have been particularly sensitive to disorders such as birth trauma, anoxia, sudden infant death syndrome, postmaturity, intracranial hemorrhage, encephalitis and brain death [Nodar et al., 1980; Salamy et al., 1980]. Infants afflicted with such disorders have been observed to have significant increases

in latency and amplitude of I.III and V peaks among other changes of BAEP parameters.

Tumors:

BAEPs are the most sensitive test for screening patients suspected with acoustic neuroma [Chiappa, 1983]. In one study comprising of 35 acoustic tumors and 7 temporal bone tumors, it was noted that, tumors that press on the VIII nerve gave rise to an interaural latency of 0.4 msec (normal<0.2 msec) at the first peak [Selters and Brackmann, 1977]. It was also found that the size of the tumor was also directly proportional to I-V interval in 18 subjects. However, it was observed that if the subject has a hearing loss >75 dB, the BAEPs yield greater false positive findings. The BAEPs may be especially useful in detecting acoustic neuromas at an early stage where the abnormalities of wave I and wave II suggest the presence of tumor ipsilaterally [Robinson and Rudge, 1982b]. The cerebellopontine tumors may cause extinction of peaks after wave II.

2.4.2 Applications of BAEPs in Prognosis:

Head Injury:

Several investigators have reported the monitoring of BAEPs in patients with severe head injury from the time of admission following injury to several months after injury [Greenberg and Ducker. 1982; Seales et al., 1979]. The presence of an intact BAEP 12 hours after the injury, even with prolonged IPL I-V is a good indication of a favourable prognosis. Facco et al. [1985] state that the break point between the irreversible brain damage and reversible dysfunction is determined by an interpeak latency of peaks I-V of 4.48 ms, as observed in 40 patients with head injury. It was found that 19 out of 29 survivors (65%) had an IPL of I-V in the range 3.82 - 4.48 ms, six months after injury.

Greenberg et al. [1982] developed grading schemes to quantify the level of abnormality of the BAEPs following head injury. According to their classification strategy, normal waveform is grade I. In a grade II waveform, only the waves I and V are discernible and delays in the latency of these waves may be seen along with amplitude reduction for other waves. In a grade III waveform, all peaks except the first peak show significant deviations from the normal. A grade IV BAEP is one in which only the wave I is seen. Based on their study of more than 100 Head Injury patients, Greenberg et al. [1982] report that, majority of patients with

grade II BAEPs survived; but patients with grade III and IV deteriorated and died or were left severely disabled. It is postulated that patients with grade II BAEPs have impaired neural systems which are still viable [Newlon et al., 1982]. Anderson et al. [1984] have also found the above scheme clinically useful for predicting the prognosis of patients with severe head injury and report that BAEPs yield a low rate of falsely pessimistic prognosis. They noted, from a data of 39 patients with closed head injury, the BAEPS proved to be the best predictors of outcome compared to intracranial pressure, pupillary reflexes and motor responses.

Karnaze [1982] studied 26 patients who were comatose following head injury and found that 19 patients (73%) with normal BAEPs on admission survived and that preservation of BAEP correlated with a good quality of survival. Karnaze et al. [1982] state that, while decerebration is associated with brainstem dysfunction, it does not always result in abnormal BAEPs, an observation also reported by Greenberg et al. [1982].

Figure 2.3 shows BAEPs of a patient with head injury and admitted to the McMaster University Hospital. One can observe that there is a poor definition of peaks accompanied

by the degeneration of morphology of the waveform.

In summary, for patients with head injury, a normal or near normal BAEP recorded within 24-48 hours after the trauma predicts good prognosis; however, abnormal waveforms are predictors of unfavourable outcome.

2.4.3 The BAEPs in Intraoperative Monitoring:

The BAEPs have been immensely useful in neurosurgical operations in the cerebellopontine angle [Grundy, 1982] whereby the changes in BAEPs have been seen with surgical retraction, operative manipulation, positioning of the head and neck for retromastoid craniectomy and a combination of hypocarbia and moderate hypotension. It is suggested that the monitoring the BAEP waveform may prevent injury to auditory nerve and brainstem during operations in the cerebellopontine angle [Samii, 1986]. It is particularly useful during procedures where hearing is at risk, such as during removal of tumor in the vicinity of cochlear nerve or vestibular nerve section [Raudzens and Shetter, 1982].

2.4.4 The Effect of Barbiturates and Similar Compounds on BAEPs:

Starr et al [1975] studied nine patients who had taken a variety of drugs including benzodiazepines, phenothiazines and propoxyphene. The BAEPs were resistant to all the above drugs and were normal when other clinical measures of brainstem function such as spontaneous respiration, cold caloric response, oculocephalic reflexes were absent or depressed. If the cortex was not damaged, these patients with normal BAEPs were found to make good recoveries. Similar results were observed in animals [Sutton et al., 1982; Bobbin et al., 1979]. It is believed that synapse is site of action of hypnotic compounds [Sharpless, 1970] and the effect of such agents would be seen minimally at the end organ or nearby synapses which generate the volume conducted potentials [Sutton et al., 1982]

2.4.5 Brain Death:

In patients supected to be brain dead, BAEPs have been used to make a definitive diagnosis. In twenty patients with isoelectric EEG, the BAEPs have been either absent or have shown only the presence of wave I which also disappeared subsequently. The components of BAEP were abnormal and disappeared in a rostro-caudal sequence [Starr, 1976]. Figure 2.4 shows a BAEP recorded in McMaster

University Hospital, from a patient with suspected brain death, who subsequently died.

2.5 Summary:

In this chapter, a summary of the characteristics of normal BAEP waveform and some of the clinical applications of BAEPs were presented. It would be useful if classification of BAEPs was performed automatically as an aid to clinical diagnosis, which is the objective of this research.

The automatic classification of biological waveforms is an important area which Pattern Recognition is addressing currently. Specifically, the automatic recognition of ECG, EMG, EEG has brought significant clinical benefits. In this context, computer based classification of BAEPs would complement the clinician in providing objective assessment of the waveform.

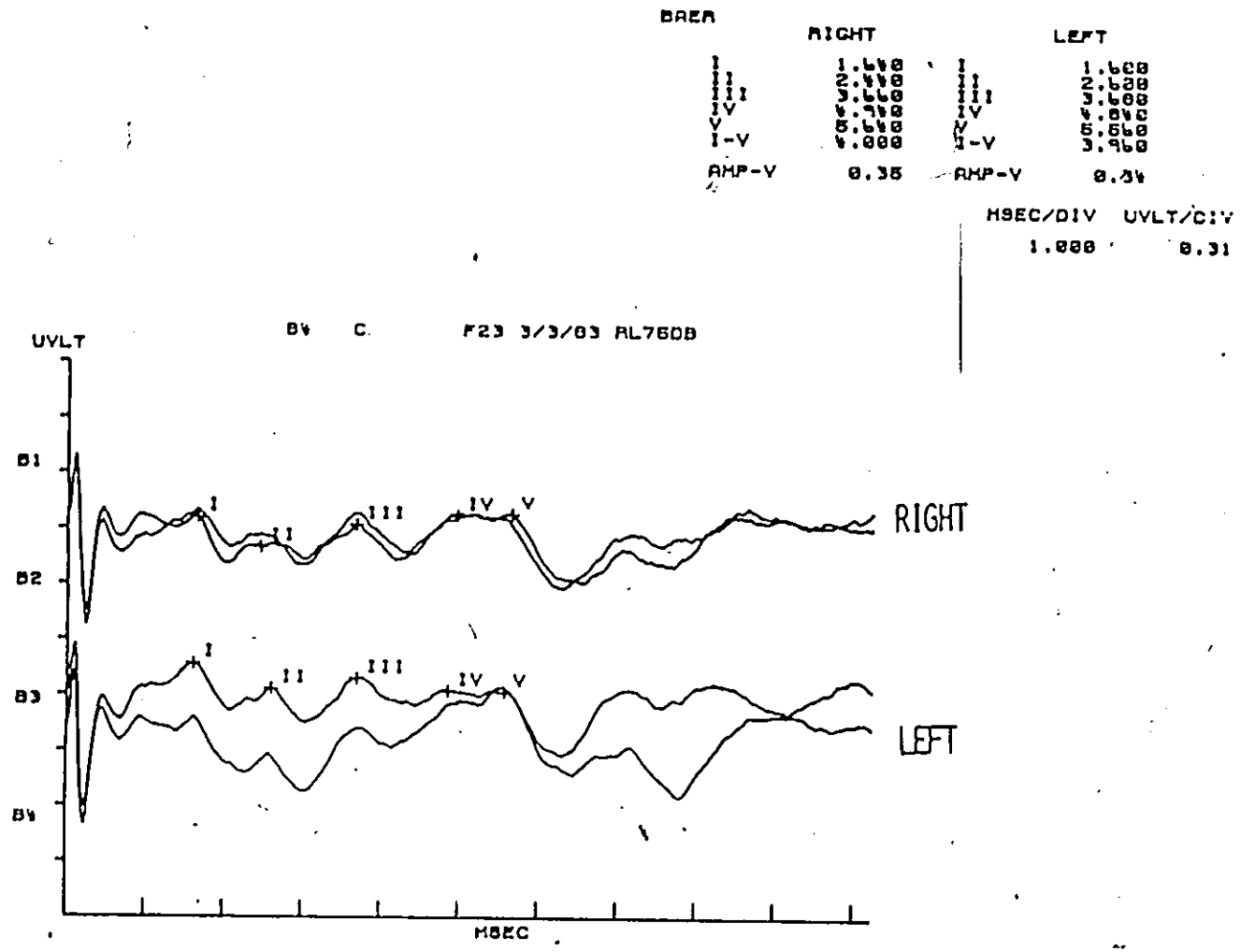

Figure 2.1 Brainstem auditory evoked potentials (BAEPs) of a normal subject. The top trace is the response to right ear stimulation and the lower trace is the response to left ear stimulation. Two trials were conducted for each side.

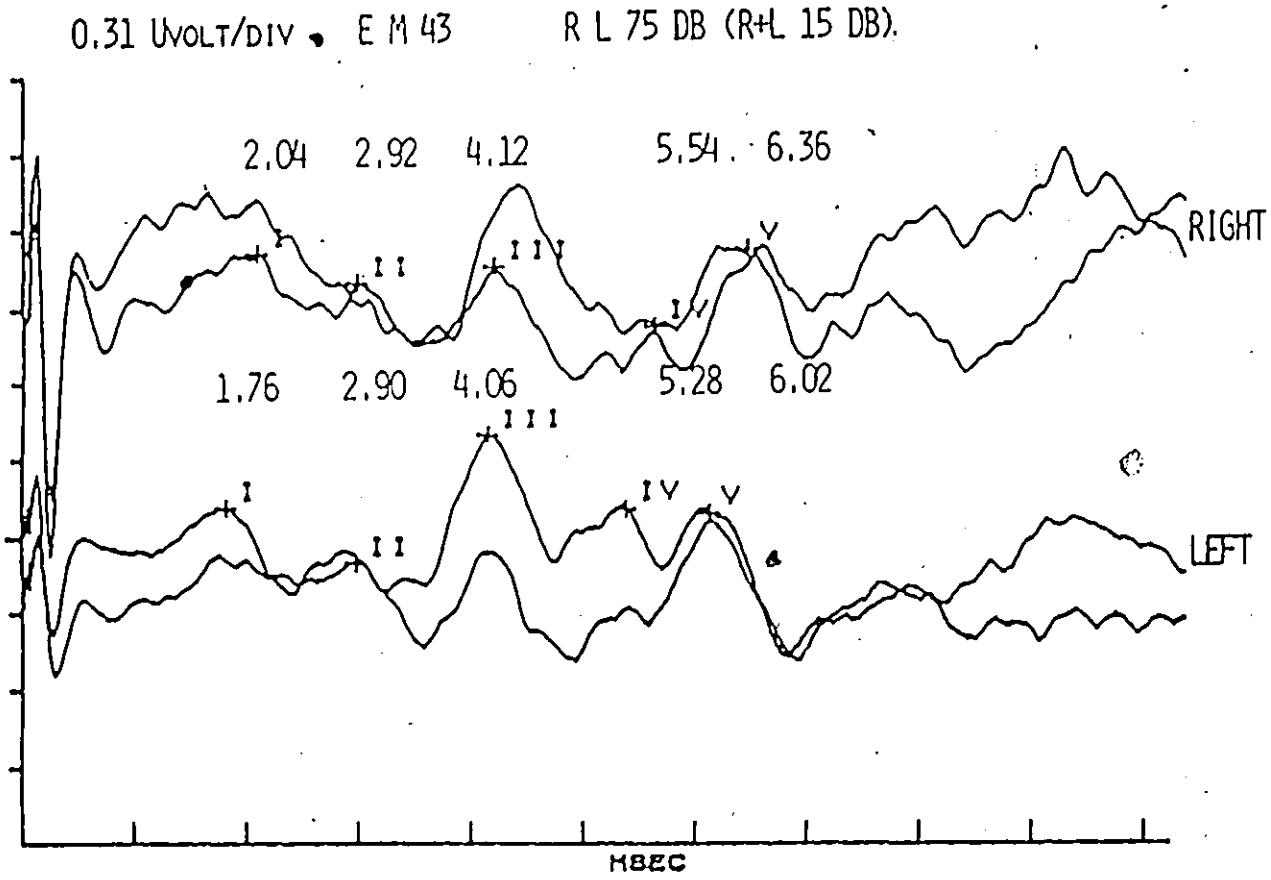

Figure 2.2 BAEPs of a patient with multiple sclerosis. Note the increase in the latencies of peaks compared to the normal BAEP.

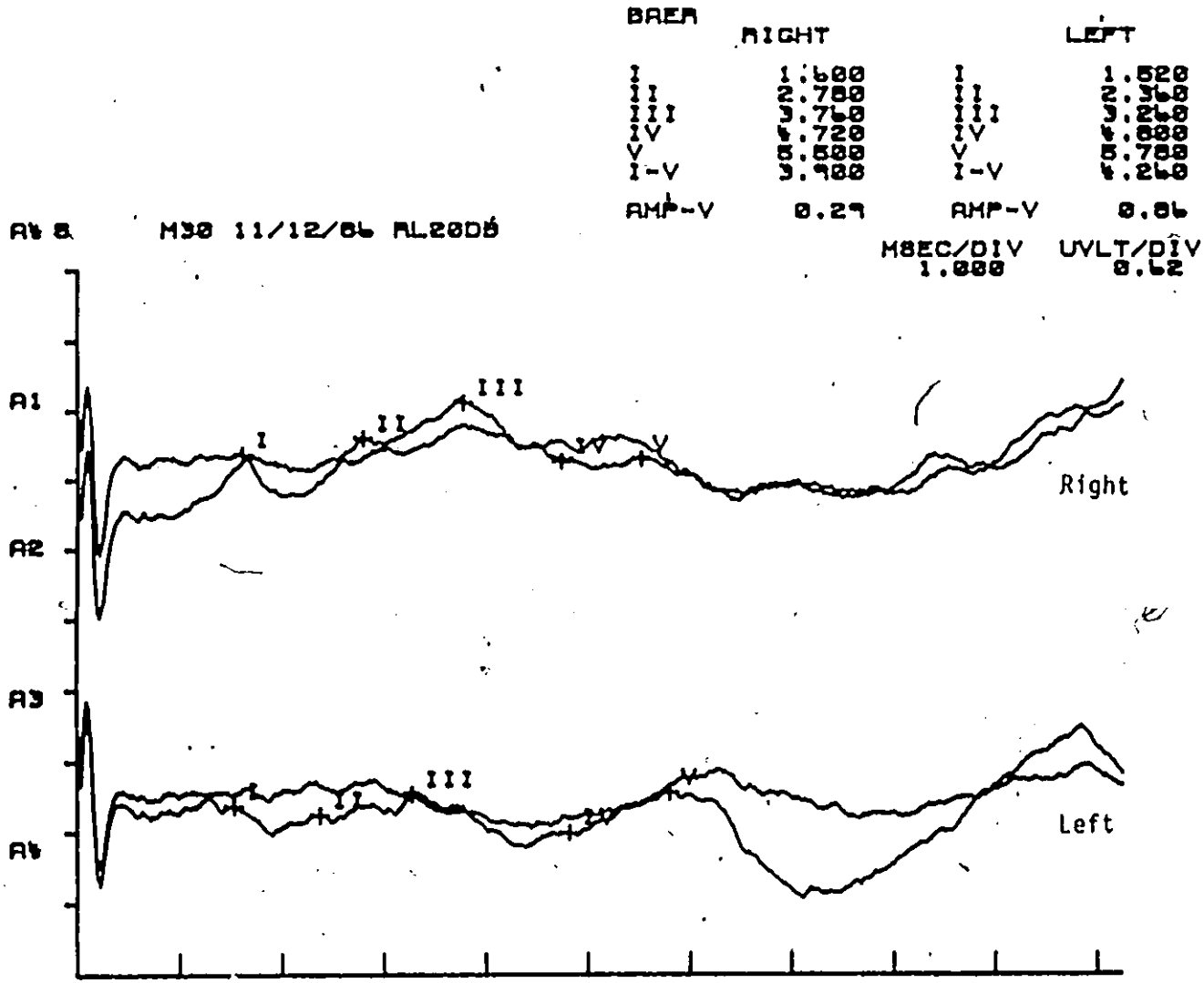

Figure 2.3 BAEPs of a patient with head injury.

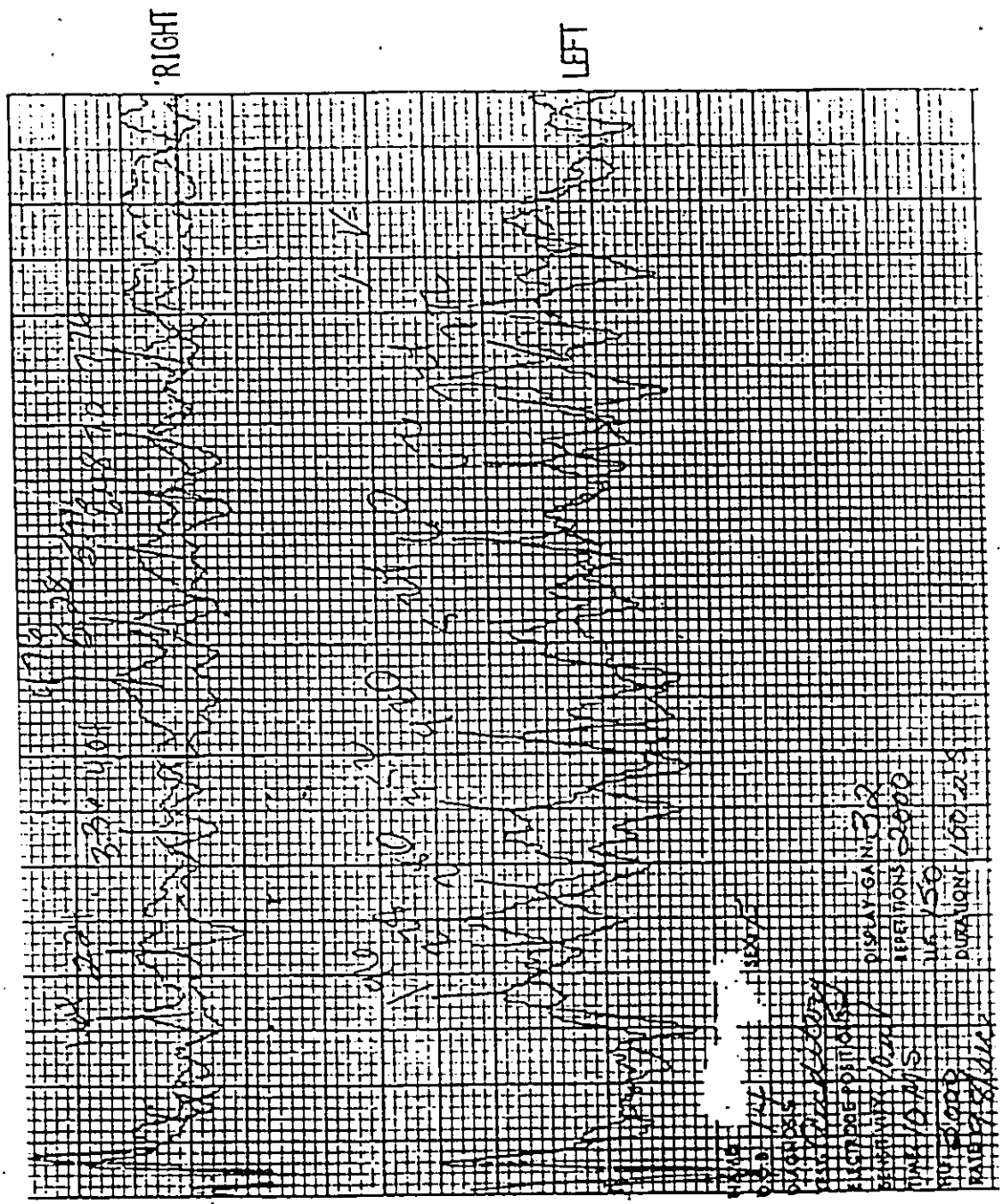

Figure 2.4 BAEPs of a patient with brain death. There are no specific peaks and the recording is not repeatable.

CHAPTER 3

AN INTRODUCTION TO PATTERN RECOGNITION TECHNIQUES AND THEIR APPLICATIONS TO BIOLOGICAL WAVEFORM PROCESSING

3.1 Introduction:

Pattern recognition has emerged as a novel discipline in the recent past with strong interdisciplinary ties. Its development has been influenced by such diverse fields as statistical decision theory, estimation theory, neural dynamics, biology, medicine, psychology and linguistics amongst others. The techniques drawn from these areas have been invoked and adapted for developing machines which measure, categorize, recognize and classify patterns. This chapter presents two such techniques which are used for classifying BAEPs in this thesis. The implementation of these classifiers is presented in the next chapter.

3.2 Concepts of Pattern Recognition:

The term, pattern, encompasses a wide variety of objects or data, including images, waveforms, handwritten and printed characters or a mathematical description of an

object or some process. A class is described by some common attributes of its members. Consequently, a pattern recognition system categorizes the input patterns or their description into identifiable classes via the extraction of significant features from a broad background or irrelevant detail [Tou and Gonzalez, 1974].

Automatic pattern recognition systems are ideally suited when the information to be handled is large: such as when the features which describe the objects are several, when there are multiple classes and when the mathematical processing is too complex to be done in a reasonable amount of time. Pattern recognition has made significant contributions in enhancement and segmentation of satellite and medical images, analysis of biomedical and radar signals, towards geophysical exploration and in economic forecasting.

Fig.3.1 shows a typical pattern recognition scheme. The incoming data from the object to be classified is sensed through some sensors. The relevant features are obtained and the classification is then carried out based on decision rules which are either specified earlier or are "learned" from the patterns. If the features convey significant and useful information for discrimination between different classes, the classifiers tend to be simple. On the

contrary, complex classifiers are needed to discriminate between patterns which are represented by features that do not differentiate various classes unequivocally. The design of subsystems for efficient feature selection, feature extraction and the implementation of classifiers which provide low misclassification rates are principal goals of pattern recognition methods.

Often, the patterns are perceived and modelled as samples from a statistical distribution and the features can be represented by numerical quantities. In such an instance, the classifiers will be a set of statistical decision rules based on class statistics such as mean vector and covariance matrix. This method of assigning patterns to different classes based on their statistical descriptors is called statistical pattern recognition.

In certain applications where structural or contextual information is of relevance, a complex pattern is divided into its simpler entities called primitives. The primitives are combined through certain grammatical rules called the pattern grammar and different classes result from various combinations of primitives. If a given unclassified pattern can be generated by a particular grammar, then the pattern belongs to the class described by that grammar. This approach is termed as syntactic pattern recognition [Fu,

1982].

Because of the quantitative nature by which the BAEPs are characterized in the present work, statistical pattern recognition techniques are used to classify the BAEPs. A description of these techniques is presented below.

3.3 Techniques of Statistical Pattern Recognition Used in The Present Work:

Whenever a set of objects are given, those objects which appear similar to each other, in general, will be said to belong to the same class. If some measurements are taken of an object or a pattern, the relative proximity or similarity of any two sets of measurements will suggest that those patterns which generated the measurements belong to the same class. An objective measure of similarity between the measurements may further help in making the decision.

Mathematically, if there are N measurements of an object, they can be represented by an N dimensional vector. Usually, these measurements are real numbers and form a pattern or a feature vector, **X**.

$$\mathbf{X} = \begin{bmatrix} x_1 \\ x_2 \\ \vdots \\ x_N \end{bmatrix}$$

where x_1, x_2.....x_N are individual measurements.

In statistical pattern recognition systems, the vector X is treated as an observation of a random variable with N dimensions. (Bold faced variables represent a vector or a matrix).

If there are no labelled samples available to the designer while developing a pattern recognition system, an initial exploratory technique such as cluster analysis may be used to examine the existence of natural classes in a given set of patterns [Duda and Hart, 1973]. Such an analysis may provide insights into the nature of patterns. If there is some previous information about the patterns, in terms of the probabilities of different classes and class conditional density functions, then the probability of each class, given that pattern X has been observed, can be computed. Bayes classifier is one such classifier, which is based on concepts of statistical decision theory, for evaluating the a posteriori probabilities of a pattern belonging to a particular class. It is used in the present work.

Bayes classifier treats each pattern as an obser-

vation of a random variable and assigns the pattern to a class with maximum a posteriori probability. The design of the Bayes Classifier minimizes the error of misclassification and consequently it is very attractive in statistical pattern classification problems.

Alternately, one may project the samples in 'N' dimensions on a line which produces a separation of the samples. This procedure is termed as Fisher's Linear Discriminant Function (FLD) and is also used in the present work to classify the BAEPs. Sections 3.4 and 3.5 describe the Bayes classifier and FLD, and present the equations used for classification.

3.4 Bayes Classifier:

In this section, the design criteria for development of Bayes classifier are presented. The following description assumes that there are only two classes. These concepts can be extended to multiple classes.

Given a pattern X, such as a BAEP, with N features (i.e. x(1), x(2).....x(N)), one can decide that pattern X belongs to class A or class B depending on,

$$P(A/X) \underset{B}{\overset{A}{\gtrless}} P(B/X) \quad \text{given} \quad X \quad \begin{cases} A \\ B \end{cases} \qquad (3.1)$$

In equation (3.1), P(A/X) and P(B/X) are the a posteriori probabilities of class A and class B, given that the pattern X has been observed. Equation (3.1) states that the decision to assign the pattern X is based on the maximum a posteriori probability of either of the two classes. By Bayes theorem [Duda and Hart, 1973], equation (3.1) can be written as,

$$p(X/A)\ P(A) \underset{B}{\overset{A}{\gtrless}} p(X/B)P(B) \qquad (3.2)$$

In equation (3.2), p(X/A) and p(X/B)are the conditional probability density functions of the observation vector X. P(A) and P(B) are the a priori probabilities of occurence of class A and class B respectively. The a priori probabilities can be estimated from a knowledge of the number of normal and abnormal BAEPs recorded in the evoked potentials laboratory. Arbitrarily, class A has been taken as the class containing the abnormal BAEPs, and class B is designated to be the normal class. The inequality sign between two sides of the equation (3.2) implies, decision is in favour of class A if the left hand side of the equation is greater than right hand side; otherwise, the decision is in favour of class B. The decision is to be arbitrary, if the

two sides are equal.

As the conditional probability density functions, describing the data in either class A or class B, are not known, an assumption that the BAEP patterns would satisfy the multivariate normal density function is made. This is acceptable in practice as multivariate density function is easily defined by the mean vector and the variance-covariance matrix.

If there are N features, the multivariate normal density is,

$$p(X) = \frac{\exp(-(X-M)^T S^{-1} (X-M)/2)}{(2\ PI)^{N/2}\ \ |S|^{1/2}} \qquad (3.3)$$

In equation (3.3), X is the data vector, M is the mean vector, S is the variance-covariance matrix, |S| its determinant and PI = 3.14159...

$$M = E[X] \qquad (3.3a)$$

$$S = E[(X-M)(X-M)^T] \qquad (3.3b)$$

In equations (3.3a) and (3.3b), E[ ] denotes the expectation operator. Equation (3.3) is usually abbreviated as,

$$p(X) = N(M, S) \qquad (3.4)$$

The 'N' dimensional multivariate normal density function, for classes A and B, is written as,

$$p(X/A) = N(M_A, S_A) \qquad (3.5a)$$

$$p(X/B) = N(M_B, S_B) \qquad (3.5b)$$

where M_A is the mean vector and S_A variance-covariance matrix for class A respectively. Similarly M_B and S_B define the mean vector and variance-covariance matrix of class B. The computation of the M_A, S_A, M_B, S_B is described in the next chapter.

From (3.2) and (3.3),

$$\frac{P(A)\exp(-((X-M_A)^T S_A^{-1}(X-M_A))/2)}{(2\,PI)^{N/2}\ |S_A|^{1/2}} \underset{B}{\overset{A}{\gtrless}} \frac{P(B)\exp(-((X-M_B)^T S_B^{-1}(X-M_B))/2)}{(2\,PI)^{N/2}\ |S_B|^{1/2}} \qquad (3.6)$$

Taking the natural logarithm and simplifying (3.6), results in the governing criterion expressed as,

$$(X-M_B)^T S_B^{-1}(X-M_B) - (X-M_A)^T S_A^{-1}(X-M_A) \underset{B}{\overset{A}{\gtrless}} 2\ln(P(B)/P(A)) + \ln(|S_A|/|S_B|) \qquad (3.7)$$

The terms

$$d^2(X, M_B, S_B) = (X-M_B)^T S_B^{-1} (X-M_B) \qquad (3.7a)$$

$$d^2(X, M_A, S_A) = (X-M_A)^T S_A^{-1} (X-M_A) \qquad (3.7b)$$

are scalar measures of distance of pattern X from the corresponding normal distribution.

If we let,

$$T = 2 \ln[P(B)/P(A)] + \ln(|S_A| / |S_B|) \qquad (3.8)$$

as a threshold, the first term on the right hand side biases the decision in favour of the class with larger probability and the second term biases the decision in favour of the class with a smaller determinant of the variance-covariance matrix. Since the determinant of the covariance matrix is proportional to the square of the volume of the probability density functions, the Bayes classifier favours the class with the smaller volume or the denser class [Duda and Hart, 1973].

The vectors M_A, M_B and matrices S_A, S_B are not known a priori and are estimated from a set of labelled patterns. The computational procedure for obtaining estimates of these parameters and the implementation of Bayes Classifiers is described in the next chapter.

3.5 Classification by Fisher's Linear Discriminant Function:

Given a set of patterns for classification, the goal of FLD is to find a line which best separates the patterns when patterns are projected on to that line. Figure 3.2 shows a two dimensional case for two classes, A and B.

A discriminant W, onto which samples are projected is:

$$y = W^T X \qquad (3.9)$$

Since projected points lie on the same line, the patterns $y_1, y_2 \ldots y_n$ become scalars. Optimally, the samples should fall into two separate clusters. One should choose a discriminant as in Figure 3.2 and not as in Figure 3.3. It has been shown that an optimum- choice for W is [Duda and Hart, 1973; Johnson and Wichern, 1982]:

$$W = S_P^{-1}(M_B - M_A)$$

Stated geometrically, S_P^{-1} rotates the vector between the means to take into account the shapes of class distributions, to find the optimal discriminant.

$$W^T X = (M_B - M_A)^T S_P^{-1} X \qquad (3.10)$$

The midpoint between the two classes is the point which demarcates the two classes and decides the class membership.

The mid point, 'm', between the two pattern classes is given by.

$$m = (M_B - M_A)^T S_P^{-1} (M_B + M_A)/2 \qquad (3.11)$$

In equation (3.11), 'm' is a scalar.

For any new pattern X0, to be classified, let.

$$Y0 = (M_B - M_A)^T S_P^{-1} X0 \qquad (3.12)$$

Allocate X0, according to the classification rule:

Pattern X0 belongs to class B, if

$$Y0 > m \qquad (3.13)$$

Pattern X0 belongs to class A, if

$$Y0 < m \qquad (3.14)$$

Computational details for the estimation of matrix S_p, are given in the next chapter.

It must be stated that both Bayes classifier and FLD are asymptotically identical under the simplifying assumption of equal variance-covariance matrices for both the classes A and B. Although, this may not be always true in

practice. FLD is an useful approach in several practical situations. For example, the FLD can be implemented separately to test the performance of Bayes classifier. This mutual test method is implemented for recognizing BAEPs from normal and patients, as described in the next chapter.

3.6 Summary:

In this chapter the mathematical preliminaries required for designing the Bayes Classifier and Fisher's Linear Discriminant Function was presented. Although, the BAEPs show considerable consistency and uniformity in normals, they do differ significantly in patients. Under these conditions, it is useful to characterize them by their statistical variations. Consequently, Bayes classifer and Fisher's Linear discriminant function are good candidates for developing appropriate classifiers as they use the underlying statistics to classify a pattern such as a BAEP waveform into appropriate class. The next two chapters describe the results of such an investigation into the efficacy of using these two classifiers for identifying the normal and pathological BAEPs.

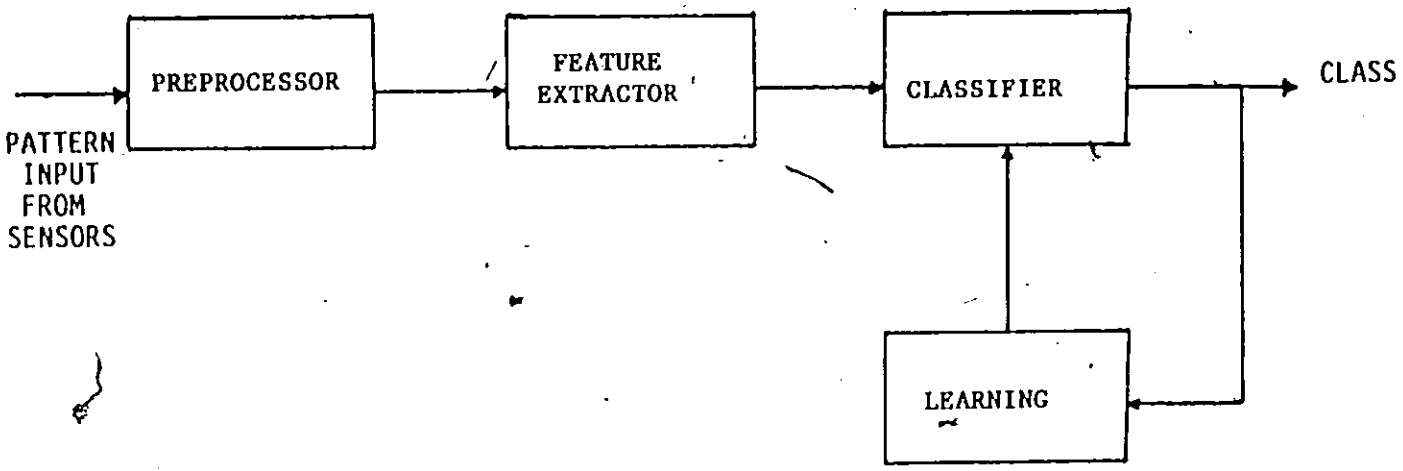

Figure 3.1 A typical pattern recognition scheme.

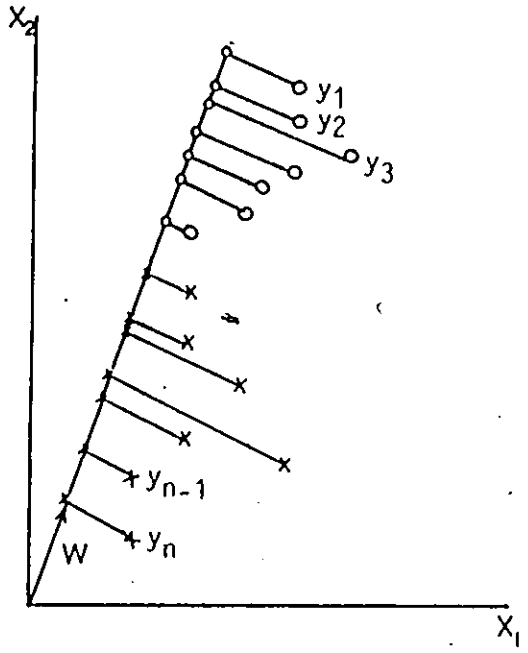

Figure 3.2 Selection of a proper Fisher's Linear discriminant in two dimensions.

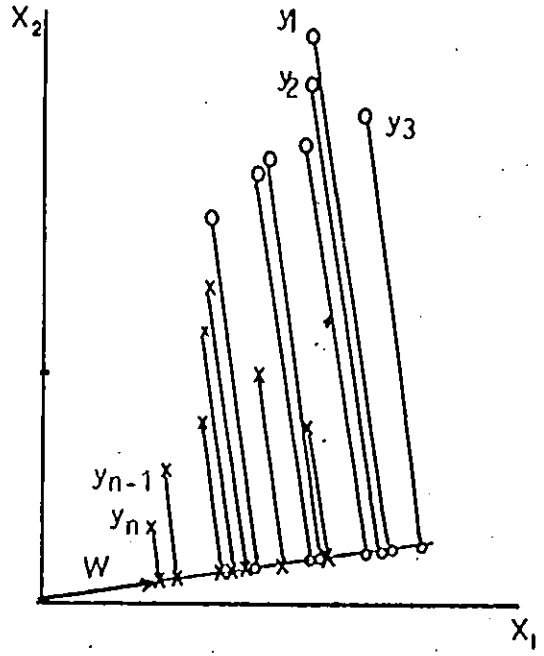

Figure 3.3 Improper selection of Fisher's Linear Discriminant in two dimensions.

CHAPTER 4

STATISTICAL PATTERN CLASSIFICATION OF BRAINSTEM AUDITORY EVOKED POTENTIALS USING TIME DOMAIN FEATURES

4.1 Introduction:

The role of BAEPs in assisting the neurophysician for evaluation of brainstem function during diagnosis, prognosis of neurological disorders, and during neurological surgery has been outlined in the earlier chapters. It is thus evident that latencies and amplitudes of the BAEPs are being used during the diagnosis of a wide spectrum of disorders of the central nervous system. It is of interest to develop classifiers which will provide information regarding the normality or pathogenicity of a given BAEP to aid the physician while making objective evaluation of the patient.

The classification of waveforms is performed by extracting relevant features from the waveform. These features must represent the waveform and its significant attributes in a concise and unique manner to provide data compression and at the same time provide acceptable accuracy of classification. Whereas, a waveform may be represented

by mathematical abstractions such as Legendre polynomials, splines or similar functions, it would be attractive to choose simpler measures of characterizing the BAEPs.

It was a logical step to attempt the BAEP classification on a computer with the latencies of the earlier five peaks used as features. The amplitudes of the peaks I-IV are not generally used in clinical practice due to their large variances. The amplitude of peak V has some relevance especially in patients with multiple sclerosis [Robinson and Rudge, 1977]. The present chapter describes the development and application of pattern classifiers to classify normal and pathological BAEPs by employing those features the neurophysician makes use of while examining the BAEPs, namely the latencies of the earlier five peaks and amplitude of the fifth peak. In the next section, justification for using the Bayes classifier and Fisher's linear discriminant (FLD) is given. The data acquisition and the design of the classifiers are presented in section 4.3. The feature selection and implementation details are given in section 4.4. The results and performance of the classifiers are presented in sections 4.5. These results are discussed in section 4.6.

4.2 Choice of the Classifiers:

The classification of BAEPs can be achieved by syntactic or statistical approaches. However, with either method, it would be advantageous to take into account the inherent statistics of normals for the design of the classifier. Under these conditions, Bayes classifier is suitable as it treats each new observation, such as a BAEP waveform as the sample or a stochastic variable. In addition, the Bayes classifier makes the classification process probabilistic, which is intuitively very attractive. The theoretical errors of classification are also minimal for the Bayes method [Hand, 1981; Duda and Hart, 1973]. Simpler statistical distributions can be devised by Fisher's linear discriminant method which was also used in this work as an alternate classifer to verify the classification accuracy.

4.3 Materials and Methods:

4.3.1 Data Acquistion

The BAEP data used in this study was recorded at the Neurology clinic of McMaster University Medical Center. Every year, a large number (n>1000) of BAEPs are recorded from patients with wide range of neurological complications. Only the BAEPs of those patients who had a normal hearing threshold were used. The BAEPs were obtained from

C_z-M_1, C_z-M_2 i.e vertex-right mastoid and vertex-left mastoid electrode locations on the scalp employing a Nicolet Pathfinder II system in our Evoked Potentials Laboratory. The contralateral mastoid was used as the reference. The stimulus was a 0.1 ms pulse delivered 9.8 times per second at 60 dB above the hearing threshold. The frequency range of recording was 150-3000 Hz. Two thousand BAEP responses were averaged, displayed and plotted on paper.

The latencies of the initial five peaks were measured from the computer display of the evoked potentials instrumentation system. The physician's diagnosis of the patient, based on the overall neurological assessment of several other criteria, is taken as the standard for evaluation of the accuracy or reliability of classification. The clinician's assessment of severity of disease was not used as a criterion for inclusion of BAEP in the study. Rather, it was the clinician's statement if the patient was healthy or pathological with a normal or abnormal waveform based on latencies that was used as the criterion to indicate the normality or otherwise of the BAEPs.

The BAEPs were obtained from two groups: a normal group of 49 clinically healthy patients (group B) and a patient group (group A) of 20 patients with confirmed multiple sclerosis (MS) and 21 patients with head injury

(HI). Thus, the patients in group A had abnormal BAEPs. The mean age of normals was 35.1±18.1 years (32 females, 17 males) and that of the patients was 34.9±18.1 years (19 females and 22 males). The BAEPs of right and left sides of all patients were used. The BAEP of each side was taken as one pattern, with the initial five latencies of the BAEP and the amplitude of the fifth peak used as features. In eight patients (6 MS, 2 HI), BAEPs from one of the sides were normal. These BAEPs were excluded from further analysis. Thus, there were a total of 172 BAEP patterns from 90 patients, used in this study. The feature selection process and implementation of the classifier are given in section 4.4.

4.3.2 Design of Bayes Classifier:

Equations (3.3) through (3.7) were implemented on a mainframe computer. The vectors M_A, M_B and matrices S_A, S_B are not known apriori and are estimated from a set of labelled patterns. In the present study, latencies from a subset of BAEPs labelled those of patients were selected to estimate M_A, S_A. Similar computations are performed for the estimation of M_B and S_B using latencies from BAEPs of normal subjects. The vectors M_A, M_B, and matrices S_A and S_B are computed as follows:

For i' = 1.2 ....N features.

$$M_A(i) = 1/n_A \sum_{j=1}^{n_A} x_j(i)_A \qquad (4.1)$$

$$M_B(i) = 1/n_B \sum_{j=1}^{n_B} x_j(i)_B \qquad (4.2)$$

In equation (4.1), $x_j(i)_A$'s are the 'j ' (totalling n_A) measurements on each of 'i ' features (totalling N) of labelled patterns from class A and n_A is the number of labelled samples from class A (called the training set). Similar computations were done for class B using individual features of labelled patterns, $x_j(i)_B$'s (equation (4.2)), where n_B is the number of labelled patterns in the training set of class B. Both M_A and M_B are vectors of dimension (N X 1) where N is the number of features. Each element $s_{i,j}$ of the covariance matrices S_A and S_B is computed as follows, from a training set of n_A and n_B labelled samples:

$$s_{i,j} = 1/n \sum_{k=1}^{n} (x_{ik} - M(i))(x_{jk} - M(j)) \qquad (4.3)$$

In equation (4.3) substitute, $n=n_A$ or n_B

corresponding to class A or class B. Also, the appropriate mean vector is substituted for M. The dimension of each covariance matrix is N X N.

4.3.3 Design of Fisher's Linear Discriminant Function:

Fisher's Linear Discriminant (FLD) projects all patterns on to a line which maximizes the separation of means between the classes when weighted by the covariance matrix. Given a labelled set of samples, the FLD is determined from:

$$W = S_P^{-1}(M_B - M_A) \qquad (4.4)$$

W = linear discriminant function

M_A = mean vector of class A

M_B = mean vector of class B

S_P = pooled variance-covariance matrix.

$$S_P = [(n_A - 1)S_A + (n_B - 1)S_B]/[n_A + n_B - 2] \qquad (4.5)$$

The computation of M_A, S_A, M_B, S_B is performed from a training set as in Bayes method. The equation (4.5) implies that the second order moments for both the classes are

equal.

4.4 Feature Selection and Implementation of the Classifiers:

Both the Bayes classifier and FLD were implemented in FORTRAN on a CYBER 170 computer system. In order to evaluate the efficacy of using each latency as a feature, the classification of BAEPs were done using one dimensional Bayes classifier given by equation (3.7) with each individual latency as the only feature. It was noted that latency of the fifth peak gave the highest accuracy of classification (76.7%) followed by the latencies of the IV peak (72.7%), III peak (71.0%), II peak (68.6%) and I peak (65.6%). The amplitude of the V peak and interpeak intervals did not yield accuracies greater than 65%. Classifiers were then designed with two, three, four "best" features (Fig.4.1). Finally, the following combination of features were utilized to develop the Bayes and FLD classifiers:

a) Latencies of initial five peaks (N = 5).

b) Latency of the first peak and interpeak intervals of the initial five peaks (N=5) .

c) Latencies of the initial five peaks and I-V interval (N=6).

d) Latencies of the five peaks and the amplitude of the fifth peak (N = 6).

e) Interpeak intervals of peaks I-II, II-III, III-IV and IV-V (N=4)

The classification of BAEPs was performed by the following procedures [Aunon and McGillem, 1982]:

1) Partition-Substitution method 2) Leave-one-out method.

1) In the Partition-Substitution (PS) method, a subset of BAEPs was used as the training set. Initially, BAEPs of 20 normal and 20 pathological subjects were used as the training set for each of the above implementation with different sets of features (a)-(e). The mean vectors, variance-covariance matrix for class A (pathological class) and class B are computed using equations (4.1)-(4.3). All the BAEPs (n=172) were then used as test patterns. The class membership of test BAEPs were determined from equation (3.7) for the Bayes classifier and from equations (3.13) and (3.14) for the Fisher's Linear Discriminant function.

The accuracy of classification was computed for each iteration using the diagnosis given by the clinician as the reference. The percentage accuracy of correct classification was computed from,

Accuracy (%) = No.of BAEPs correctly classified X 100/NT

(4.6)

where NT = 172 i.e., total no. BAEPs.

The training set was slowly increased from 20 to 70 (in steps of 10) in each of the two classes, whereas the test set was always the set of all the BAEPs. The class membership was computed for each new implementation of the classifier. The percentage accuracy was plotted as a function of the number of patterns in the training set.

2) In the Leave-one-out (LO) method, all patterns except one BAEP to be classified, were used as the training set. The classifiers were designed, and the test BAEP was then classified using Bayes and FLD classifiers. After classification, the test BAEP was returned to the training set. In turn, each BAEP was removed from the training set, new classifiers were designed and the BAEP was subjected to classification. The accuracy of classfication was computed

from the equation (4.6), after all the BAEPs were classified [Fukunaga, 1972]. The feature selection method described above was also performed using LO method.

The PS method yields optimistic results. Although a significantly large amount of computation is involved , the LO method uses all samples for both training and testing and yields a conservative estimate of the accuracy of the classifier [Fukunaga, 1972; Aunon and McGillem, 1982]. The performance of the classifiers were evaluated by computing the sensitivity, specificity, positive predictive value and negative predictive value for the LO method [Sackett et al., 1985]. Table 4.1 show sample computations for the evaluation of the Bayes classifier with three 'best' features, namely latencies of peaks V, IV and III.

4.5 Results:

Figure 4.1 shows the results of feature selection procedure using LO method. The accuracy of classification attained a maximum at 85.3% for three features, namely the latencies of peaks V, IV and III. These features are hence termed as optimum features. Addition of latencies of peaks II and I did not affect the classification accuracy significantly. Figures 4.2 through 4.7 present the results of applying Bayes classifier and FLD to classify BAEPs with

combinations of latencies, interpeak intervals, the I-V latency and the amplitude of the fifth wave used as features. The accuracy of classification for PS method steadily improved with the increasing number of patterns in training sets. This improvement may be attributed to better estimates of underlying statistics of the distributions due to larger training sets, as well as to the overlap of the test and training patterns.

Table 4.2 presents the results of accuracy of classification with different sets of features each for Bayes and FLD classifiers, using Leave-one-out method. The highest accuracy of classification achieved using Bayes classifier was 85.3% for the LO method, 87.1% for the PS method with a training set size of 70 (Figure 4.2). These results show that the latencies of peaks V, IV and III used as features gave the best performance for classification by both the PS method and LO method.

Figures 4.8 and 4.9 show the results of evaluation of the performance of all the classifiers using sensitivity, specificity, positive predictive value (PPV) and negative predictive value (NPV) as the criteria. The classifiers with features (a) and (b) gave the overall best performance for the Bayes and FLD method as assessed by accuracy, sensitivity, PPV and NPV. Further, the classifier with

optimum features (N=3) yields performance equal to, if not better than the above two classifiers.

The Appendix A, presents typical mean values and covariance matrices of normal and pathological classes. Sample computations for two BAEPs (Fig.4.10 of a normal subject and Fig.4.11 of a patient) are illustrated in Appendix A. It may be noted from these sample computations, the determinant of the covariance matrix of class A is several hundred times that of the determinant of covariance matrix of class B. Thus, the class B is denser compared to class A, a characteristic which facilitates the discrimination between the two classes [Kamath et al., 1986a and 1986b].

4.6 Discussion:

The classification procedures described in this chapter employed features derived from visual identification of peaks. Hence those BAEPs for which some of the peaks were absent or could not be identified, such as for patients with severe head injury, have not been included. Consequently, the recording conditions in the evoked potential laboratory are critical to obtain good and reproducible waveforms. The stimulus rate and intensity levels must be predetermined and set. Ambient noise must be

low. McMaster Neurology Clinic has been using the parameters described in section 2.2. These parameters have been reported to yield good waveform reproducibility and smaller variance of conduction time. The BAEPs from both right and left sides in the normal population did not differ significantly, and data from both the sides have been pooled together for this work while developing the statistics of the normal class. The latencies of the affected side(s) were utilized for computations of pathological class.

It is not surprising that the latencies of the successive peaks I-V become relatively more valuable as features. The delays (when present) of individual peaks accumulate, with the result that latency of peak V turns out to be the most valuable feature.

Chiappa [1984] states that absolute latencies should not be used by the clinician for interpretation of BAEPs since they are affected by stimulus intensity changes and other extraneous factors all of which induce excessive variability. It has also been recommended that interpeak intervals be used during diagnosis. But one may argue that there is no significant difference between using latencies or interpeak intervals for classification as same information is present in both sets of features. Indeed, our results demonstrate only marginal difference in any one

criteria measure for classifiers designed with these two sets of features (i.e. set (a) and set (b)). For example, sensitivity for Bayes method equals approximately, 80% for classifiers designed with these two sets of features.

Further, our results show that the classification of BAEPs may be performed on a computer with only three features as seen in figure 4.1 and table 4.2, comparable to that obtained by other feature sets. The accuracy of classification in figure 4.1 decreased with the addition of latencies of peaks II and I as features. It is noted that the addition of these two features reduces the quality of the feature set. Hence, latencies of waves I and II may not provide sufficient discriminatory information. The accuracy of classification did not improve with the addition of either the amplitude of wave V or the I-V interval as a feature [Kamath et al., 1987b]. Alternatively, it has been noted that both the latency and structural information of peaks II-III-IV-V were useful in the design of syntactic classifiers which yielded a classification accuracy of 83% [Madhavan et al., 1984, 1985, 1986].

Whereas significantly larger amount of computation is involved in the implementation of Leave-one-out method, compared to the Partition-Substitution method, the results obtained independently from both methods agree with each

other thus validating the techniques. The classification accuracy decreased with a training set of 60 samples (Fig.4.5). This decrease may be attributed to either variations in covariance matrix or to increased sensitivity of the feature set (s). A large training set is necessary for implementation of the classifiers especially in clinical settings, where a wide spectrum of diseases that result in abnormal BAEPs are diagnosed. for representing the pathological class. Similarly, data banks of BAEPs may be created for different age groups.

This work did not address the question of whether the classifiers, described herein, are more efficient in picking out BAEPs of patients with HI or MS. Individual class probabilities and larger training sets would be needed for such work. For classification of BAEPs from patients with severe HI or MS and where peaks can not be identified easily, features from frequency domain analysis may provide additional discriminatory information. An investigation to address this latter question is presented in subsequent chapters [Kamath et al, 1984; Kamath et al., 1987a].

The performance of Bayes classifier was generally better than FLD, as measured by accuracy and other criteria (Figs.4.1- 4.9 and Table 4.2) especially for classifiers using optimum features and using feature sets (a) and (b).

It can be shown that the Bayes classifier is asymptotically identical to the FLD under the condition that covariance matrices for the two classes with multivariate normal density function are equal [Hand, 1981]. Hence the improved accuracy obtained by using the Bayes method implies that not only are the first order statistical variables (mean) different for normal and pathological classes but that the second order moments described by the covariance matrices also differ for these two classes (see Appendix A).

The a priori probabilities for both the classes depend upon patient population at each clinic and would have to be tuned to an individual site. The a priori probabilities can be computed by a careful analysis of previous BAEP records in the clinic, and may be updated periodically. Precisely computed a priori probabilities would be especially useful if in a particular geographical area, there is preponderance of a specific pathology.

On-line implementation of the classifiers described in this work, on a microcomputer for example, would provide supplemental information to the clinician. Appropriate filtering and peak detection algorithms could be substituted for manual peak detection to automate the procedure [Fridman et al., 1982].

4.7 Summary:

In this chapter the development and results of classification schemes to recognize and classify normal and patients' BAEPs using time domain data were presented. The results indicate that automatic classification using features of BAEP waveforms may be performed, which may finally aid the physician. It was also noted that the latencies of peaks V, IV and III can be used to effectively classify BAEPs with similar results as with a larger set of features. The appendix A shows a sample set of computations on two BAEPs.

TABLE 4.1

EVALUATION OF CLASSIFIER PERFORMANCE

The following results were obtained for the Bayes classifier using optimal features (latencies of peaks V, IV and III). The sensitivity , specificity, positive predictive value (PPV) and negative predictive value (NPV) were computed as shown below:

		Reference Diagnosis	
		Pathological	Normal
Classification Result	class A	59 (a)	10 (b)
	class B	15 (c)	88 (d)

a + b + c + d = 172

Accuracy = (a+d)/(a+b+c+d) = 147/172 = 85.3 %

Sensitivity = a/(a+c) = 59/74 = 79.7 %

Specificity = d/(b+d) = 88/98 = 89.7 %

PPV = a/(a+b) = 59/69 = 85.5 %

NPV = d/(c+d) = 88/103 = 85.4 %

TABLE 4.2

RESULTS OF CLASSIFICATION OF BAEPS

USING LEAVE-ONE-OUT METHOD

Number/and Description of features	Percentage Accuracy	
	Bayes Classifier	Fisher's Linear Discriminant
3/Latencies of peaks III.IV and V	85.3	80.1
5/Latencies of initial five peaks	84.1	80.1
5/Latencies of initial five peaks and interpeak intervals of I-II. II-III. III-IV and IV-V.	83.3	80.0
5/Latencies of 5 peaks and I-V interval	75.0	80.0
6/Latencies of 5 peaks and amplitude of fifth peak	80.0	83.0
4/Interpeak intervals of I-II. II-III. III-IV and IV-V peaks.	78.3	73.8

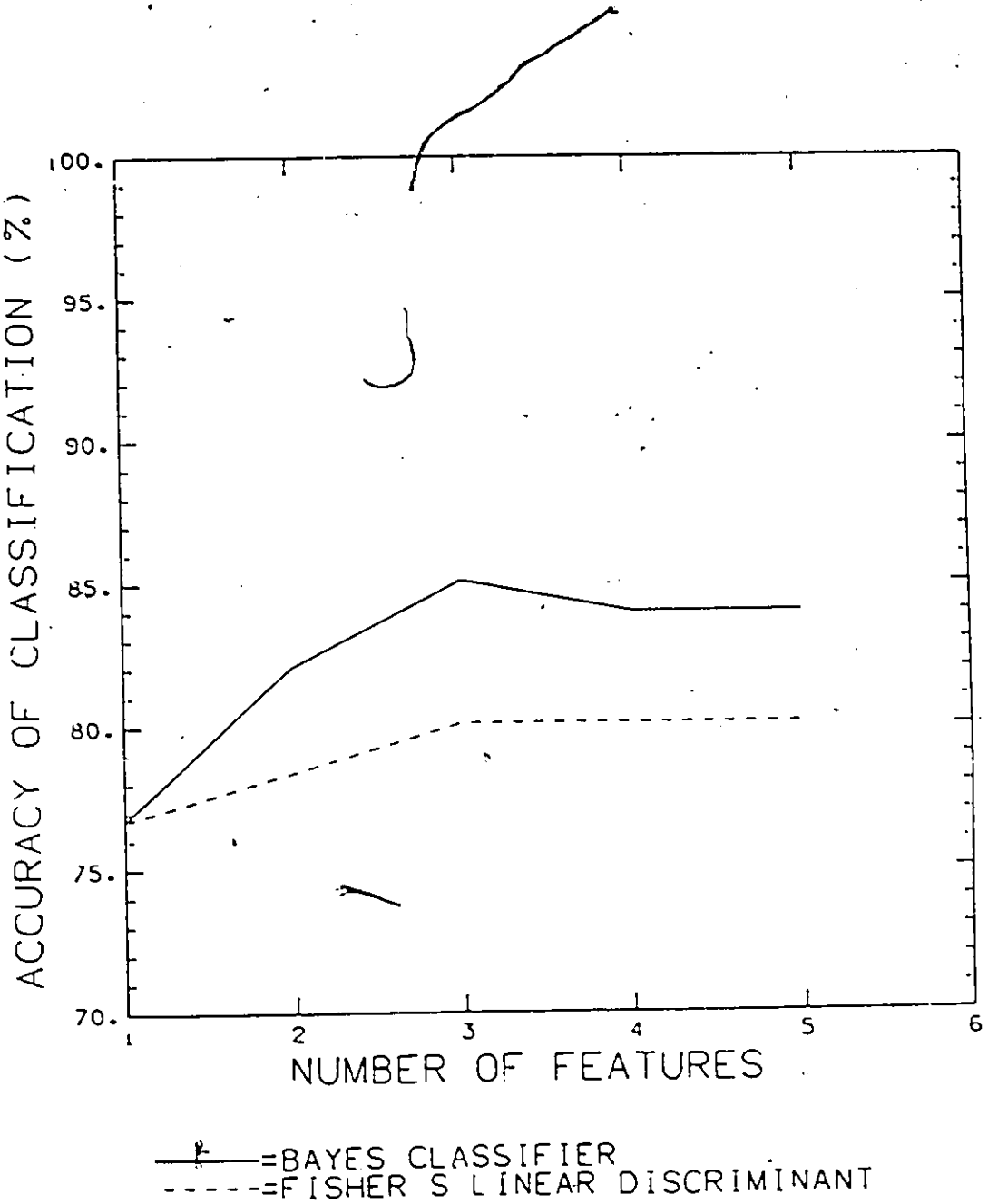

Figure 4.1 Results of feature selection by Leave-one-out method.

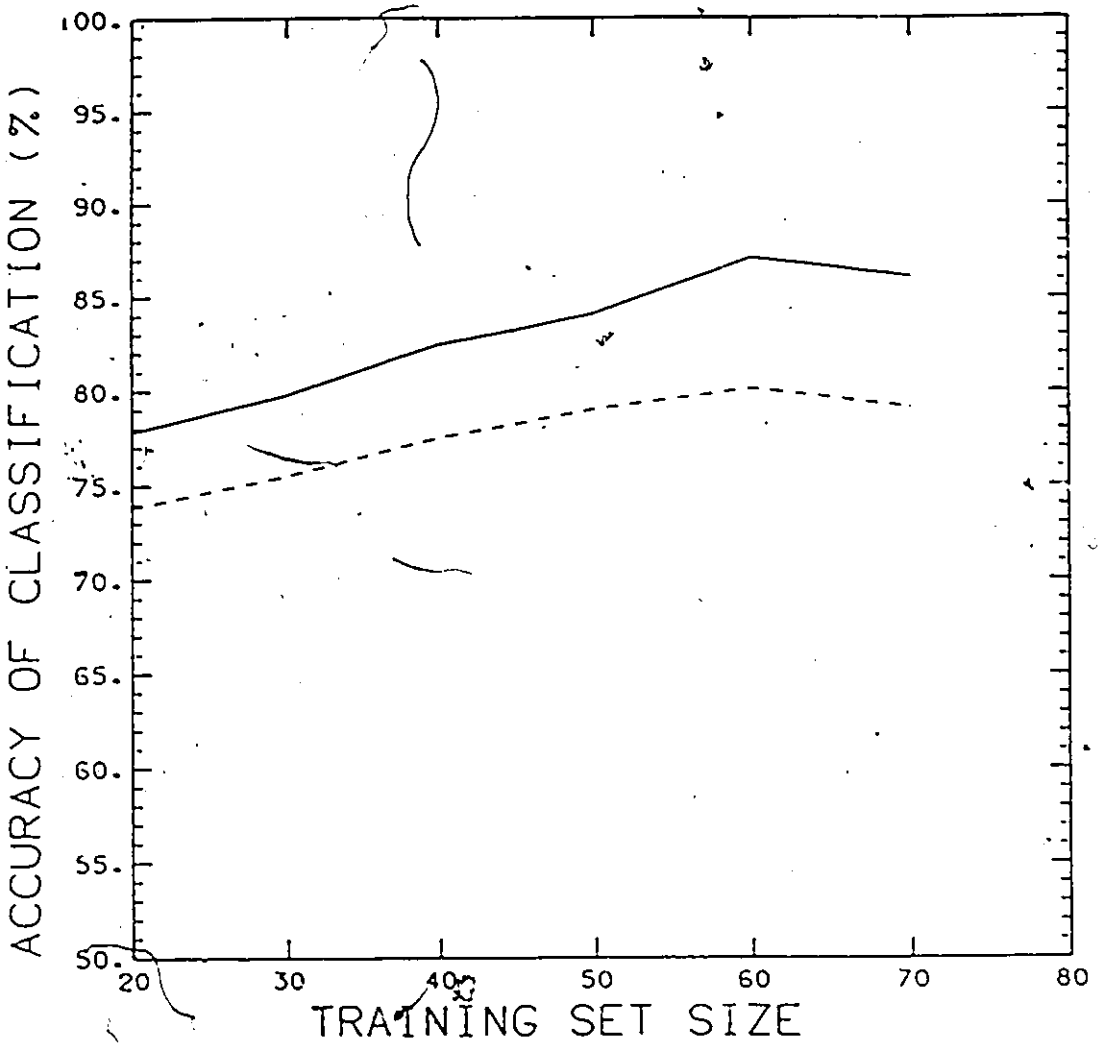

Figure 4.2 Result of pattern classification of BAEPs by Partition-Substitution (PS) method using the best three features.

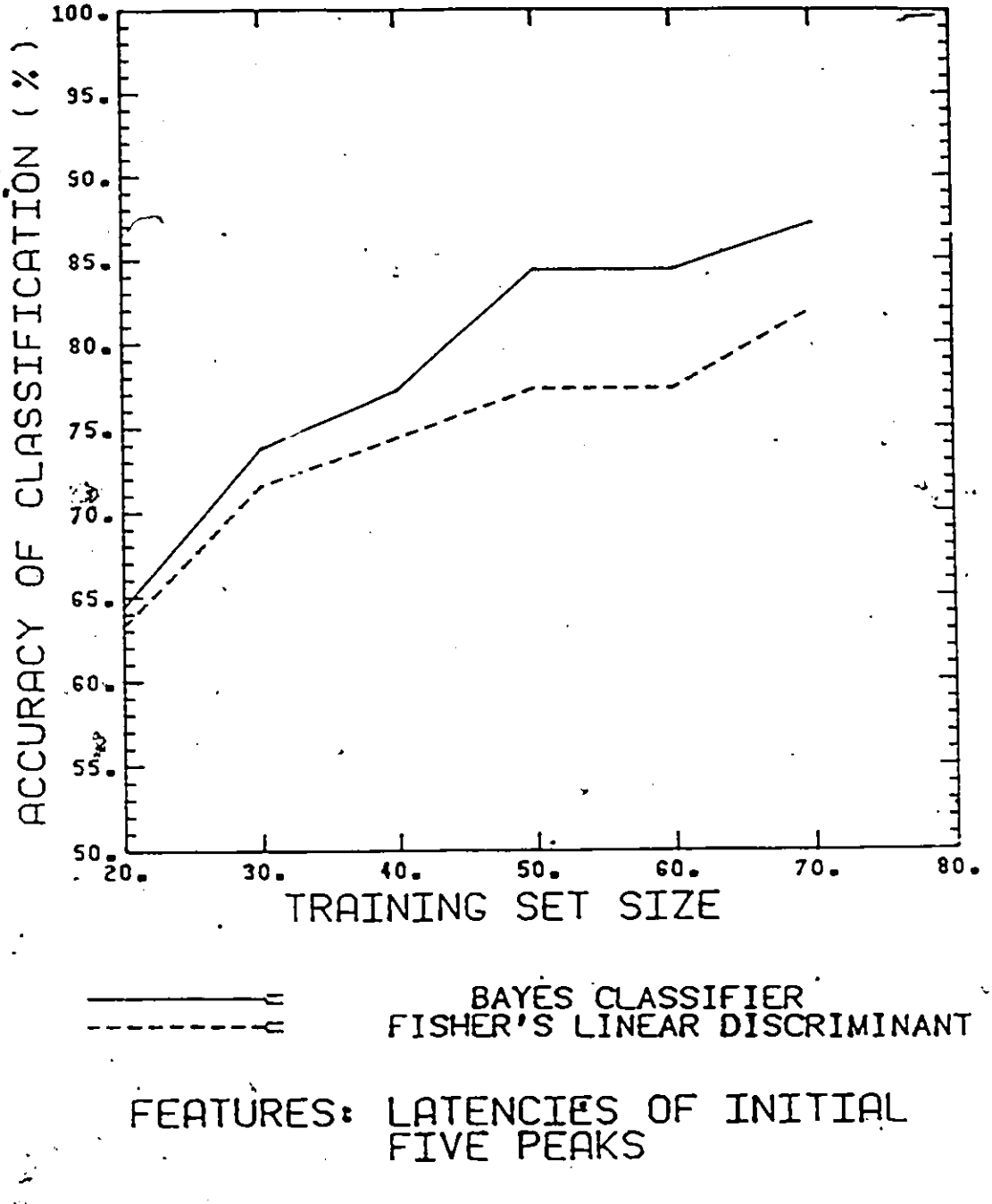

Figure 4.3 Results of pattern classification of BAEPs by PS method using latencies of initial five peaks as features.

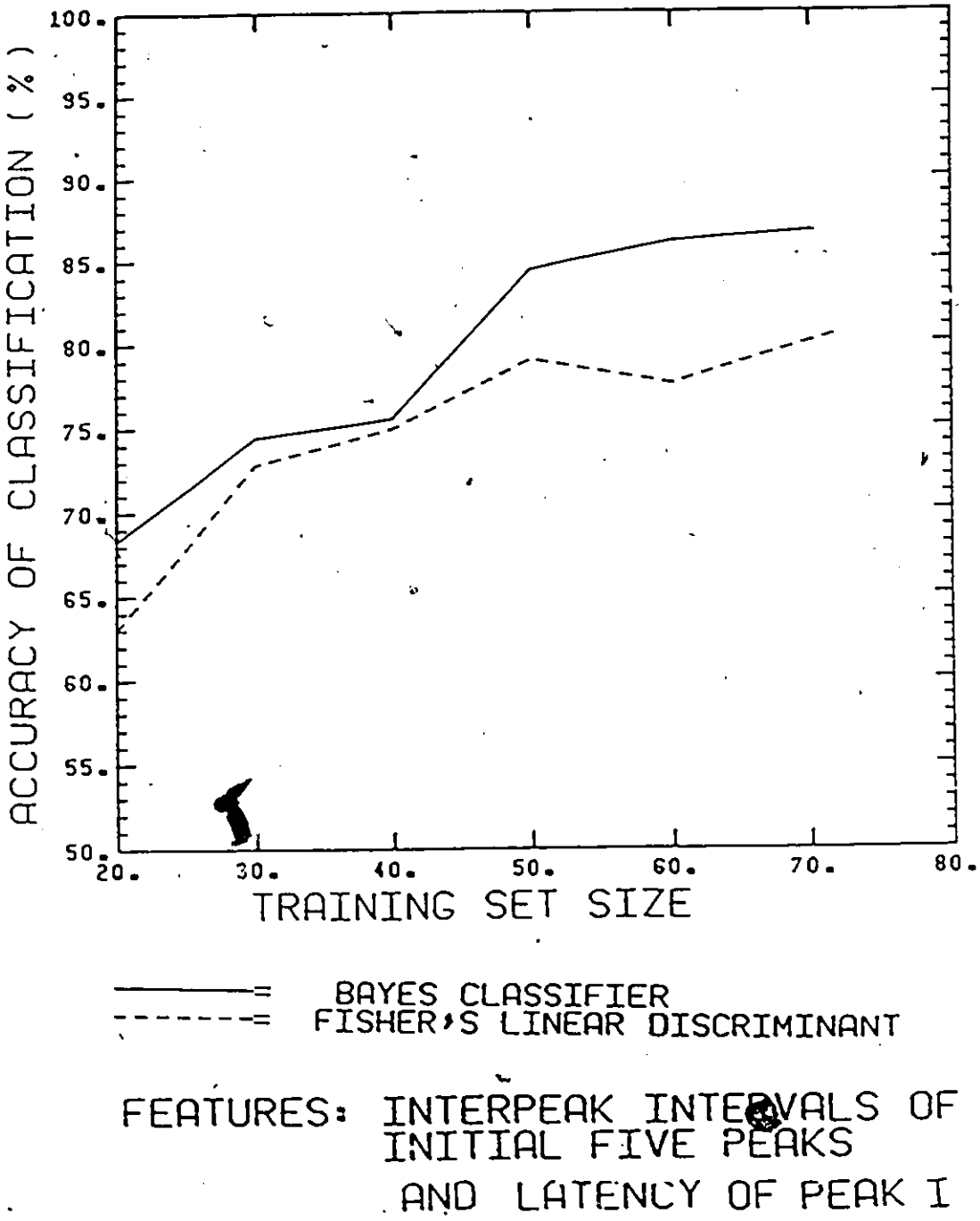

Figure 4.4 Results of pattern classification of BAEPs by PS method using latency of the first peak and interpeak intervals of the initial five peaks.

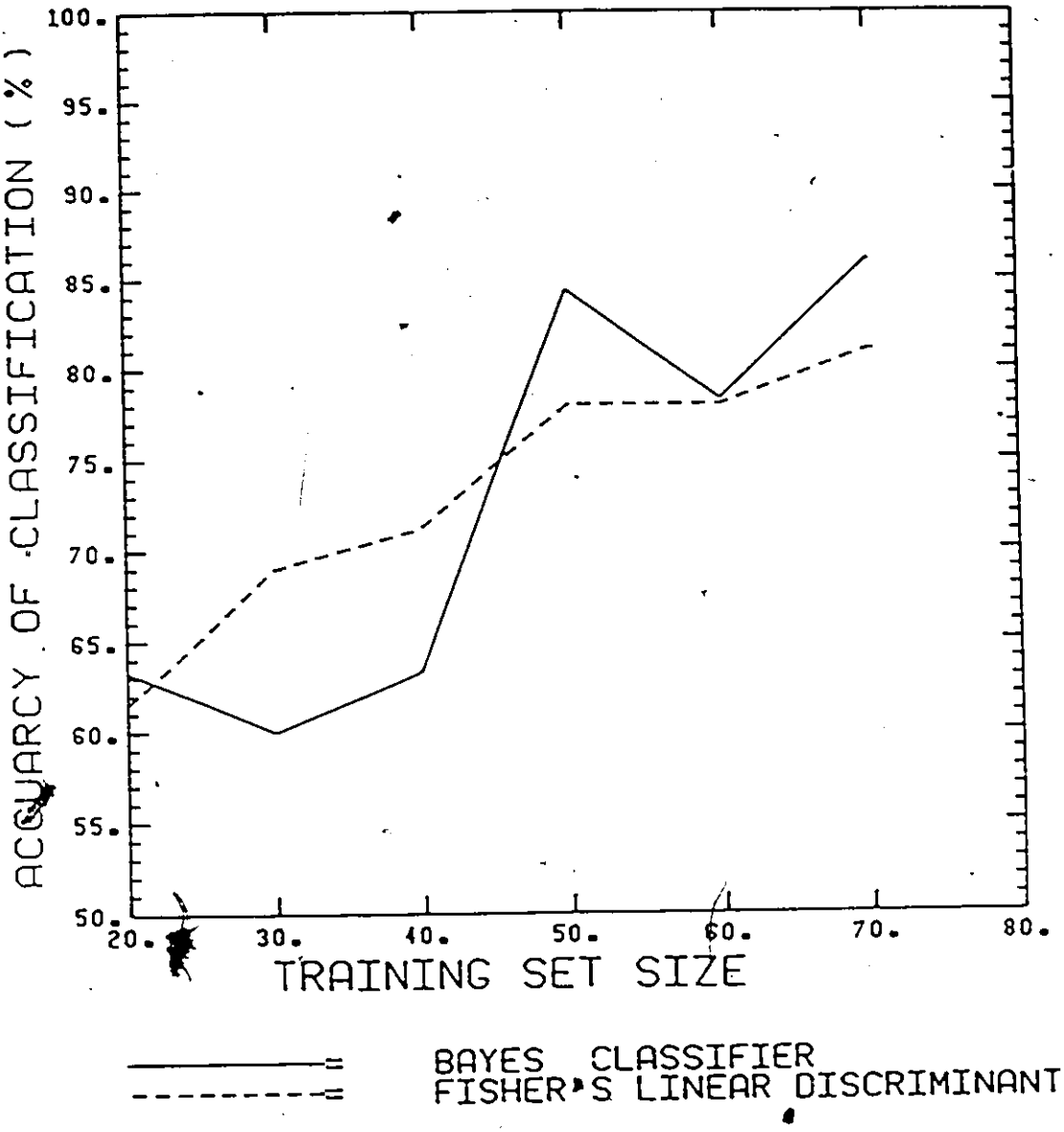

Figure 4.5 Results of pattern classification of BAEPs by PS method using latencies of the first five peaks and the I-V interval.

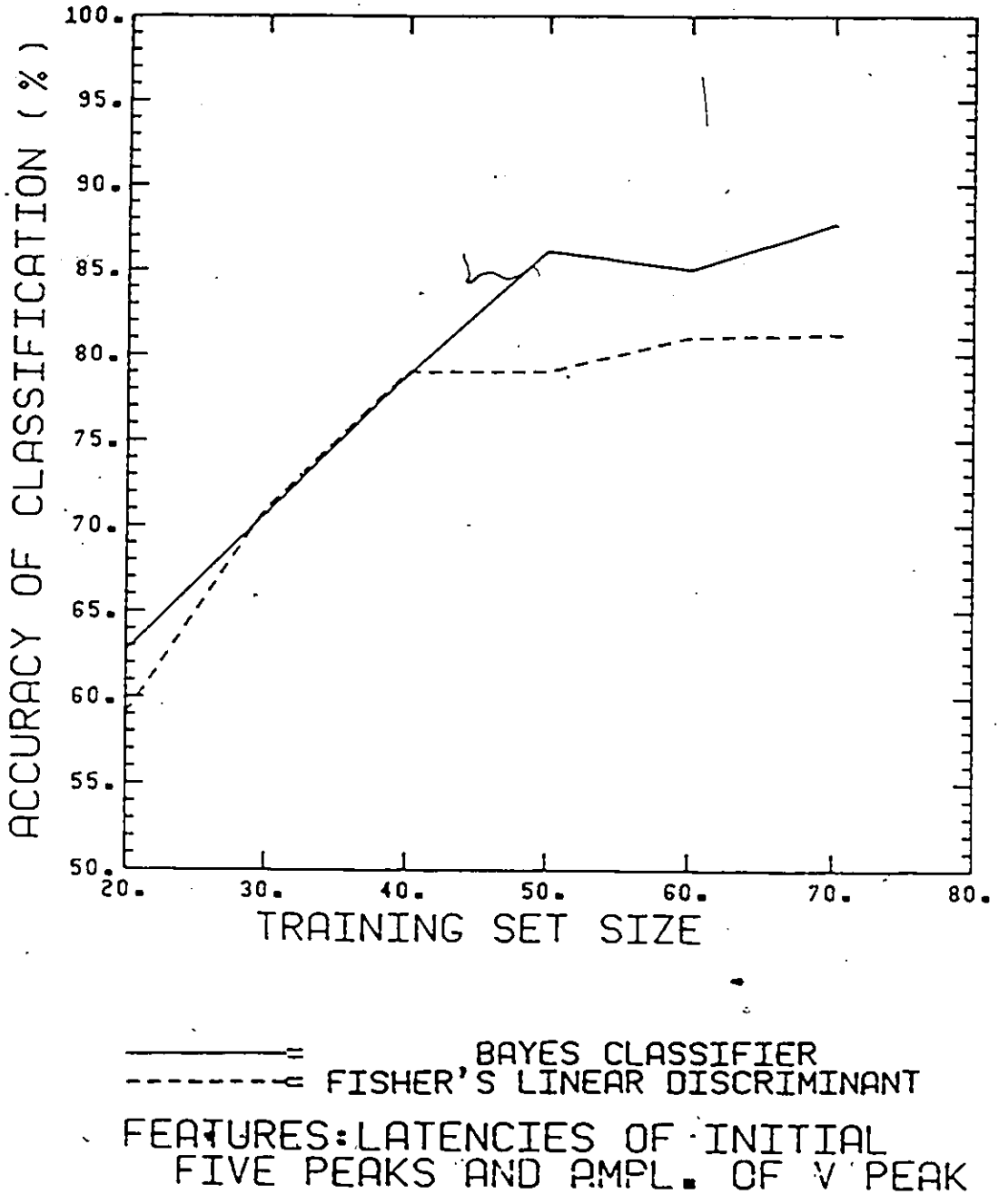

Figure 4.6 Results of pattern classification of BAEPs by PS method using latencies of the five peaks and amplitude of the fifth peak.

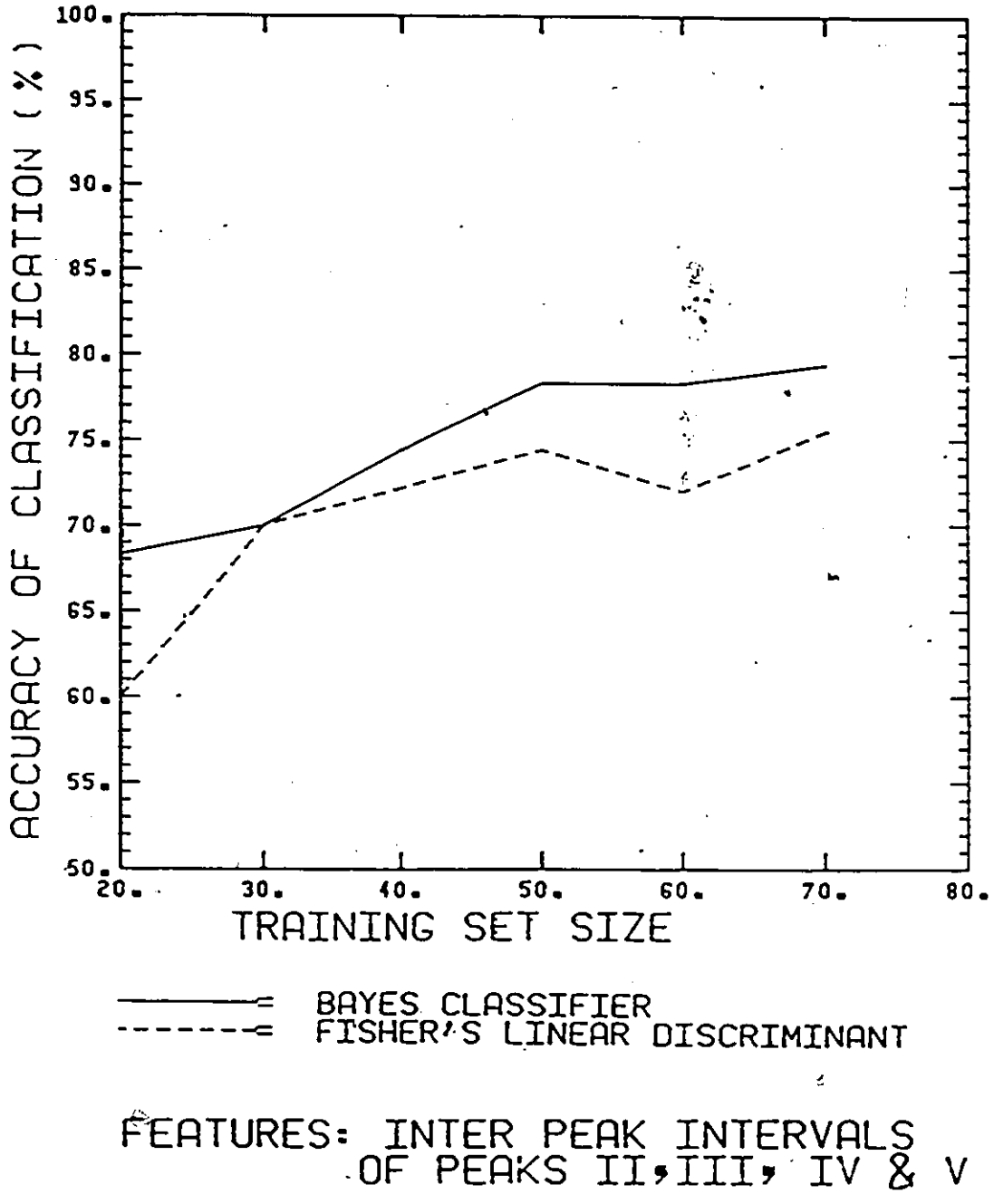

Figure 4.7 Results of pattern classification of BAEPs by PS method using interpeak intervals of peaks I-II, II-III, III-IV and IV-V.

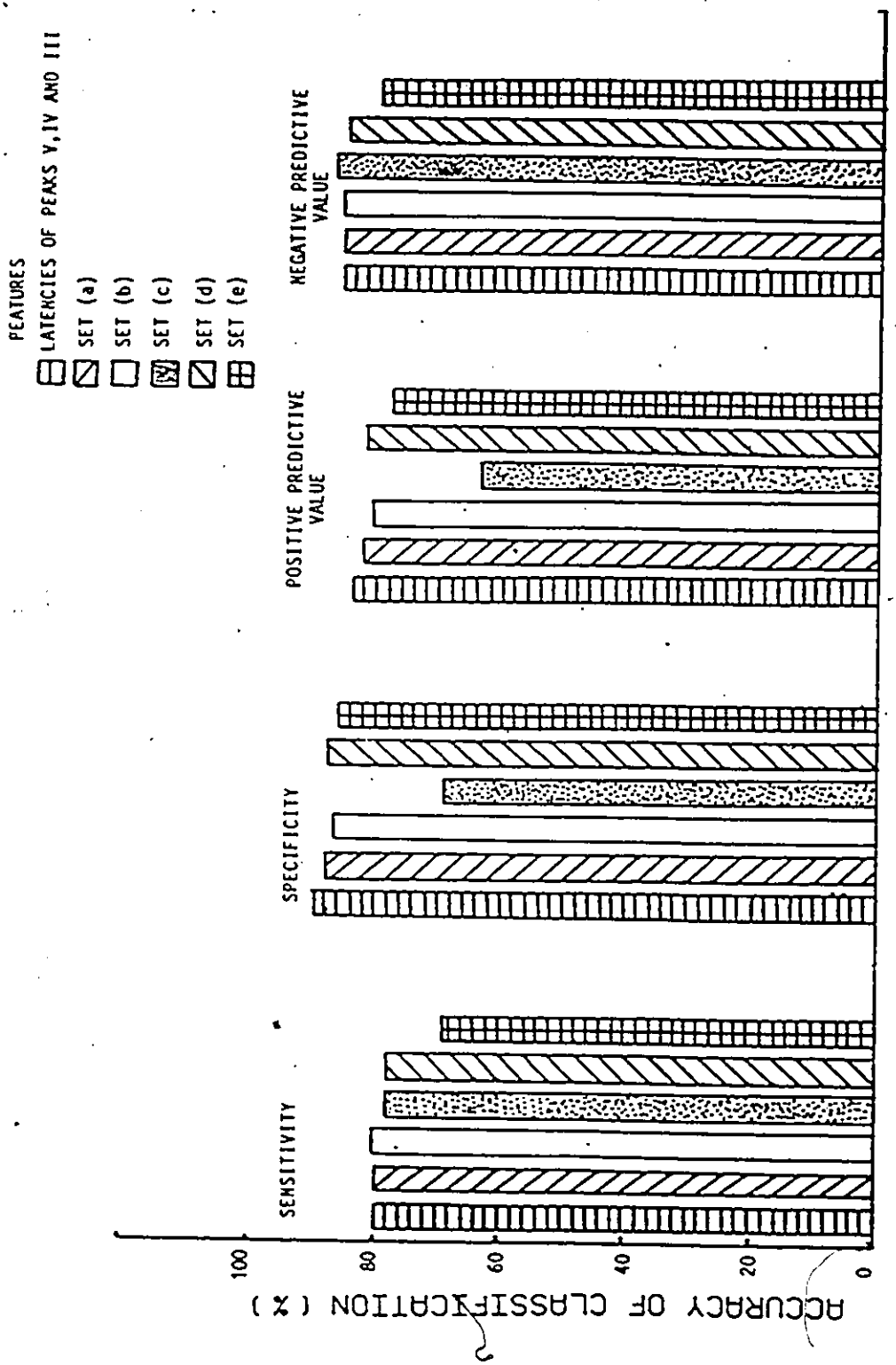

Figure 4.8 Evaluation of the performance of Bayes classifiers employing time domain features.

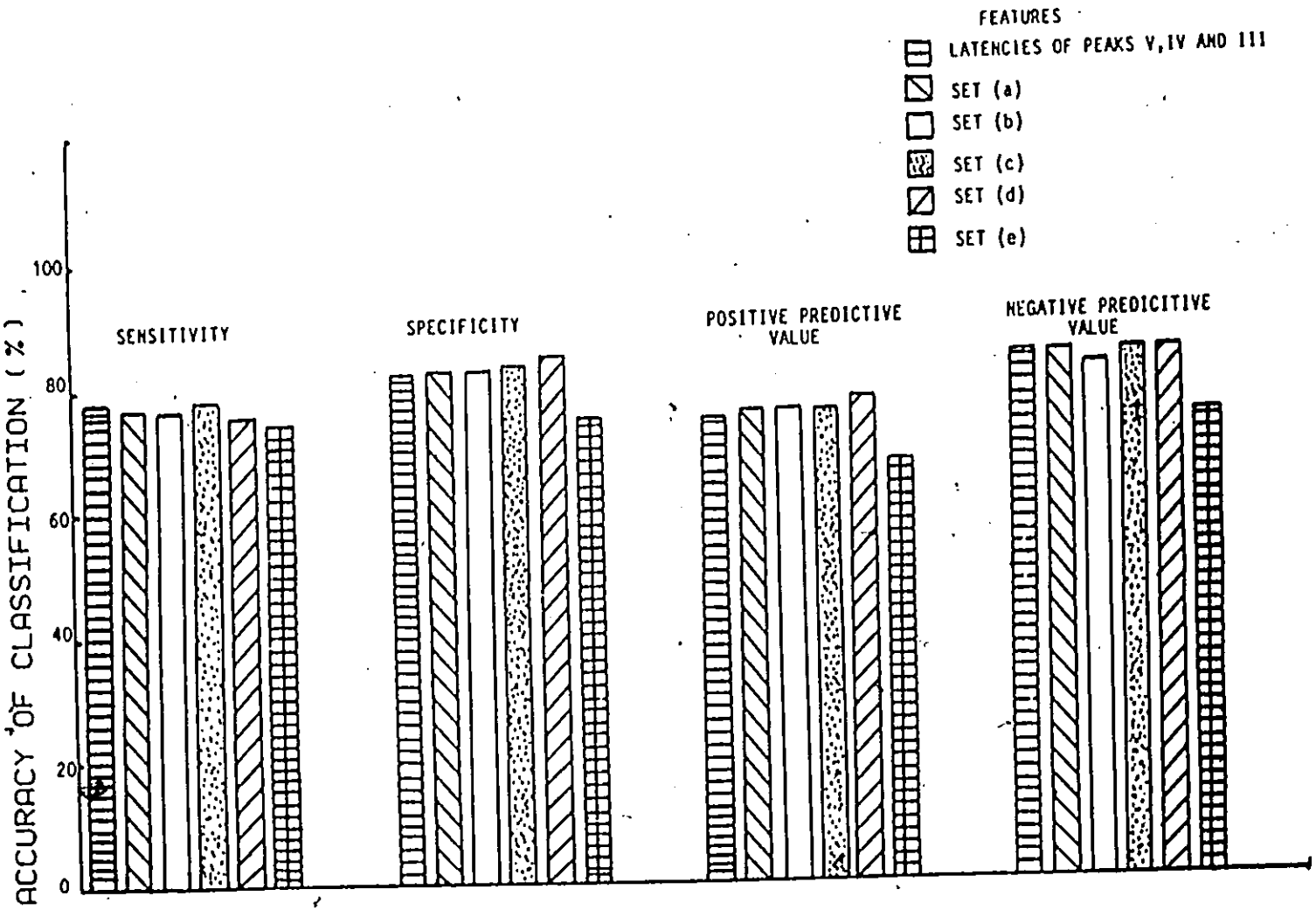

Figure 4.9 Evaluation of the performance of Fisher's Linear Discriminant Function employing time domain features.

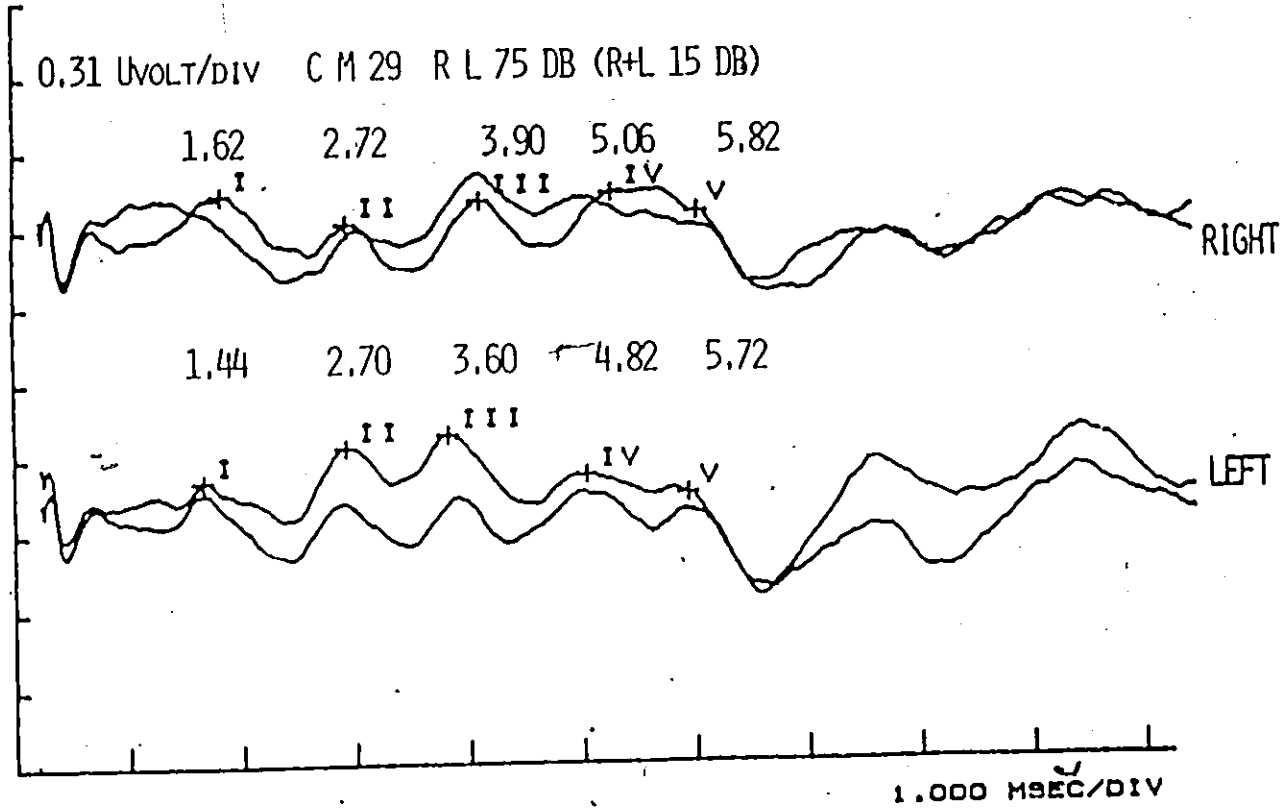

Figure 4.10 BAEPs of a normal subject.

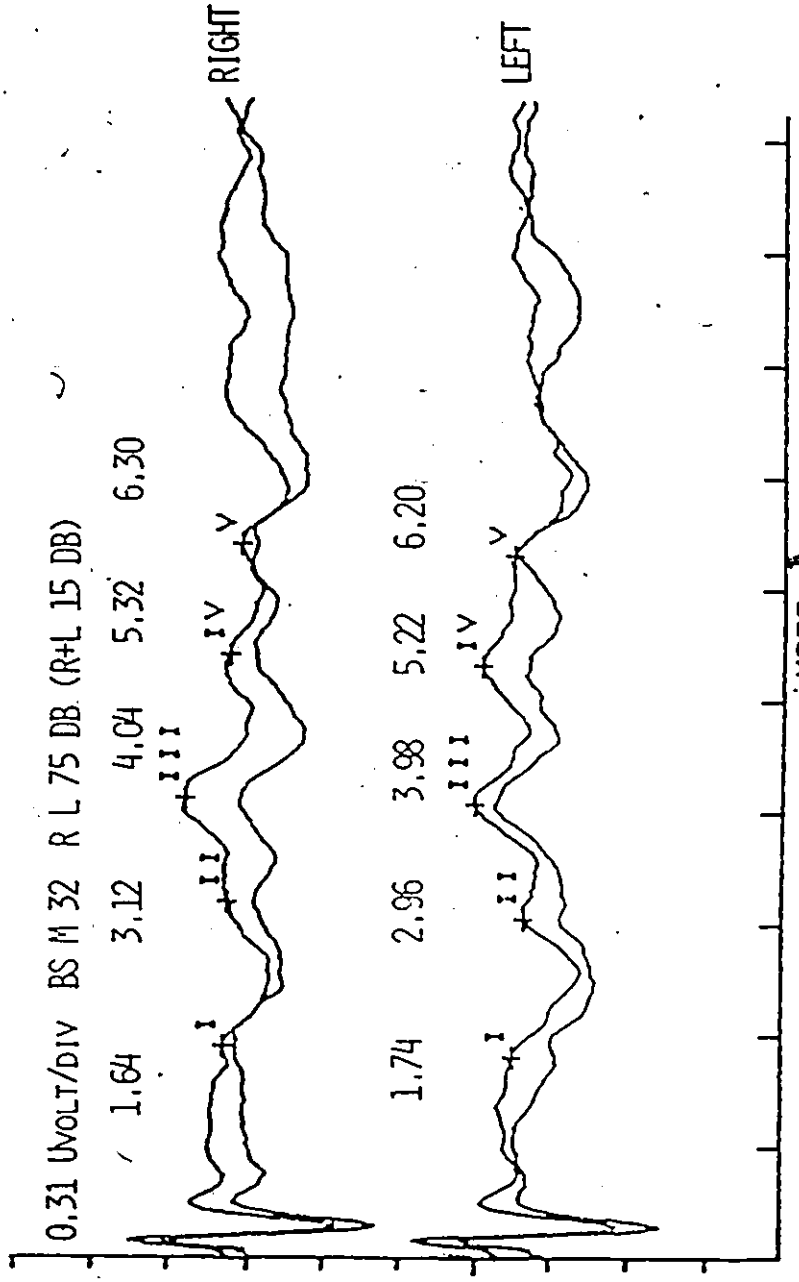

Figure 4.11 BAEPs of a patient with multiple sclerosis.

CHAPTER 5

POWER SPECTRAL ANALYSIS AND PATTERN CLASSIFICATION OF BRAINSTEM AUDITORY EVOKED POTENTIALS USING FREQUENCY DOMAIN FEATURES

5.1 Introduction:

Whereas the time domain features for classifying BAEPs resulted in a performance as described in the previous chapter, such classifiers depend on accurate identification of peaks in the BAEP waveform. Although the exact location of peaks is easy to identify in normal subjects (such as in Fig.5.1), it may be difficult to localize the latencies when there are random components in the BAEP or when the peaks become diffused as a result of pathological conditions such as head injury etc.; this is illustrated in Fig.5.2, in the case of a patient with acoustic neuroma on the left side where peaks are either absent or are hard to identify. In such cases, the possibility of using frequency domain peaks is very attractive. In this chapter, the power spectral analysis of BAEPs is described in order to obtain features for classification of BAEPs.

The section 5.2 describes the applications of power spectra of signals of biological origin. This is followed by a mathematical description of the power spectra in section 5.3. The data acquisition and computational procedures for estimating the power spectra are discussed in section 5.4. The characteristics of normal and pathological BAEP power spectra and the results of classification of normal and pathological BAEPs using the features derived from frequency domain are delineated in section 5.5. Finally, the results of power spectral estimation and classification are discussed in section 5.6.

5.2 Some Applications of Power Spectra of Biological signals:

Power Spectral analysis of biological signals, mostly based on the assumption of stationarity, provides quantifiable information about the frequency components in the signal. Information about the frequency composition of the signal can then be used to compare the normal and pathological states. For example, Sklar [1971] has successfully used spectral analysis of EEG to differentiate between normal children from dyslexic ones. Correlation

between the muscle function and motor recruiting patterns has also been studied by spectral analysis of EMG [Yoo et al., 1979]. Heart rate variability power spectra reveal the status of sympathetic and parasympathetic systems for controlling heart rate and arterial pressure [Kamath et al., 1987c].

Thus, frequency analysis of biological signals often provides insights into the origin of the waveform and physiological relevance of its various components. However, the spectral components of BAEP have not been examined critically, except to provide design criteria for filters for instrumentation to record the BAEPs [Boston et al., 1980]. Hence, power spectral analysis of BAEPs was performed initially to examine the nature of frequency content of the BAEPs [Kamath et al., 1984].

An alternate method of studying a signal along with its spectrum is to develop a model, again under the assumption of stationarity, such that the power spectrum of the model approximates that of the signal. The model parameters can then be used to compare two sets of signals. Signal modelling has found applications in analysis of waveforms such as EEG and short term speech among other signals [Jansen et al., 1981; Makhoul, 1975]. Usually, the

number of model parameters required to describe the signal is significantly less than the original data length or its spectrum. Since variability between signals will be reflected in their model parameters, it should be useful in the analysis of BAEPs.

5.3 Power Spectral Analysis and Autoregressive Modelling:

5.3.1 Power Spectrum:

Unless it is visibly rhythmic, the periodicities in a given signal x(t), can not be easily determined. If x(t) is periodic with additive random component or if x(t) is a stationary random process, the periodicities can be better understood by its autocorrelation function $R_{xx}(\tau)$, given by

$$R_{xx}(\tau) = \lim_{T\to\infty} \int_0^T x(t)x(t+\tau)dt \quad ..(5.1)$$

for a continuous signal.

However, periodicities in a given signal can often be better quantified into the frequency domain via the Fourier transform. According to Wiener-Khintchin theorem, the Fourier transform of the autocorrelation function of the signal is its power spectral density (PSD).

Thus, the power spectrum $S_{xx}(f)$, of $x(t)$ is given by,

$$S_{xx}(f) = \int_{-\infty}^{\infty} R_{xx}(\tau)\exp(-j2f\pi\tau)d\tau \quad .. \quad (5.2)$$

The power spectrum of a given signal represents the average distribution of power in the signal as a function of frequency. The power spectrum brings out the existence and location or dominant frequencies and the power contained at those frequencies. The estimation of the power spectrum via the correlation function is known as the Blackman-Tukey (BT) method. This method has been applied for power spectral analysis or auditory evoked responses due to psuedo random noise excitation [Reddy et al., 1979].

5.3.2 Modelling and Computation of the Power Spectrum by Maximum Entropy Method (MEM):

In recent years, a number of nonlinear spectral analysis techniques have been proposed and implemented on various kinds or signals including those of biological origin [Jansen, 1981; Childers, 1978; Haykin, 1979]. These methods characterize a signal by a model. The model parameters describing the signal are determined and the parameters are subsequently used to estimate the power spectrum of the signal.

In one such model commonly used in signal processing, a discrete signal x(n) is considered to be the output of a system with an input gaussian sequence u(n). The output x(n) is represented as a combination of the previous inputs and outputs:

$$x(n) = - \sum_{k=1}^{p} a_k x(n-k) + G \sum_{i=1}^{q} b_i u(n-i) \quad ..(5.3)$$

where a_k $(1<k<p)$, b_i $(1<i<q)$ and G are the parameters of the system.

The coefficients $b_1 \ldots b_m$ are known as the zeroes and $a_1 \ldots a_p$ are known as the poles. The model is called Pole-Zero model. In time series literature, this formulation is referred to as autoregressive-moving average model. It is possible to use only an all-pole or autoregressive model to represent a signal. The poles of the model can be estimated by solving a set of linear equations and hence the all-pole model is favoured in signal analysis.

In the autoregressive (AR) modelling approach, the estimate of the signal amplitude, x(n), at a given instant 'n' is represented as a weighted linear sum of its 'p'

previous samples plus u(n):

$$x(n) = -\sum_{k=1}^{p} a_k\, x(n-k) + u(n) \qquad \ldots\ldots \quad (5.4)$$

where the process u(n), n=1.....N, form the samples of a stationary Gaussian white noise process. The parameters a_1, a_2, ... a_p are to be estimated from the signal and are called the AR parameters.

Since u(n) is a Gaussian white noise, one can write [Makhoul 1975] from equation (5.4) an expression for power spectra, P(f), of x(n):

$$\bar{P}(f) = \frac{G^2}{\left| 1 + \sum_{k=1}^{p} a_k \exp(-j2fk\pi\Delta t) \right|^2} \qquad (5.5)$$

where Δt is the sampling interval and G^2 equals the variance of the white noise u(n).

Several methods have been developed for computation of AR parameters from the signal [Childers, 1978]. In one such formulation, known as maximum entropy method (MEM), the

spectrum which corresponds to the most unpredictable time series; and whose autocorrelation approaches that of the given signal for the given set of lags is chosen. In the maximum entropy method, the autoregressive parameters are so estimated as to reduce the errors by running the model in forward and backward directions. Such a computation of the model parameters has been shown to be equivalent to maximizing the entropy of the spectrum of the model [Kay and Marple, 1981].

The final prediction error (FPE), which is defined as sum of the squares of the errors between the measured signal x(n), and the predicted signal, is used as an index for predetermining the optimum number of parameters required to estimate the MEM spectrum. The first local minimum of the FPE as a function of order often indicates the optimum model order.

5.4. Materials and Methods:

5.4.1 Data Acquisition:

The BAEPs of 60 subjects were recorded from vertex-right mastoid and vertex-left mastoid locations, in the Evoked Potentials laboratory of McMaster University

hosptial. The subjects comprised of 23 Normals (age 29+16 yrs.), 19 with multiple sclerosis (MS) (40±9 yrs.), 13 with head injury (HI)(16±15 yrs.) and 5 with acoustic neuroma (AN) (40±9 yrs.). Two patients from HI group and one patient from MS group exhibited normal BAEPs from one of the two sides: the spectra of these three BAEPs and those of patients with AN were not included in the subsequent analysis although their power spectra was computed for verification. Thus, 107 BAEP waveforms were analyzed for this study.

The stimulus was a 0.1 ms pulse delivered at the rate of 9.8 times per second at 60 dB above the hearing threshold. The recording of the BAEP was done for 10 ms following the auditory stimulus over a frequency range of 150-3000 Hz. Two thousand BAEP responses were averaged and plotted on paper. The plotted BAEP signal of 10 ms duration was digitized on a Summagraphics Bit Pad into 256 samples corresponding to a sampling rate of 25.6 KHz. The digitized signal was transmitted to and anlayzed on CYBER 170 computer.

5.4.2 Computation of Power Spectrum by Blackman-Tukey (BT) method:

Classical methods of power spectral estimation are based on cosine transforms and subsequent smoothing in the frequency domain. However, with the advent of fast Fourier transform (FFT) algorithm and high speed computers, the power spectrum is estimated by Welch Periodogram [Welch, 1967] or the implementation of Blackman-Tukey (BT) correlation method partially or fully with FFT algorithm [Schwartz and Shaw, 1975]. Herein, the correlation function was estimated directly and then the smoothed power spectrum was estimated as the Fourier transform of the estimated correlation function.

The power spectrum of each digitized BAEP waveform is computed by the BT method as follows:

Let the discrete version of the BAEP signal be represented as x(0), x(1)....x(i).....x(N-1), where 'N' is the number of samples. The autocorrelation function of x(i) then is :

$$R(m) = 1/N \sum_{n=1}^{N-m-1} x(n)x(n+m) \quad \ldots\ldots (5.6)$$

where m=0,1....K is the number of lags.

The autocorrelation function R(m), is multiplied by a

lag window such as Bartlett window. Next. the spectrum is computed using the relation.

$$S(f) = \Delta t \sum_{m=1}^{M} W(m)\, R(m) \exp(-j2fm\Delta t) \quad \ldots(5.7)$$

where Δt is the sampling interval and W(m) is the Bartlett window for m=1,2,....M.

The FFT procedure is invoked for efficient computation of this equation. The various parameters used in the computation are shown in Table 5.1. For each power spectrum, S(f), its decibel equivalent 10log10 S(f) was computed to yield the power spectrum on a decibel scale for convenient plotting. The power spectra or BAEPs from both right and left side were computed and plotted using CALCOMP plotter.

It was noted that there were three principal peaks in the normal BAEP power spectra at 170 , 520 and at 950 Hz. In order to quantitate the power spectra of BAEPs of normals and patients, the power contained in each spectrum was divided into five principal bands (Table 5.2); each of the first three bands included a peak. The fourth and fifth bands were chosen to separate the power beyond 2 KHz.

Finally, a mean power corresponding to each frequency band was computed for each normal, MS and HI groups. In order to test the hypothesis that mean power across each frequency band in MS and HI groups equals that of the mean power in a corresponding frequency band in a normal group, the student 't' test was performed at 95% level of confidence.

5.4.3 Autoregressive Modelling and Computation of MEM Spectra:

Of the various methods used in practice for computing the AR parameters of the BAEP signal, the MEM due to Burg was chosen [Ulrych, 1975]. From these AR parameters, the power spectrum of BAEP was estimated using equation (5.4). Power spectral estimates for different model orders were also computed and plotted one above the other (Figs. 5.12-5.14) to facilitate the examination of the MEM spectra for various model orders. The final prediction error was plotted as a function of the model order for each of the signals.

5.4.4 Feature Selection and Classifier Design:

Since the mean power in the bands lying around the frequency peaks 170, 520 and 950 Hz differed significantly

(Table 5.2), between normals and patients ($p<0.05$), these powers were used as the features. The total powers in the frequency range 1.05 - 2.0 KHz and from 2.05 -12.8 KHz did not differ significantly between the normals and patients ($p<0.05$) and consequently were not used as the features.

Bayes classifier and Fisher's Linear Discriminant Function were implemented in FORTRAN on CYBER 170 computer using leave-one-out method as described in the last chapter. Briefly, all BAEPs except the one to be classified are treated as design set. Both Bayes classifier (equation 3.7) and FLD (equation 3.10) were designed using equations presented in the chapter 3. The test BAEP was subjected to classification after which it was returned to the design set. This procedure was repeated for all 107 BAEPs. The accuracy of classification was estimated from physician's diagnosis as the reference.

In order to evaluate the relative merit of using each of the features mentioned above, both Bayes classifiers and FLD were designed with a single dimension and classification accuracy was computed. It was noted that power in the band containing 950 Hz peak gave the highest accuracy of classification, of 74.2% (Table 5.3). The classifiers with two best features and the three features were then designed

and accuracy of classification was evaluated. The performance of the classifiers (both Bayes and FLD) with all the three frequency domain features were assessed using sensitivity, specificity, positive predictive value and negative predictive value as the criteria.

5.5 Results:

The results of spectral analysis by Blackman-Tukey and by Burg's method as well as of classification by frequency domain features are presented below. The differences in spectra of normal and patients' BAEPs are described. The results of evaluation of the performance of the classifiers described in the section 5.4 are also presented.

5.5.1 Blackman-Tukey (BT) PSDs of BAEPs of normals and patients:

For comparative purposes, the hypothetical ideal BAEP of Figure 1.1 [Stockard et al., 1977a] was digitzed and its PSD was estimated (Fig.5.3). The PSD exhibits three principal peaks at 200 Hz, 500 Hz and 900 Hz. In order to determine which component(s) of the signal contributes towards the power at each of the three principal frequency

bands of BAEP power spectrum. an artificial signal was generated on the computer by combining three sinewaves at the above frequencies along with some added noise (inset of Fig.5.4) The power spectrum of the simulated signal (Fig. 5.4) indicates that the power in the frequencies near 200 Hz corresponds to the part of the waveform starting at the valley following the third peak in the time domain and ending at the valley following the fifth peak. an interval that is roughly 2.5 ms; this component resembles half a sinewave (without the fourth and fifth latency peaks). The first three waves in normal BAEP appear about 1 ms apart (for example. in Fig. 5.1) and provide the major contribution to the power at 1000 Hz. The peak around 600 Hz is due to wavelets containing the peaks VI and VII in the time domain.

The power spectra of normal BAEPs were computed. The BT power spectra of the normal subject in Fig.5.1 is shown in Fig.5.5. To visually compare the BAEP power spectra across different normal subjects, the power spectra of ten normals were plotted. one above the other. by shifting the power spectra and eliminating the hidden lines (Fig. 5.6). Prominent peaks were located in all the power spectra. Three major peaks appear at 170±55, 520±40 and 950±50 Hz. while a minor peak appears at 1950±100 Hz. The spectral

energy decays rapidly after 1500 Hz.

The BAEP power spectra of patients differed from those of normal subjects with respect to their location and spread of power. The power spectra of patients with AN had no well derined peaks. However, the spectra of the unaffected side appeared normal. For example, Fig.5.7 shows the power spectra of the BAEP in Fig.5.2. The peaks in the power spectra of BAEP from the left side affected by acoustic neuroma are not well formed.

In patients with demyelinating disease such as multiple sclerosis (MS) the conduction abnormalities are manifested in BAEPs as delays in one or more latencies as well as reduced amplitudes of some of its components [Chiappa, 1980]. In the frequency domain, these variations from normal waveform transform to dispersion of power in the frequency bands corresponding to the affected components. As an example, Fig. 5.8 shows the BAEPs of a patient afflicted with MS; the latencies of peaks IV and V are delayed and the amplitudes of wave V are reduced bilaterally. Figure 5.9 shows the computed BT power spectra of the BAEPs in Fig. 5.8. The first three peaks in the time domain, which appear approximately one millisecond apart bilaterally, result in a 850 Hz peak in the right side and a

comparatively large power around 800-900 Hz on the left side. The abnormal temporal relationships between different time domain peaks has resulted in the loss of a peak at 550 Hz in the power spectra of right side BAEP and in the appearance of a peak at 320 Hz on the left side.

In patients with head injury, the BAEPs are often delayed on the side with injury: sometimes one or several of the peaks are absent, or not well formed, depending on the nature and severity of injury. Typical BAEPs of a patient with head injury are shown in Fig.5.10. The patient suffered injury to the right pareito-temporal region in a motor vehicle accident. The waves I,II,III are not well represented, wave IV is not very sharp, and wave V is delayed in the right side. The damage to the left side is minimal. Fig.5.11 depicts the BT power spectra of BAEPs in Fig.5.10. The power spectrum of the right side differs from normal BAEP power spectra. The left side was unaffected clinically and the corresponding PSD has well defined peaks at 220 Hz,600 Hz and 1020 Hz.

The mean power in the two lower frequency bands were significantly higher for PSDs of BAEPs of patients with HI and MS ($p<0.05$) whereas the normal subjects had higher power in the 850-1200 Hz band in their BAEP PSD ($p<0.05$). Thus an

increase in the BAEP latencies or augmented waveform morphology for pathological states (in MS and HI) results in a PSD quite different from normal BAEP PSD. Because of the small sample size, the results of AN patients were not subjected to statistical analysis.

5.5.2 MEM Power Spectra of Normal and Patients' BAEPs:

The MEM power spectra were computed for orders varying from 15-49 with an arbitrary step size of 2. Figures 5.12, 5.13 and 5.14 show the MEM power of BAEPs in Figs. 5.1, 5.8 and 5.10. At low model orders, the major frequency peaks present in the BT power spectra do not appear distinctly. Only when the model order is greater than 30 does the MEM power spectra appear well formed and stable. The power spectra corresponding to model orders predicted by a local minima in the final prediction error (FPE) were examined. A plot of FPE vs. model order for BAEPs (shown in Figs. 5.1, 5.8 and 5.10) is given in Fig. 5.15.

It was noted from such plots for all the BAEPs, that a first local minimum in FPE correlated with well formed peaks in the MEM power spectra (the same frequencies of the BT power spectra) only in 10% of the BAEPs. Usually, an AR

model greater than one indicated by the local minimum in FPE was needed for an acceptable MEM spectra. Hence, optimum model orders were obtained by a visual examination of plots of the MEM spectra for increasing model orders for all the BAEPs used in this study. Typically, 40 or more AR parameters were necessary to represent the BAEPs The mean order (nearest integer±s.d.) for characterizing BAEPs was 42±4 for normals, 40±5 for patients with MS and 42±4 for patients suffering from head injury. The sample size of patients with AN was too small to estimate the mean order required to represent the BAEPs. Figure 5.16 shows a plot of optimum order number for individual BAEPs in normal, MS and HI and AN groups. The frequencies at which peaks appear in MEM power spectra, at the optimum order chosen (as described), were obtained in all normal subjects. These spectral peaks were found to be at 165±55, 550±45 and 1000±55 Hz.

5.5.3 Classifier Performance:

The percentage accuracy of classification for individual and combination of features is listed in Table 5.3. It can be observed that the maximum classification accuracy of 77.4% was obtained with the powers in three principal frequency bands, namely at 170, 520 and 950 Hz, as

the features. The power in the frequency band 850-1200 Hz yielded the maximum accuracy of classification (74.2%) . Addition of other two features increased the accuracy of classification by only 3.2% . The Bayes classifier gave marginally better classification accuracy than FLD. Figure 5.17 shows the classifier performance for both the Bayes classifier and FLD. It may also be noted that the performance of the Bayes classifier as measured by sensitivity. specificity. positive predictive value and negative predictive value was close to that using FLD. Appendix B gives sample calculations for classification of two BAEPs using frequency domain features.

5.6 Discussion:

This chapter presents an attempt at characterizing the power spectra of the BAEPs from normal and pathological subjects. by Blackman-Tukey (BT) method and maximum entropy method. (MEM). in order to examine their frequency composition [Kamath et al.. 1987a]. The efficacy of using frequency domain features for classifying normal and pathological BAEPs is also examined.

The observation that power spectra computed by BT and MEM show peaks at frequencies that agree with one another.

to within one frequency resolution of the computation (i.e. 50 Hz) tends to confirm the validity of these methods in analyzing the BAEPs. The minor peak observed at about 2 KHz in the BT power spectra of BAEPs of normal subjects was not always seen in the MEM power spectra, because the relative power at this frequency tended to be small compared to the major peaks at 170 Hz, 520 Hz and 1 KHz.

The student 't' test, performed on BT power spectra, shows that power contained in three specific frequency bands of BAEPs of patients with multiple sclerosis and head injuries differ significantly from the power spectra of normal BAEPs. This observation prompted the development of classifiers based on frequency domain features.

A major limitation of the Fourier transform based methods (such as the BT method), for estimating the power spectra is that the signal exists outside the data window being analyzed. Consequently, in the power spectra computed using the BT methods there is a leakage of power into the neighbouring frequency bands. A number of window functions have been recommended to minimize the leakage of power. But the window functions are not specifically tailored to take into consideration the statistical properties of the individual signal. The BAEP lasts less than 10

milliseconds, and because of its short duration, the MEM method appears to be well suited to examine the periodicities and to model it.

However, for estimation of the MEM power spectra of a BAEP signal, the order of the model generating the signal is important. The order corresponding to a minimum FPE is usually chosen as the optimum model order. Although selection of a model order based on minimum FPE works well for modelling pure autoregressive (AR) processes, the FPE criteria underestimates the model order in many practical applications. It has been observed that harmonic processes with noise require as many as N/3 to N/2 MEM parameters to describe the signal for a record length of N [Ulrych et al., 1979].

Recently, Shangkai and Loew [1986] have reported the use of AR model of the BAEP signal for hearing threshold detection, with only five parameters and using FPE as the criterion for selecting the order number. However, they have not shown the efficacy of their model in estimating the power spectra as delineated in this work: nor was the procedure for estimating the optimum model order based on matching the power spectra obtained from the signal as suggested in literature [Makhoul, 1975]. Our results show

that BAEPs sampled with 256 points can be represented with less than 50 parameters i.e. about 20% of the original record length.

However, the features derived from BT method gave sufficiently good accuracy of upto 77.4% during classification. The relative increase in classifier performance by using AR parameters instead of the presently used features i.e. the total power in three principal frequency bands, has not been attempted in this research.

Although, the time domain features provided better classification performance, the frequency domain features are useful in cases where the time domain features (i.e. location of peaks) are not easily available. Hence, it is suggested that freqeuncy domain features be used where latencies can not be unequivocally located and that both techniques can be used to give the clinician a larger range of objective criteria. It is also observed that both Bayes classifier and FLD yield similar peformance (Fig. 5.17), an indication that the second order moments of the frequency domain features do not differ significantly from each other for the normal and pathological classes.

5.7 Summary:

The power spectra of normal and patients' BAEPs are examined in this chapter. More than 100 BAEPs were subjected to power spectral analysis. The normal power spectra show three principal bands. The total power in each of these bands for patients' BAEPs differed significantly from that demonstrated in the normal subjects. Further, when these total powers in each band were used as features, Bayes classifier and FLD yielded 77% and 76% classification accuracies respectively. The MEM method was also used to verify the location of peaks in the power spectra. However, since the number of MEM parameters required to characterize the BAEPs was observed to be greater than 40, they have not been used further in this research.

TABLE 5.1

BLACKMAN-TUKEY POWER SPECTRAL ESTIMATION

Variable	Value
T	Total duration of the signal: 10ms
N	Number of samples :256
f_s	Sampling rate : 25.6 KHz
F_{max}	Maximum Frequency ($f_s/2$) :12.8 KHz
K	Number of Lags :128
M	Length of Lag window :256
F	Frequency resolution: 50 Hz.

TABLE 5.2

TOTAL POWERS IN SPECTRAL BANDS OF BAEPS (micro volts^2)

Frequency band	Normal Subjects (n=46)	Multiple Sclerosis (n=37)	Head Injury (n=24)
0-350 Hz	14121.1±3247	16965.5±3080*	18265.9±3183*
400-800 Hz	8328.2±2205	7072.3±2523*	6522.2±2715*
850-1200 Hz	2915.5±1213	1673.4±919*	1044.2±500*
1.25-2.00 KHz	588.1±219	455.1±147	356.9±71.9
2.05-12.8 KHz	335.7±45.6	329.0±51	310.3±35.9

*denotes statistically significant power from that of the normal subject ($p<0.05$)

TABLE 5.3

ACCURACY OF CLASSIFICATION FOR INDIVIDUAL FEATURES AND COMBINATIONS OF FREQUENCY DOMAIN FEATURES

FEATURE(S)	PERCENTAGE ACCURACY	
	BAYES CLASSIFIER	FISHER'S LINEAR DISCRIMINANT
1	66.98	67.92
2	60.37	63.20
3	74.20	74.00
1 and 2	76.42	76.42
1 and 3	76.66	75.80
2 and 3	76.42	75.35
1.2 and 3	77.40	76.70

FEATURE 1 : POWER IN FREQUENCY BAND 0-350 Hz

FEATURE 2 : POWER IN FREQUENCY BAND 400-800 Hz

FEATURE 3 : POWER IN FREQUENCY BAND 850-1200 Hz.

BAER

	RIGHT		LEFT
I	1.680	I	1.520
II	2.880	II	2.840
III	3.880	III	3.820
IV	4.700	IV	4.820
V	5.680	V	5.480
I-V	4.000	I-V	3.840
AMP-V	0.40	AMP-V	0.52

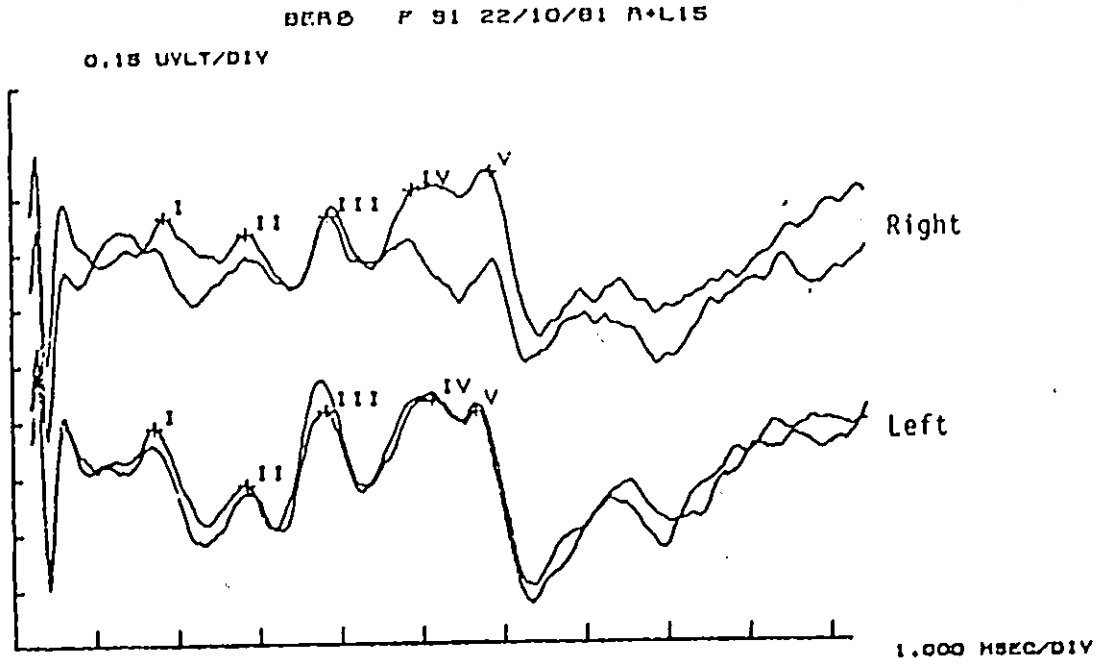

Figure 5.1 BAEPs of a normal subject (BERB).

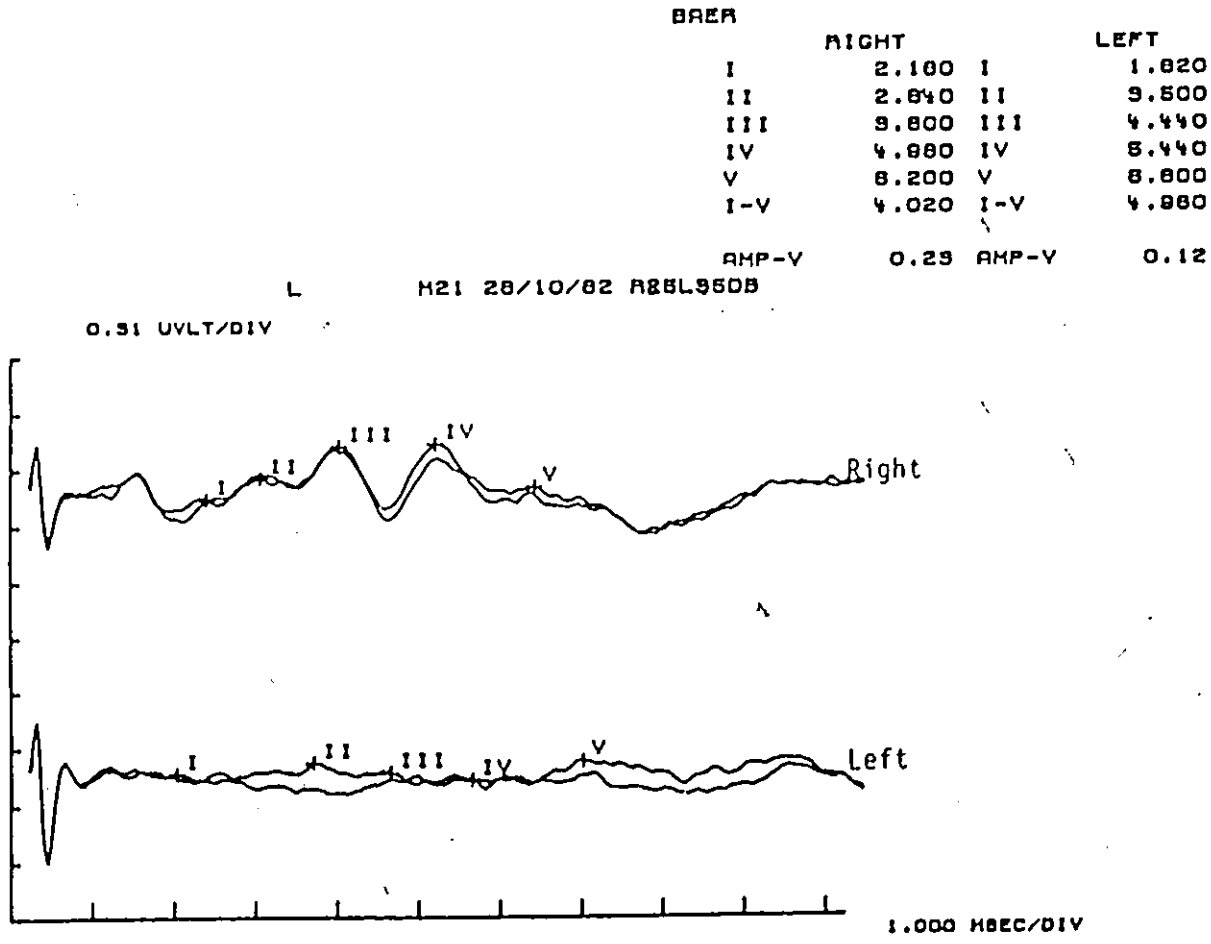

Figure 5.2 BAEPs of a patient (L) with acoustic neuroma on the left side.

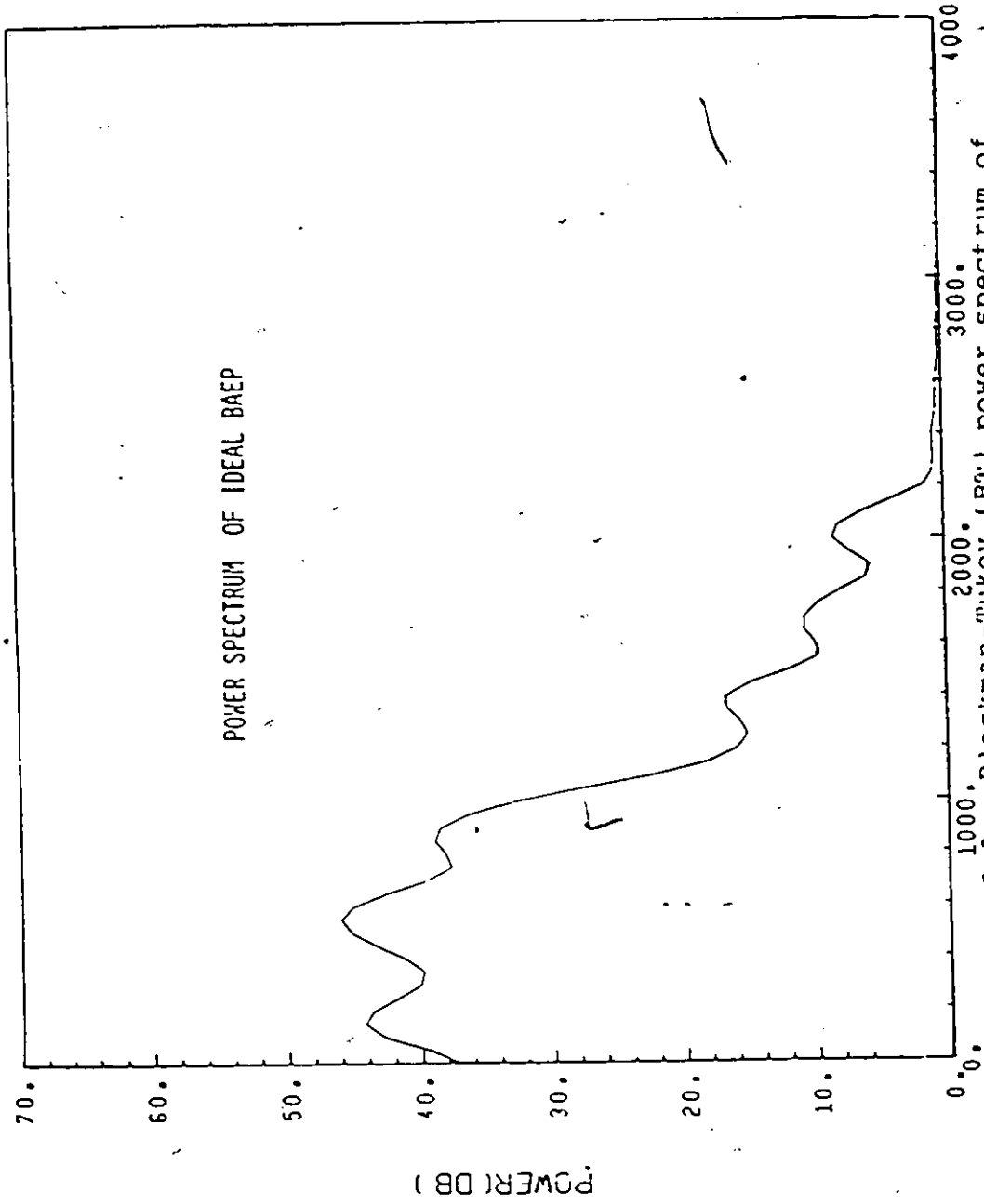

Figure 5.3 Blackman-Tukey (BT) power spectrum of hypothetical idealized BAEP (of Figure 1.1).

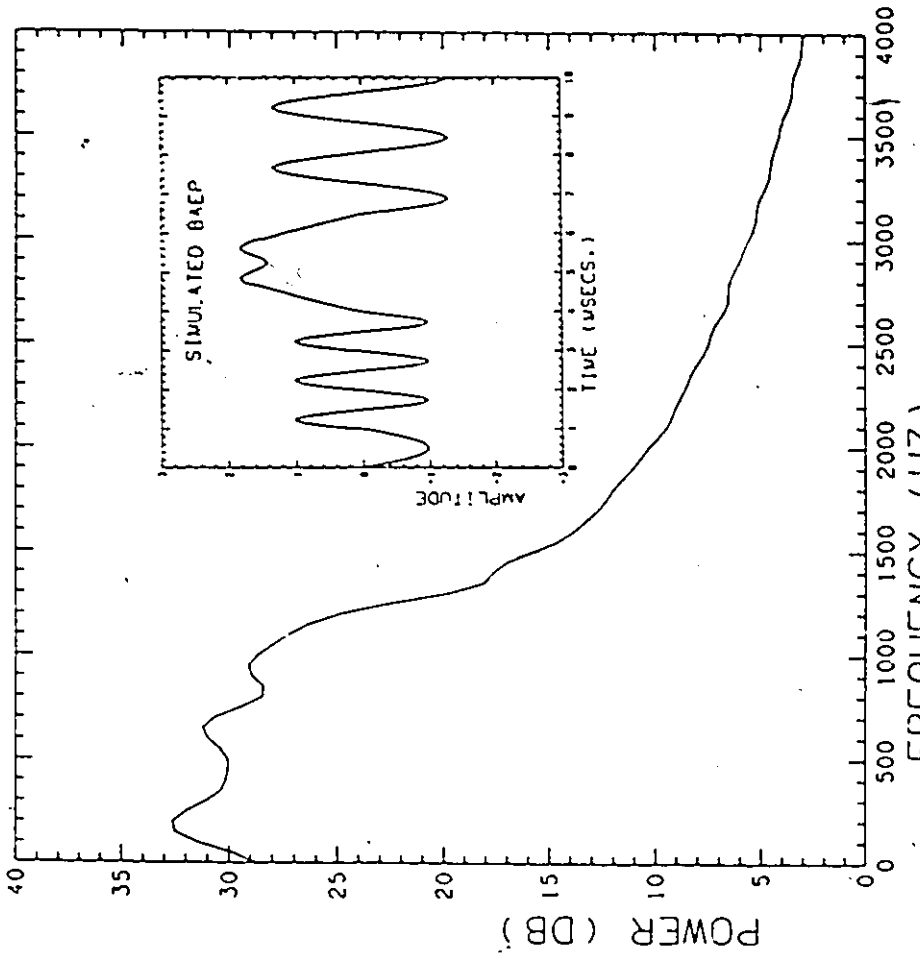

Figure 5.4 Simulated BAEP and its power spectrum.

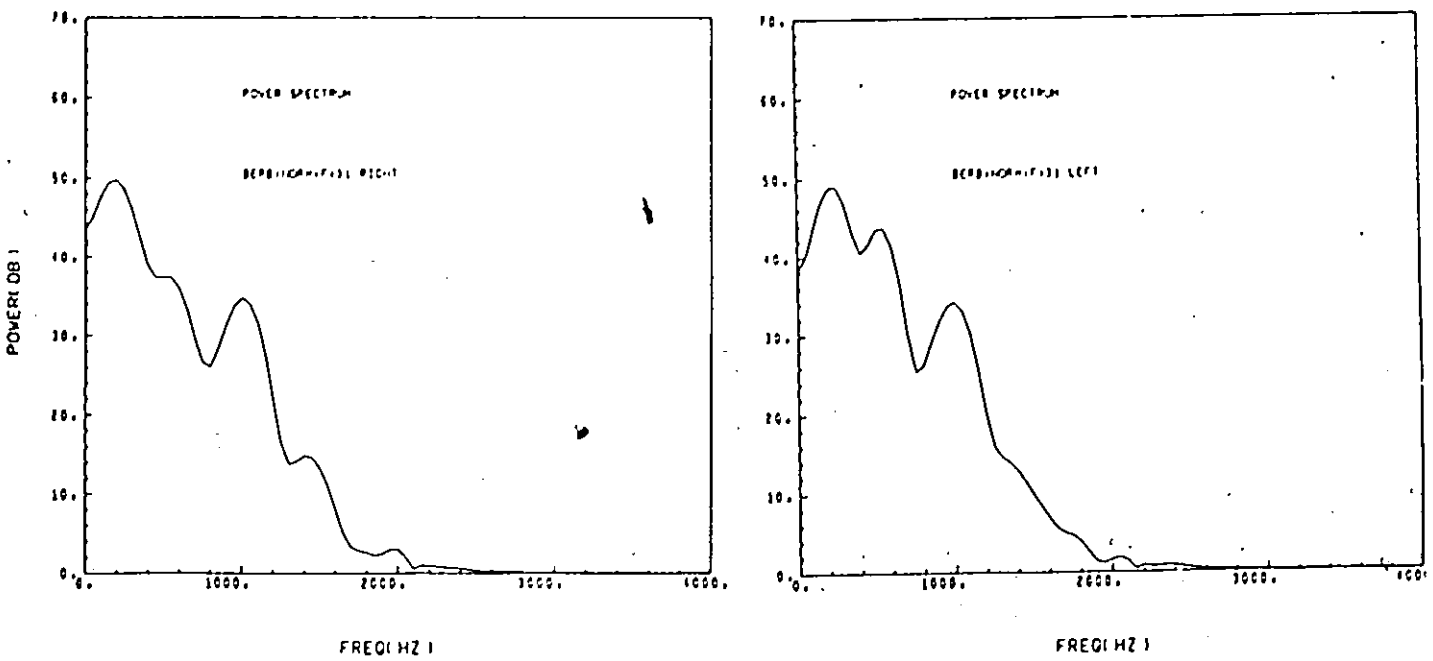

Figure 5.5 BT power spectra of BAEPs of normal subject (BERB) shown in Figure 5.1.

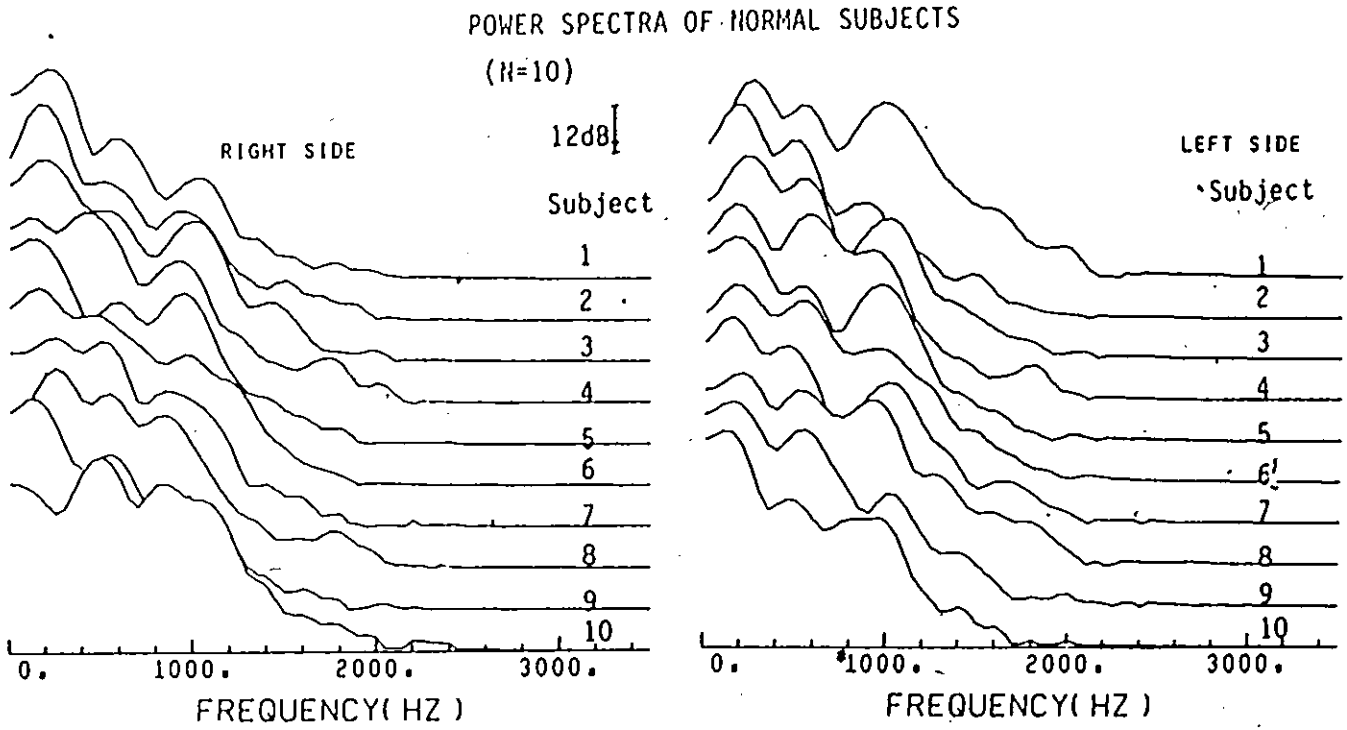

Fig. 5.6 BT power spectra of ten pairs of normal BAEPs.

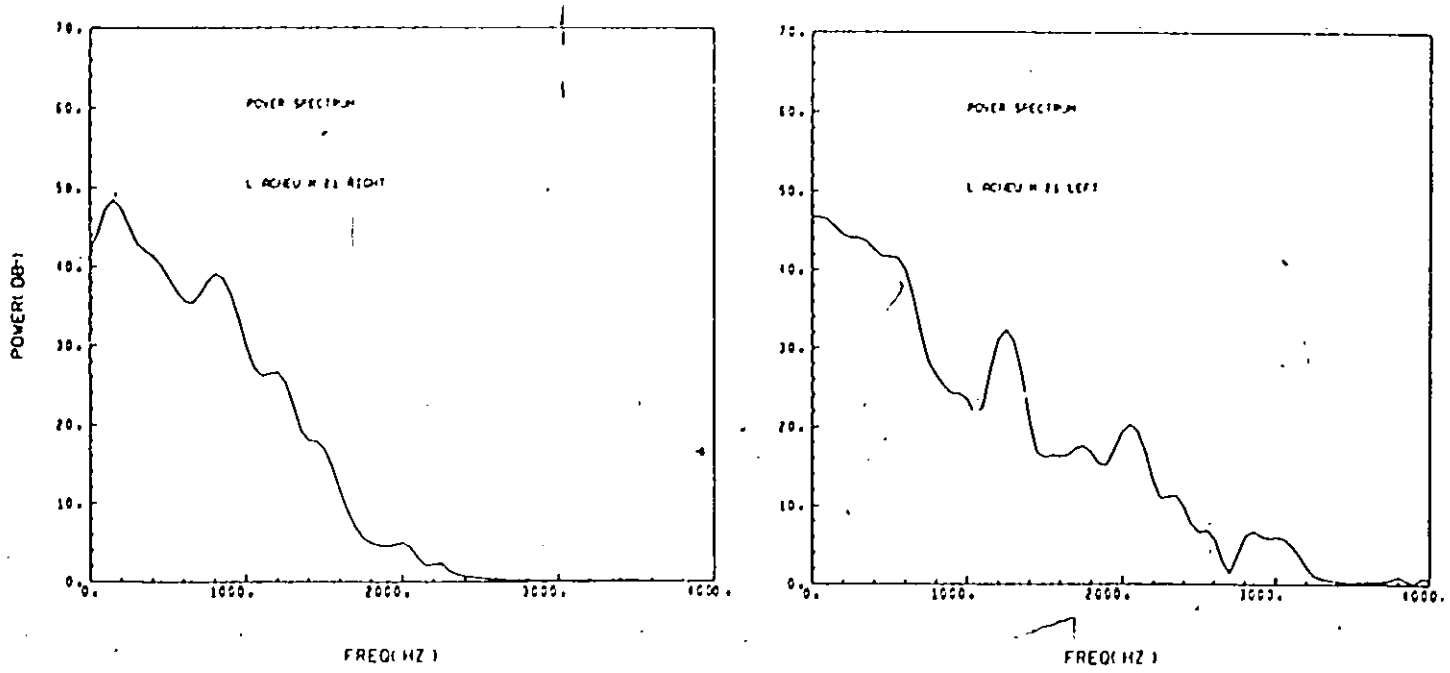

Figure 5.7 BT power spectra of patient L (Figure 5.2) with acoustic neuroma on the left side.

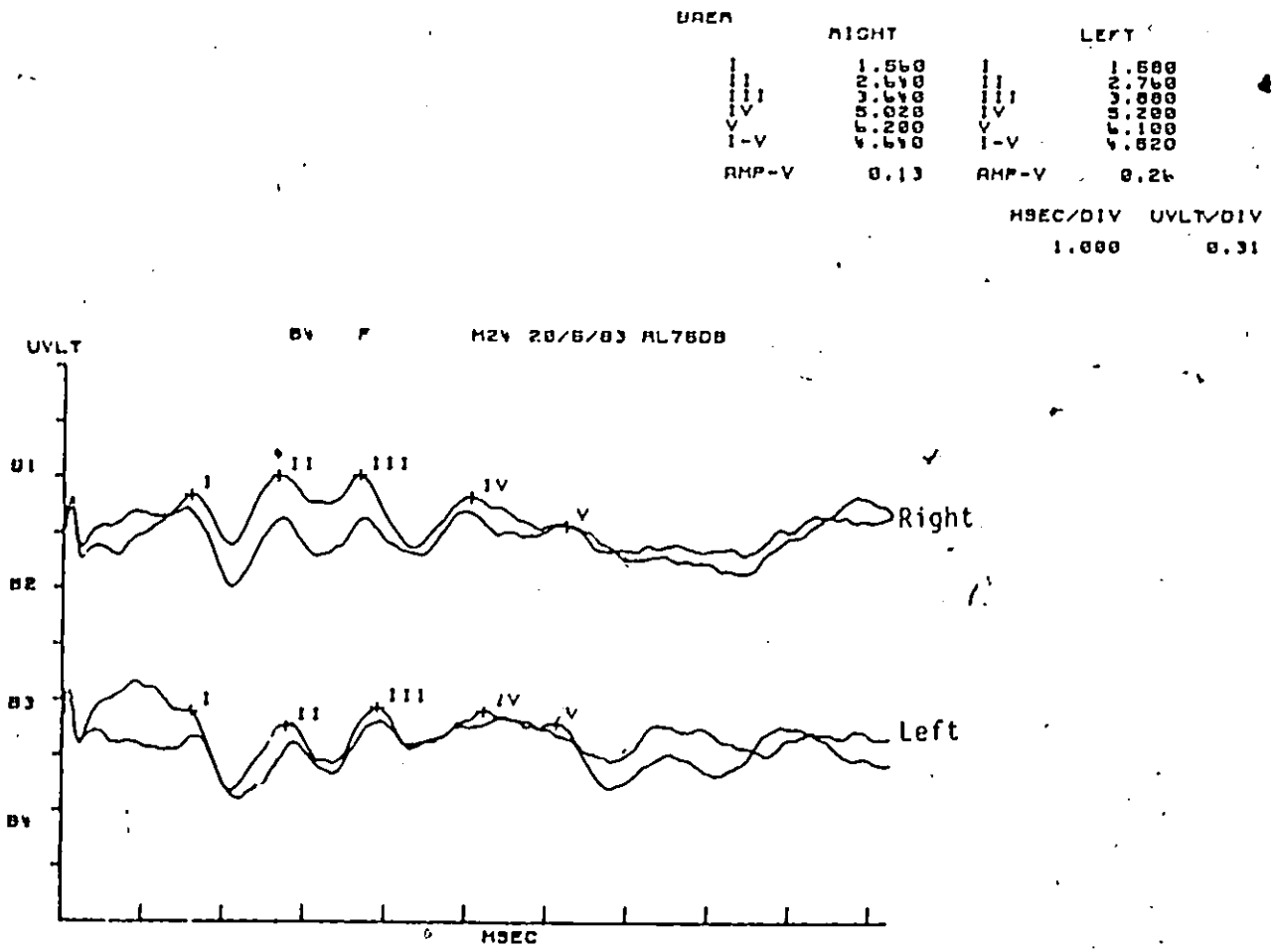

Figure 5.8 BAEPs of a patient (F) with multiple sclerosis.

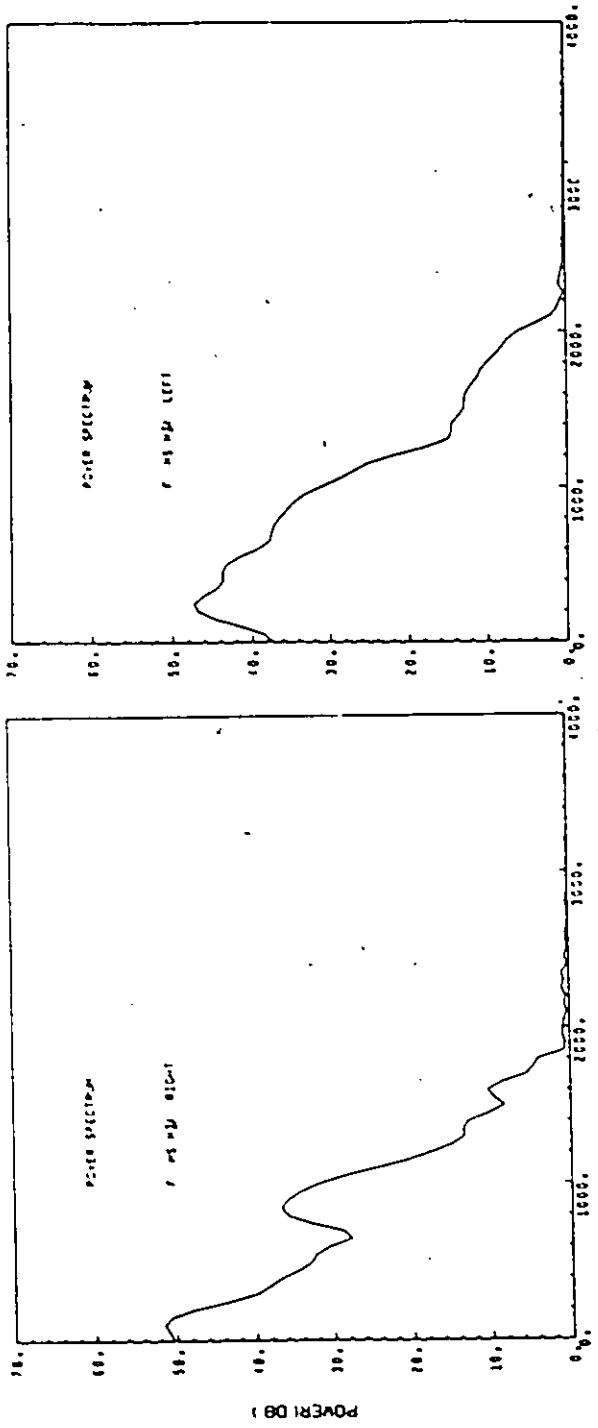

Figure 5.9 BT power spectra of BAEPs of patient F.

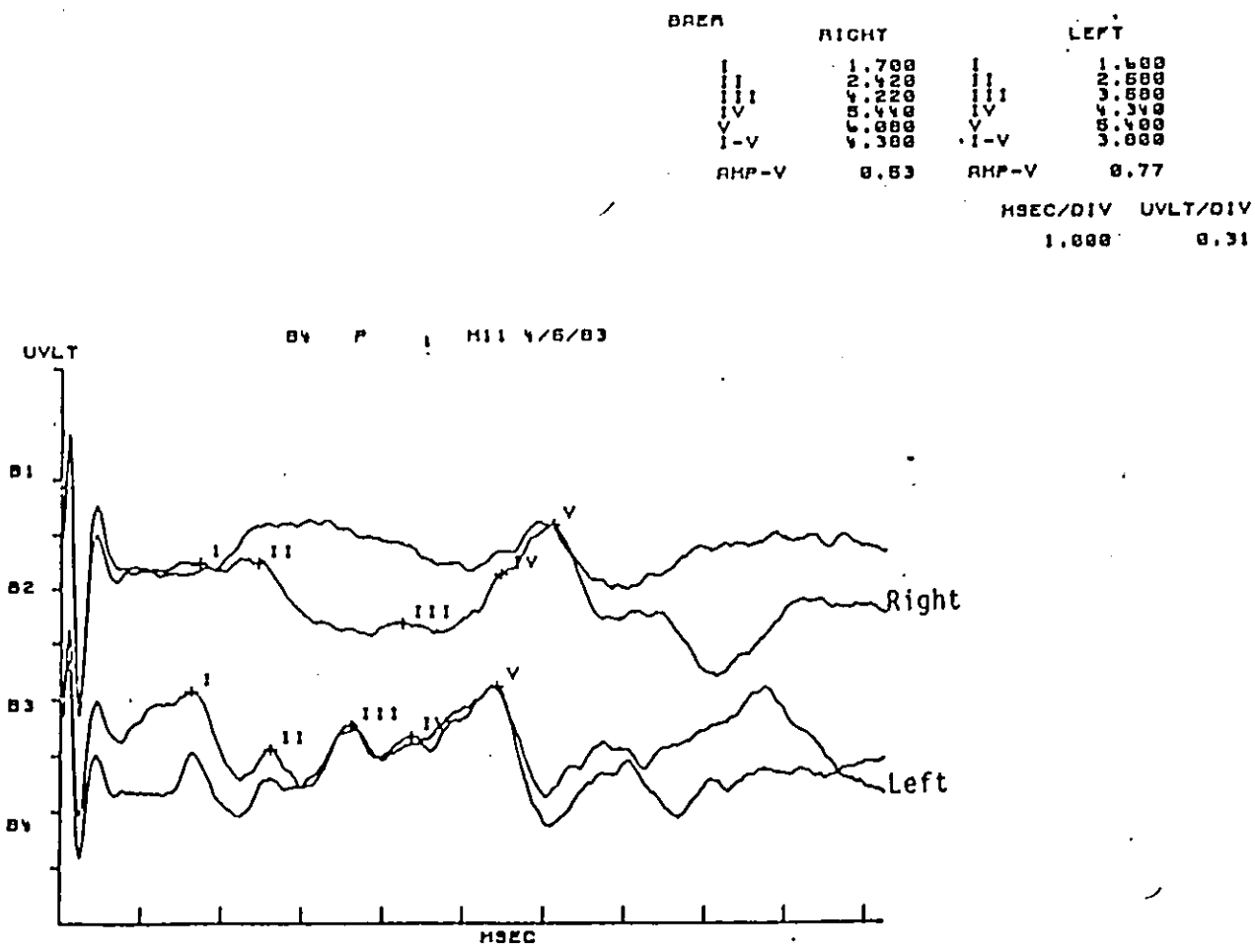

Figure 5.10 BAEPs of a patient (P) with head injury.

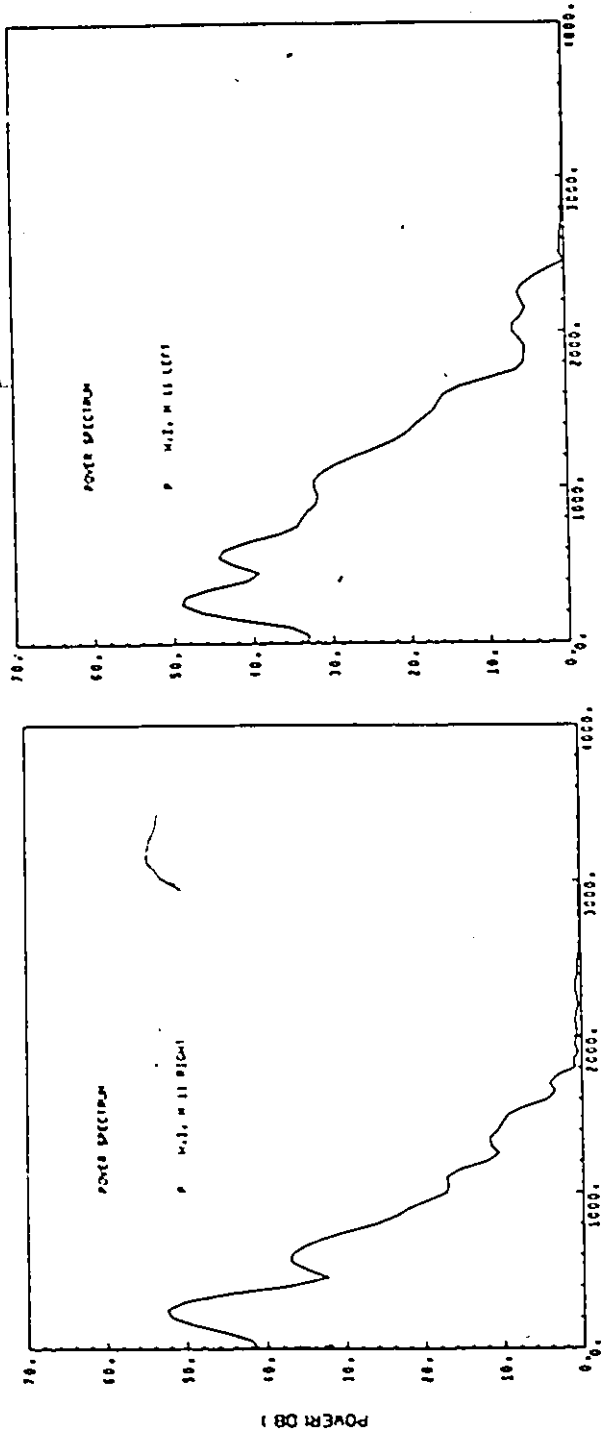

Figure 5.11 BT power spectra of the BAEPs of patient P, with head injury.

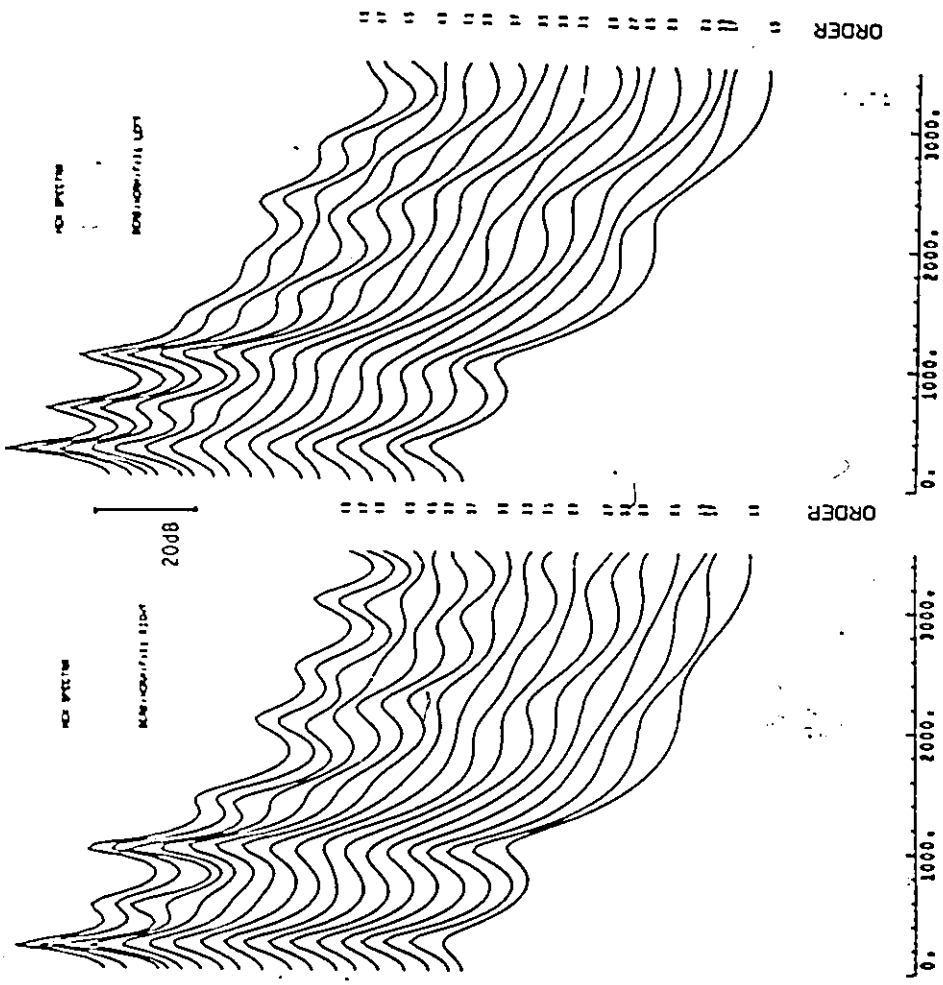

Figure 5.12 Maximum entropy (ME)power spectra of BAEPs of subject BERB.

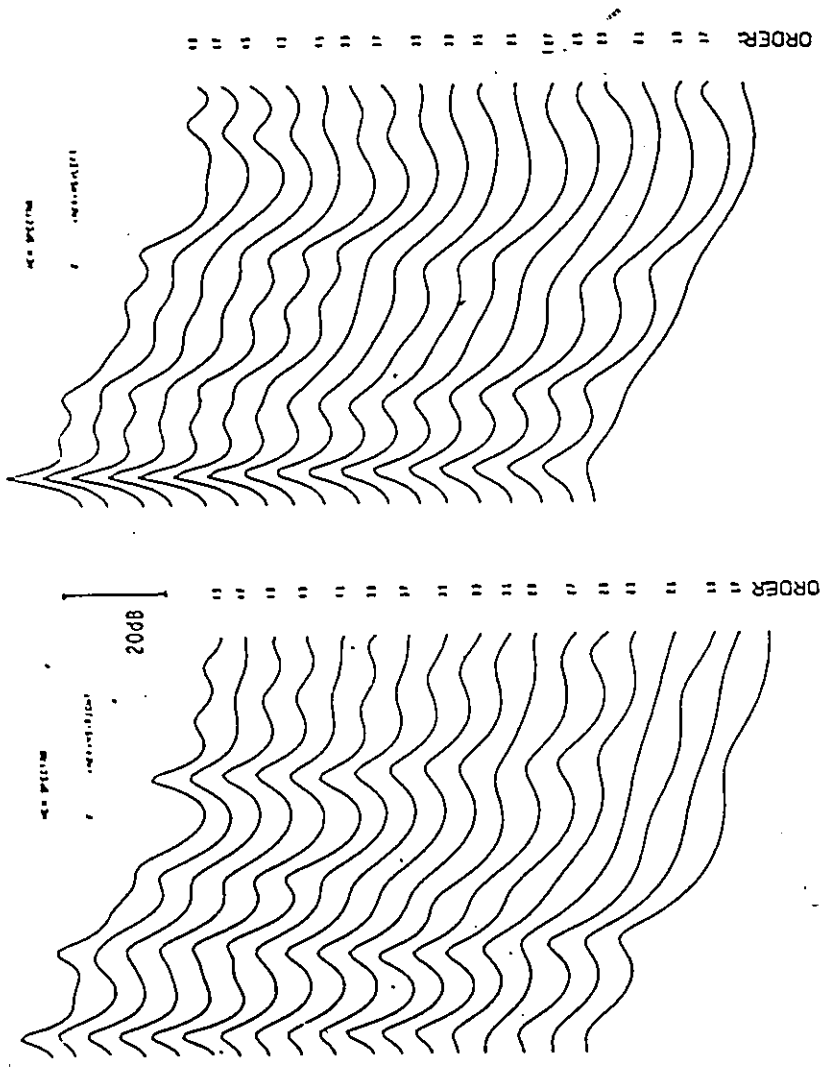

Figure 5.13 ME power spectra of the BAEPs of patient F with multiple sclerosis.

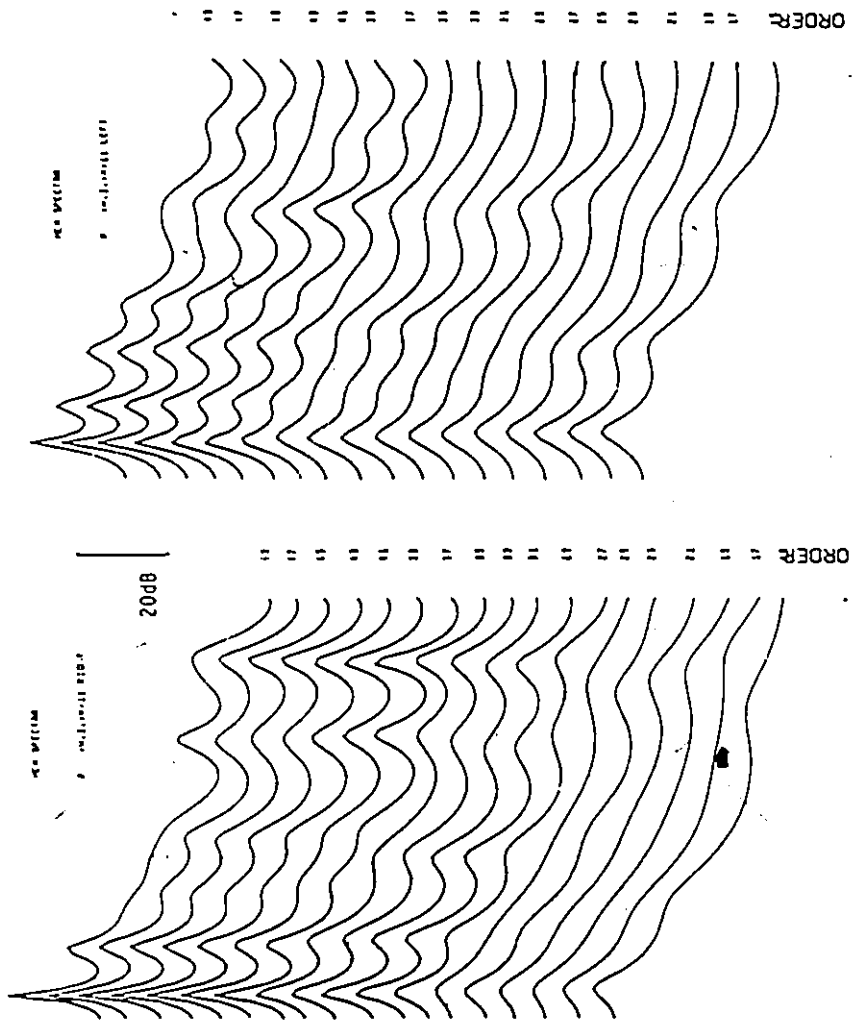

Figure 5.14 ME power spectra of the BAEPs of patient P with head injury.

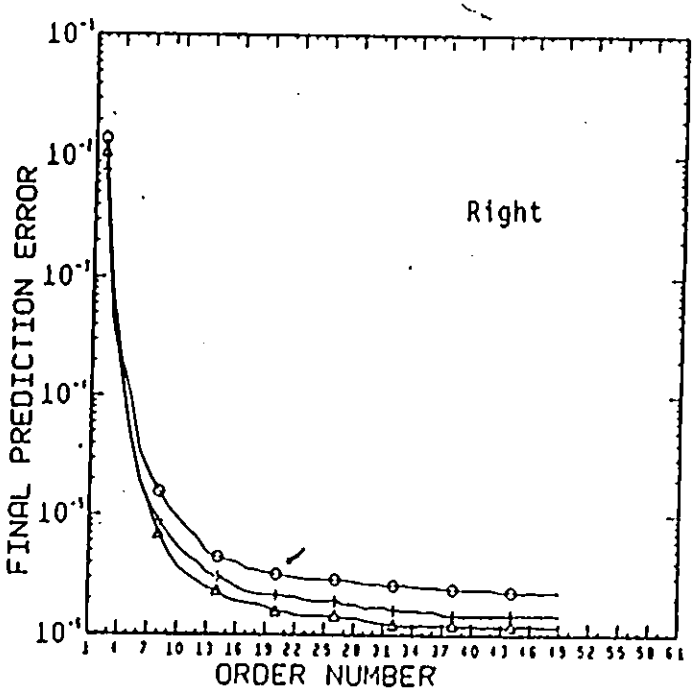

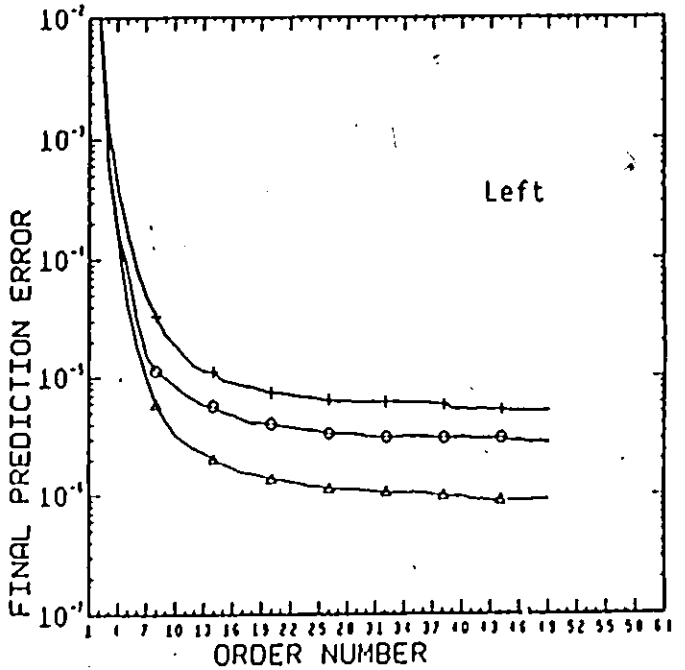

FINAL PRED.ERROR VS ORDER NO.

FINAL PRED.ERROR VS ORDER NO.

Figure 5.15 A plot of the final prediction error vs order number for BAEPs in Figures 5.1, 5.8 and 5.10.

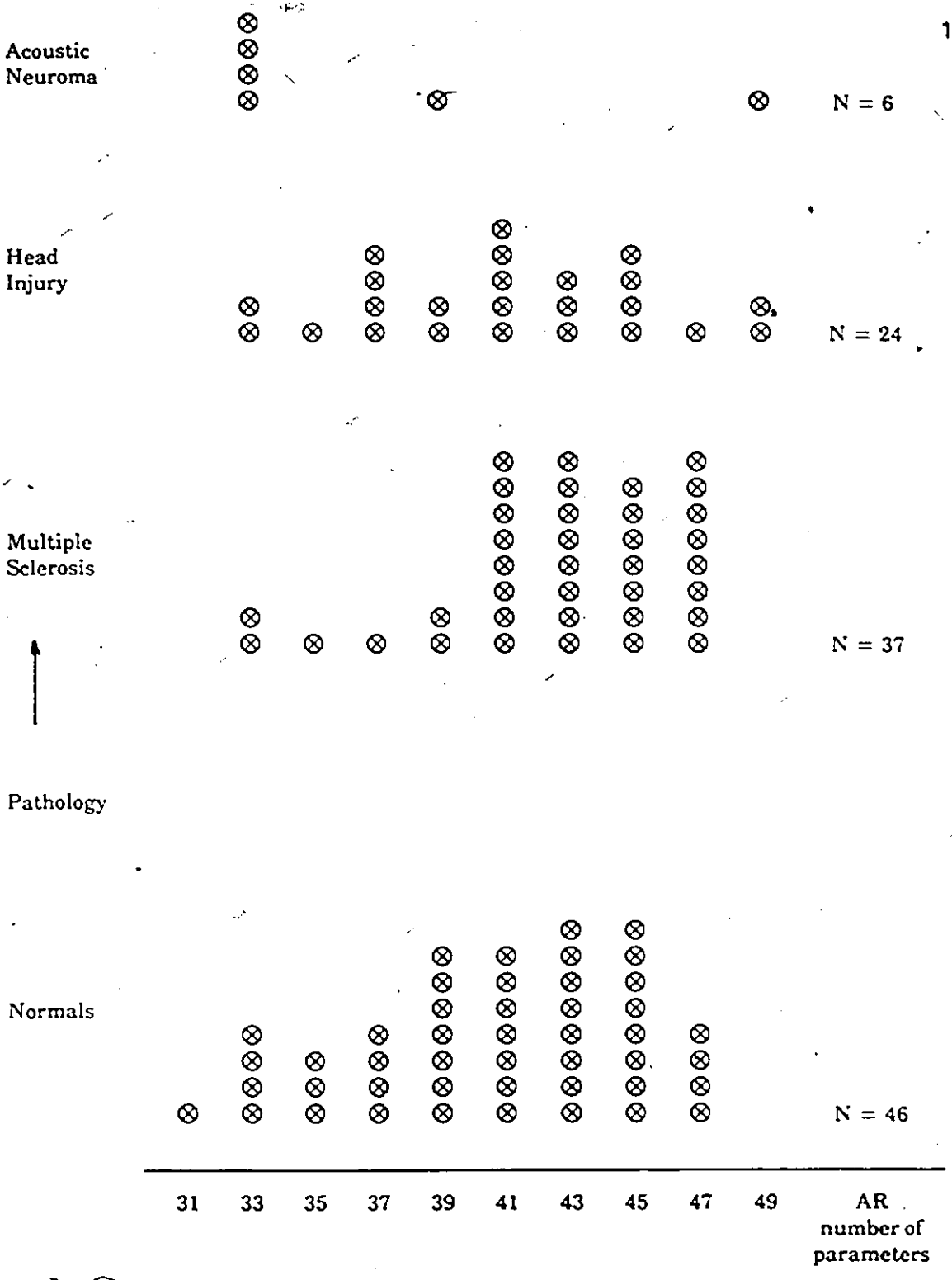

Fig. 5.16 Plot of the distribution of optimum number of parameters required to represent normal and patients' BAEPs.

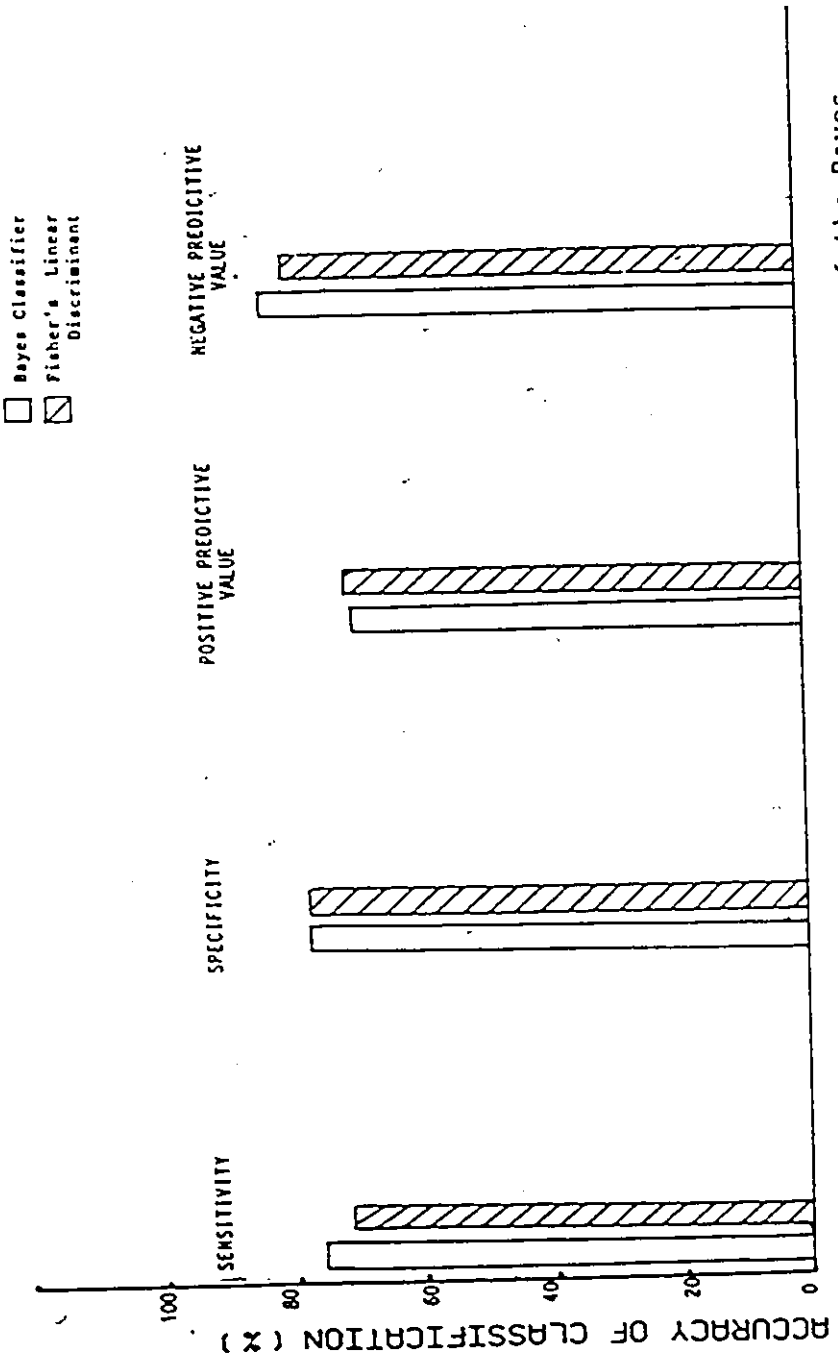

Figure 5.17 Evaluation of the performance of the Bayes classifier and Fisher's Linear Discriminant employing the frequency domain features.

CHAPTER 6

SUGGESTIONS FOR FUTURE WORK AND SUMMARY

In this chapter some recent work on BAEPs will be discussed in light of the pattern classification of the waveforms presented in this dissertation. Some new ideas will also be outlined to further the work on BAEPs. Finally, a summary of the work reported in chapters 1-5 will be presented.

6.1 Some Recent Work on BAEPs and Possible Directions for Future Work:

It is imperative that, to obtain a better knowledge of the central nervous system, non-invasive techniques such as evoked potentials should be used along with other clinical information for improved diagnosis. In recent years, there is a trend towards using multimodality evoked potentials in clinical practice, especially when a patient with severe head injury is being examined [Greenberg and Ducker, 1982]. In such cases, changes in patient's condition need to be objectively assessed. The pattern classification

or evoked potentials offers such a technique to establish if a patient has improved from a pathological class to a normal or near normal class. Further, finer gradations of changes in BAEPs amongst other evoked potentials may be quantified, if features similar to or better than those described in this work are developed.

Applications of BAEPs in certain critical areas of medicine such as in an operating theatre or in an intensive care unit are presently limited due to the time (several minutes) it takes to obtain 2000 averages. Such time required for recording of BAEPs may be reduced by using adaptive filtering techniques currently being developed. According to some recent work, typically 32 stimuli (which would take only 0.2 seconds) are adequate for obtaining a BAEP [Thakor, 1986]. This would permit frequent monitoring of changes (if any) of the status of the patient, if the evoked potential computation can be done reasonably quickly. Madhavan [1985] reports recording single stimulus evoked potentials using adaptive filtering.

The exact origin of each component of the BAEP waveform is yet to be understood. Animal models and human experiments have thus far provided significant evidence and clues to pin-point the origin of different components of BAEPs [Wada et al., 1983]. There is no reported work to

this author's knowledge, about the application of electromagnetic theory to elucidate possible sites of genesis of different components of BAEPs. It is suggested that computer simulation of electromagnetic field models of the brain using field equations and validation by actual recording be attempted in order to address this issue. Some progress in this direction for visual evoked potentials has been reported [Thickbroom, 1985].

The quantification of BAEPs may be done in several ways. The work reported herein has used clinically relevant features (latencies of peaks) and also the total power in different frequency bands. It seems logical to derive mathematical descriptors of the waveforms such as by bezier polynomials, splines or other orthogonal polynomials. Improved recording methods combined with better waveform descriptors would further the applications of BAEPs.

One such method to quantitate the BAEPs has been explored briefly, as a part of the present research [Kamath et al., 1986a]. It is known that the equation (3.7b) or (3.7b), usually called pattern to class distance, can provide a quantification of the given pattern, in terms of the distance of the pattern from either the disease class or the normal class. As an example, consider figures 5.1 and 4.10, the BAEPs of normal subjects. The computed distance

from the normal class of the BAEPs (see Table 6.1) are given to be 5.41, 2.17, 3.23 and 7.21. The latencies of the five initial peaks of the BAEPs were used as features.

However, patients' BAEPs (Figures 6.1-6.2) show the distances of 8.92, 24.30, 11.86 and 55.21. It can be seen that the latencies of the peaks in patients' BAEP waveforms are significantly more than those in the normal BAEPs and consequently the distances of the patients' BAEPs rise with increase in the latencies. The distance $d^2(X, M_A, S_A)$ did not yield a monotonic increase for rise of the latencies, perhaps because of large volume of this distribution. On the other hand, the normal class is quite compact (as evidenced by the smaller value of the determinant of the covariance matrix S_B). It would be interesting to examine the effect of changes in these distances as a result of modification of the BAEPs due to therapy or some other causes.

With the advent of more recent technologies, such as artificial intelligence in medical research, BAEP analysis could be incorporated into an expert system to help the clinician with diagnosis, therapy and during surgical interventions.

In summary, future work on BAEPs would entail providing insights into both the mechanisms and recording of

BAEPs as well as developing better methods of recognizing BAEP patterns and using such information effectively.

6.2 Summary

A summary of the work outlined in the previous chapters is presented in this section along with some of the significant results.

The objectives of this work, as outlined in chapter 1, centered on deriving objective measures of the BAEPs for possible pattern classification on a digital computer. It was also proposed that frequency analysis of the waveform be performed in order to examine the relevance of power spectra in pattern classification. Chapter 2 outlined the recording methods and presented a repertoire of applications of BAEPs.

A review of the techniques of the pattern classification used in the present work is presented in chapter 3 along with the classifier equations. Because of the wide variability in the nature of the data (especially in patients), it was decided that statistical pattern classification techniques be invoked to design the appropriate classifiers. The actual selection of features, design of the classifiers as well as the evaluation of their performance is presented in chapter 4. It was found that time-domain

features gave accuracies of upto 85% using Bayes classification method. The performance of an alternate classifier, namely Fisher's linear discriminant (FLD), was close to that of the Bayes classifier.

In patients where the peaks (and hence the latencies) of BAEPs are either absent or are not easily located, frequency domain features provide an alternate method of identifying pathological waveforms. Chapter 5 explores the power spectral characteristics of the normal and patients' BAEPs. It was noted that the normal BAEP power spectra has three distinct peaks and mean power in the frequency bands containing the peaks offer useful features as observed by the student 't' test. Subsequent design of the classifiers using powers in these frequency bands as peaks resulted in accuracies upto 77% using Bayes classifier and 76% using FLD.

The maximum entropy method (MEM) offered a second method for computing the power spectra using model based techniques. However, the size of the model order (>45) required to describe the BAEP was considered too large. It is likely, that feature reduction techniques [Fukunaga, 1972], may reduce the dimension of the feature vectors describing the BAEPs, and permit classification of of BAEPs using the MEM parameters.

TABLE 6.1

STATISTICAL DISTANCES FROM NORMAL CLASS OF SELECTED BAEPS

FIGURE	PATIENT	SIDE	PATHOLOGY	$d^2(X, M_B, S_B)$
5.1	Berb	R	Normal	5.41
	Berb	L	Normal	2.17
4.10	C	R	Normal	3.23
	C	L	Normal	7.21
6.1	M	R	MS	8.92
	M	L	MS	24.30
6.2	H	R	H.I.	11.86
	H	L	H.I.	55.21

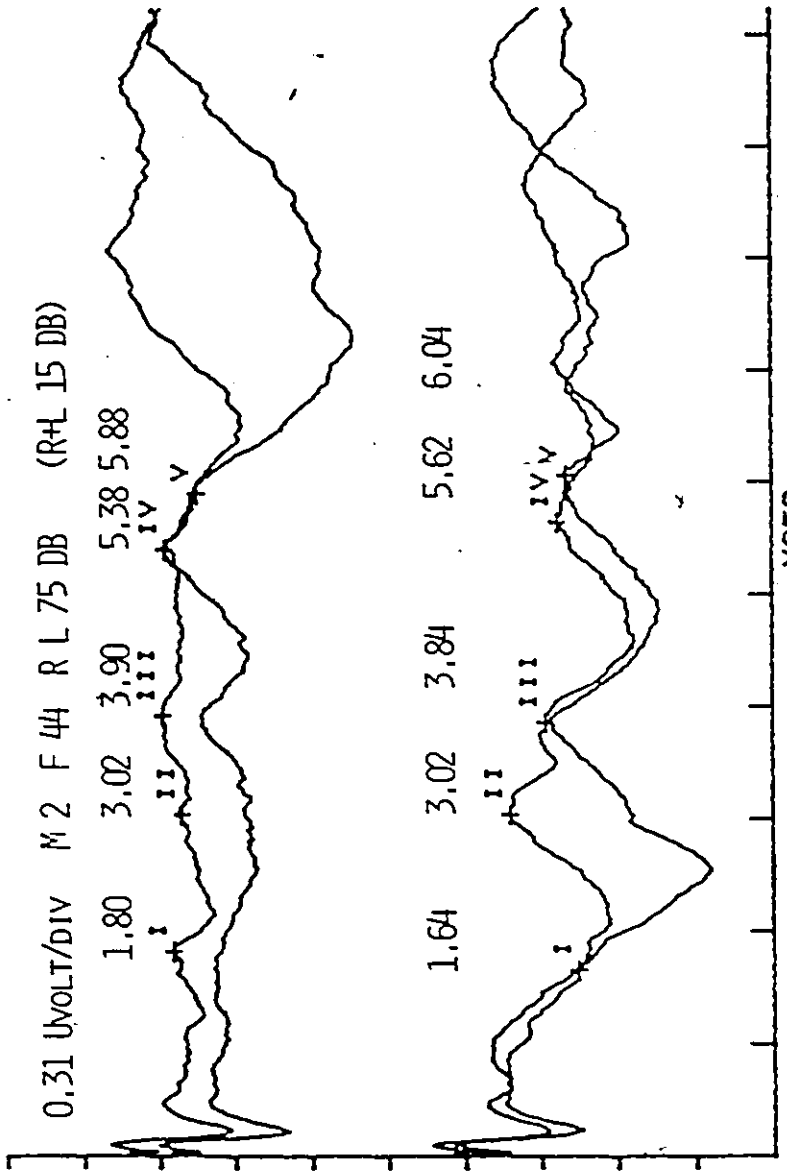

Figure 6.1 BAEPs of a patient with multiple sclerosis.

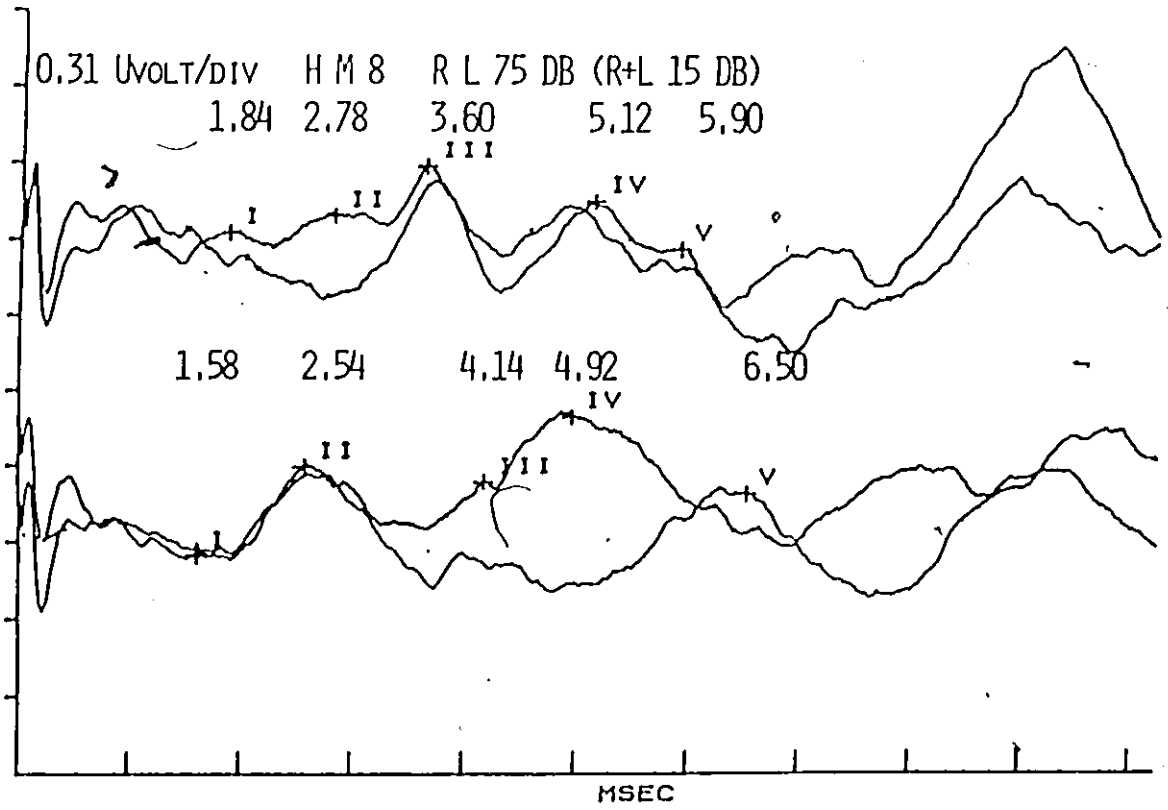

Figure 6.2 BAEPs of a patient with head injury.

CHAPTER 7

SPINAL CORD BLOOD FLOW AND ITS RELEVANCE IN SPINAL CORD INJURY RESEARCH

7.1 Introduction:

Spinal cord injury (SCI) affects a large number of people in North America. In Canada, the incidence of SCI is estimated to be 30-50 per million [Hansebout, 1983]. The magnitude of the loss suffered by these patients is amplified by the fact that a majority of these patients are in the younger age groups, many with a long life span ahead of them. Efforts initiated by Sir Ludwig Guttman and his colleagues during the post-World War II era in treating patients with SCI were pioneering in nature. Research into SCI since then, has prompted significant advances in its treatment. One such therapeutic intervention which has received considerable attention recently, is the cooling of the cord within 4-8 hours following injury, to 15-20 degree Celsius (at the centre of the cord).

In two recent reports, on the evaluation of cooling,

performed for one to four hours at eleven centres on 70 SCI patients (with complete cord injury). it was concluded that 54% of the patients improved neurologically while 14% of the patients became ambulatory [Hansebout et al..1984 and Hansebout. 1986]. The mortality rate of such patients was only 13%. which is one third of the observed mortality in SCI patients treated by other methods. Some of these patients received steroids along with cooling. Although parenteral administration of steroids does help patients with SCI. the exact mechanism of action of steroids is unknown. For cooling of cord to be clinically viable. effects produced by cooling must be studied on physiological variables. such as changes in conduction along the cord. blood flow to cord. among others. In the second part of the thesis. i.e. in chapters 7 - 10. we examine the effects of cooling on spinal cord blood flow in canine experimental model.

This chapter presents the rationale for the study of spinal cord blood flow in animal models during cord cooling and describes the experimental set-up developed by us to measure the effects of cooling on SCBF. A brief review of the literature on the spinal cord blood flow in mammals with particular relevance to cooling is also presented.

7.2 Rationale and Justification:

In severe cord injury, the blood vessels are damaged leading to hemorrhage and edema formation [De La Torre, 1981; Hansebout, 1986]. It has also been observed that there is a sudden onset of weakness or paralysis following SCI, with a degeneration of somatosensory evoked response (SSER), reflecting a loss of axonal function [Hall and Braughler, 1982]. Thus, both mechanical injury to axons and alterations in SCBF are clearly implicated in the pathophysiology of SCI. These two factors, combined with an interruption of neurochemical transmitters in ascending-and descending tracts, result in abnormal conduction of electrical activity in the cord and in afferent and efferent nerve fibres [De La Torre, 1981].

In experimental spinal cord injury on animals, the observations of spinal cord blood flow following SCI are equivocal. Whereas, some investigators recorded global reduction in SCBF both in white and gray matter [Rivlin and Tator, 1978; Senter and Venes, 1978], others have reported increased blood flow in white matter and reduced blood flow in gray matter [Smith et al., 1969; Kobrine et al., 1974; Bingham et al., 1975]. However, it has been shown that reduction in the SCBF is related to the force causing the

injury [Sandler and Tator, 1976a]. It is also hypothesised that localized cord ischemia results in post-traumatic parenchymal cord lesions [Kelly et al., 1970].

Localized cooling of spinal cord following injury in experimental animal models has been demonstrated to improve functional recovery [Albin et al., 1965; Hansebout, 1982]. It was found that cooling applied to cord within 4-8 hours following injury for one to four hours gives the best prognosis. If applied too late or for too long, cooling produces no improvement [Wells and Hansebout,1978]. It is likely that hypothermia may reduce the demand for oxygen and may induce a lower metabolic activity in the tissues. However, there have been no reports to our knowledge, elucidating the preservative and protective mechanisms, due to cord cooling.

It is of interest, therefore, to examine the effect of localized cooling, a therapeutic intervention for preserving the spinal cord viability, on SCBF, a physiological variable which plays a central role in SCI. Previous work in this area is represented by two papers, with one report indicating increased SCBF during local cord cooling, and the other showing decreased cerebral blood flow during whole body hypothermia [Zielonka et al., 1974; Meyer and

Hunter,1957]. In order to resolve these apparently conflicting observations. we decided to investigate the effect of localized cooling on normal animal spinal cord. uncomplicated by injury. The following experiments, presented in the next section, were developed for this purpose.

7.3 Experimental Protocol and the Necessary Instrumentation:

In order to investigate the effect of cooling on the canine cord three important experimental subsystems must be set up:

1) The animal model which is amenable to replication. A canine experimental model was chosen because much of the previous work and experience in our laboratory has been on dogs.

2) Instrumentation to measure the spinal cord blood flow serially in time. so as to compare the blood flows before, during and after cooling. Also. blood flows at multiple (cooled and control) sites must be monitored so as to afford comparison of SCBF in the same dog.

3) A cooling apparatus which provides uniform cooling over a localized cord surface.

The experimental set up used for this work is shown in Figure 7.1. The coolant, usually a mixture of cooled water and isopropyl alcohol at 6 degrees Celsius, was circulated through the saddle at a uniform rate, propelled by a roller pump. A cooling saddle made of silastic had been developed by Romero-Sierra et al. [1974] in collaboration with Dr.Hansebout. This saddle was especially appropriate for the present work as a similar saddle, also made of silastic, but of slightly modified design was being used in the human cord cooling. Finally, of the several methods used for measuring the SCBF, hydrogen polarography was chosen. The next chapter presents an outline of these methods and also describes our design of a microcomputer based instrumentation system developed for measuring the SCBF used in this work.

Initially, a series of pilot experiments on six dogs were run to test the experimental protocol and instrumentation. These trial runs gave us further experience and permitted us to minimize extraneous variables. The investigation of canine spinal cord blood flow which was conducted after these pilot studies, is the subject of this part of the thesis and is presented in the next three chapters.

7.4 Summary:

The blood flow in spinal cord plays a key role and it is believed that SCBF is augmented during injury to the cord. It is not known if the blood flow is altered during cord cooling, a modern therapeutic technique. We decided to investigate the effects of cooling on the normal canine spinal cord. Such an experiment was expected to provide the experimental data of the phenomena as well as an understanding of the physiology of SCBF during cooling, which may help in clinical applications of cord cooling, namely in spinal cord injury.

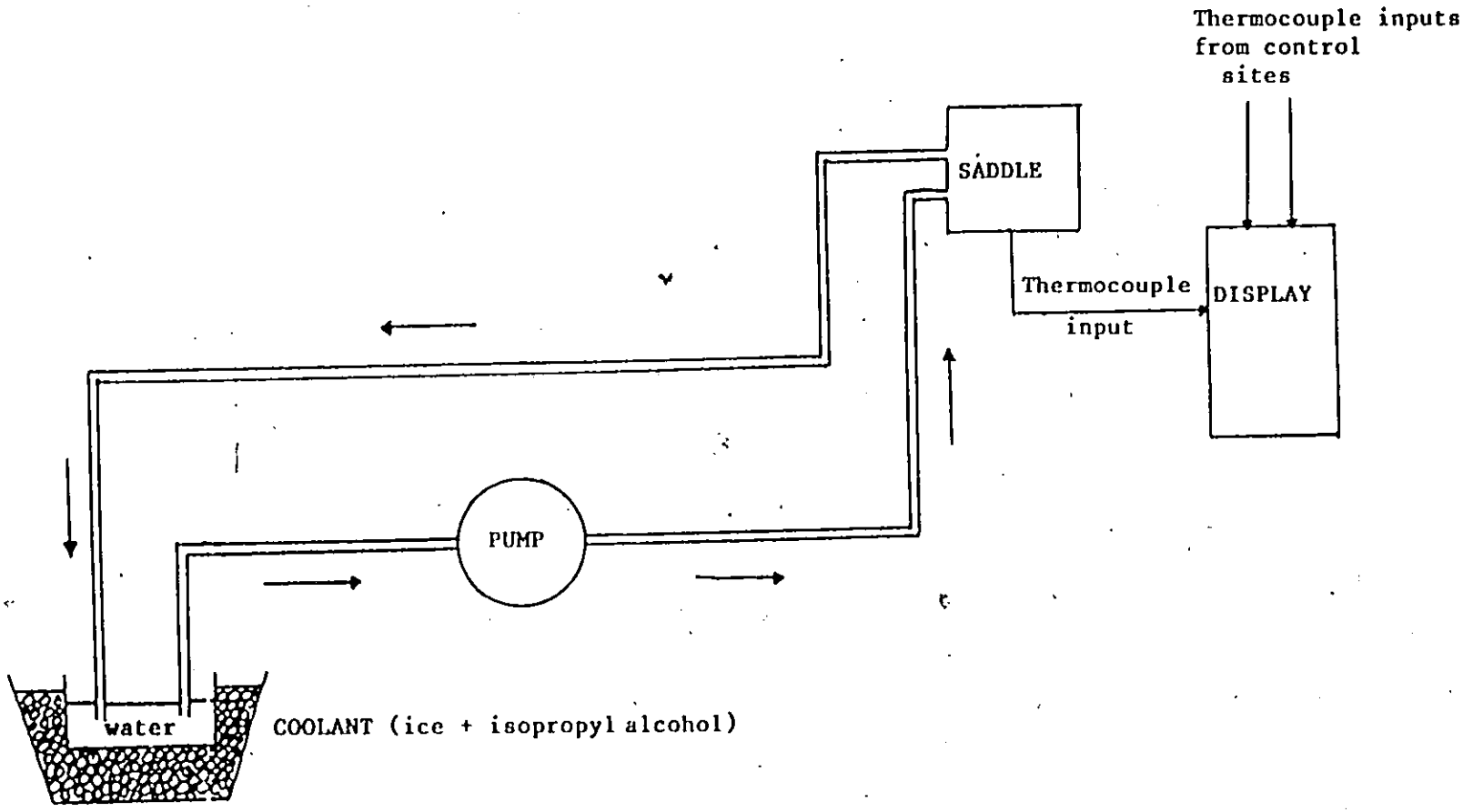

Figure 7.1 Schematic of the cooling set up used for the study.

CHAPTER 8

DEVELOPMENT OF A MICROCOMPUTERIZED INSTRUMENTATION SYSTEM FOR MEASUREMENT OF SPINAL CORD BLOOD FLOW

8.1 Introduction:

In this chapter, we examine the state-of-the-art of spinal cord blood flow monitoring and describe the development of a microcomputerized instrumentation system for monitoring spinal cord blood flow. In the present study, blood flow is measured before, during and after cooling. Such an experiment in animals requires cooling of exposed cord, performing serial measurements of the blood flow at the site of cooling as well as at control sites. Hydrogen polarography is one such technique which allows the measurement of SCBF under these conditions and hence was suitable for our study. The details of the computerized instrumentation developed for SCBF measurement are presented.

In the next section, we review the state-of-the art of spinal cord blood flow measurement. This is followed by a

description of the technique for estimating the blood flow by hydrogen polarography. The results of our developmental effort in measuring the SCBF, the experience gained thereof while measuring SCBF using the system are then presented in this chapter.

8.2 State-of-the-art of Spinal Cord Blood Flow Measurement:

The measurement of spinal cord blood flow has been confined to experimental animals in the laboratory at the present time and all the available techniques are invasive in nature. In spite of advances in the measurement of blood flow to tissues and other organs [Mathie, 1982; Woodcock, 1975], a reasonably safe, relatively inexpensive and quantitative spinal cord blood flow measurement technique applicable to humans in the clinical setting is yet to be developed. Relative inaccessibility of the spinal cord and its related vasculature for blood sampling is the main difficulty that has to be overcome in this area.

In animals, the SCBF is measured by techniques adapted from similar methods that are used to measure blood flow in other tissues or organs. There are four principal methods which are described below, all using the Fick principle [Kety, 1951] :

a) Inert gas clearance: A biologically inert gas such as Hydrogen, (or Argon) is administered to the animal by inhalation and the decay of the gas concentration in the spinal cord tissue is measured using a platinum electrode. Fick's principle is then invoked to estimate the blood flow. The principle states that the amount of inert gas, dQ_i, given off by a homogeneously perfused tissue in time dt is given by:

$$dQ_i = (C_a - C_{vi})\, F\, dt \qquad (8.1)$$

where F = blood flow in ml.

C_a = arterial concentration of hydrogen

C_{vi} = venous concentration of hydrogen

But,

$$dQ_i = W\, dC_i \qquad (8.2)$$

where W = volume of tissue

C_i = concentration of hydrogen in the tissue.

It has been shown that [Kety, 1960], for lipid soluble gases such as hydrogen, the tissue is in instantaneous diffusion equilibrium with venous blood during both saturation and desaturation, i.e.,

$$C_i = YC_{vi} \qquad (8.3)$$

where Y is the tissue/blood partition coefficient for the gas.

Substituting equation (8.2) and (8.3) in (8.1), we get,

$$W\, dC_i = F(C_a - C_i/Y)\, dt \qquad (8.4)$$

During the SCBF measurement using hydrogen polarography, the administration of the gas is stopped when the concentration of the gas in the tissue reaches a plateau, whereby concentration in the arterial blood , C_a = 0. In practice, an interval of one minute beyond the stoppage of the hydrogen gas is usually required for this to happen [Kety, 1951; Kety, 1960]. Then, from equation (8.4),

$$dC_i/C_i = (-F/YW)\, dt \qquad (8.5)$$

Integration of equation (8.5) gives,

$$C_i = C_{io} \exp(-kt) \qquad (8.6)$$

where $C_{t\,o}$ is the concentration of the gas in tissue at t=0 and

$$k = F/YW \qquad (8.7)$$

The variable 'k' has the dimension of ml/min for each gram of tissue and is computed from the slope of the line passing through the logarithms of the observed electrode voltages. Thus, k=(0.693/T-half), where T-half is the time taken for the electrode voltage to fall to half the observed value. A linear regression is performed on the logarithm of decay curve. Usually, blood flow is expressed per 100 grams of tissue. The partition coefficient, Y, has been measured between spinal cord tissue and blood and is approximately equal to unity [Aukland, 1964].

The hydrogen clearance technique offers repeatability and hence permits serial measurement of SCBF at the same site. The disadvantage of the technique is that some tissue injury results due to insertion of a platinum electrode into the cord. The hydrogen clearance technique has been widely used in dogs [Kling et al., 1986], rhesus monkeys [Kobrine et al.,1974], and in baboons [Griffiths et al., 1975] to measure SCBF for a variety of experimental paradigms.

b) Radioactive tracer clearance technique:

An injection of ^{133}Xenon (2 micro litres for goat cord) is given into the spinal cord, 4-6 mm below the cord surface. The clearance of the ^{133}Xenon is measured with a crystal scintillation probe placed superficial to the cord. The SCBF is then estimated from the clearance curve as described in section (a), for inert gas clearance technique. That the anatomical area in the cord at the site of injection is not certain, is the main limitation of this method. Smith et al. [1969], have used the ^{133}Xenon clearance method for measuring SCBF in goats while Ducker and Perot [1971], have applied this technique to measure the SCBF in dogs.

c) & d) Indicator fractionation techniques:

A slightly modified form of Fick principle is used to estimate the SCBF, using ^{14}C-antipyrine as the diffusible tracer. The rate of change of the concentration with time, of the tracer within the tissue, is equal to the difference between the rate at which the substance is brought to the tissue in the arterial blood and removed from it in the venous blood. This can be expressed mathematically as [Kety, 1951; Kety, 1960]:

$$C_i(T) = Y\, k_i \int_0^T C_a \exp[-k_i (T-t)]\,dt \qquad (8.8)$$

where:

$C_i(T)$ = concentration of the tracer in the tissue at time T

Y= tissue blood partition coefficient for the tracer

k_i = (blood flow/ minute/ unit weight of the tissue)/Y

C_a = concentration of the tracer in the arterial blood

The tissue partition coefficient of the tracer, the concentration of the tracer at time T (which is 1 minute after the start of the tracer infusion), and the time course of the change of the arterial tracer concentration should be known. The partition coefficient is measured in a pilot series of experiments [Reivich et al., 1969].

The compound is mixed with saline and infused intravenously into the animal for a limited interval of time (approx. 1 min.), after which cardiac arrest is induced in the animal. Arterial blood is sampled at frequent intervals during the infusion of the indicator and the exact amount of compound in the blood is measured. The cord is removed from the dead animal, sectioned and placed in contact with x-ray

film to obtain the autoradiographs. These autoradiographs are then compared with reference autoradiographs using a scanning densitometer to obtain the concentration $C_i(T)$, of the ^{14}C-antipyrine in the tissue. The tracer concentration C_a, in the arterial blood in conjunction with $C_i(T)$ are used to estimate the SCBF [Sandler and Tator. 1976a], through equation (8.8).

An alternate and more recent approach for determining SCBF by indicator fractionation method involves, the tagging of microspheres with radioactive compounds [Hales, 1974, Heyman et al., 1977]. The microspheres used for SCBF measurement are made of inert plastic and range in size from 15-20 microns in diameter. They are labelled with different gamma or beta emitter nuclides (such as strontium-85, neobium-95, or tin-113) which are injected into the left ventricle of the heart. The microspheres enter the circulation and are entrapped by the arteriolar or capillary vascular system of the spinal cord. Blood samples are drawn from femoral and/or brachial artery by an intra-arterial line at frequent intervals. The animal is sacrificed at the end of the study. The radioactivity of the arterial blood samples and the spinal cord samples are measured in a gamma (or beta) counter. Then, one may compute F, the spinal cord blood flow as:

$$F = \frac{\text{counts/100 gms. of spinal cord tissue}}{\text{counts/ml./minute in arterial blood}} \quad (8.9)$$

where F is the tissue blood flow in ml./100 gms.tissue/min.

Serial SCBF measurements can be performed in the same animal by tagging microspheres with isotopes that produce different spectral peaks and injecting the microspheres sequentially in time (whenever a measurement of SCBF is required).

Whereas, ^{14}C-antipyrine technique yields excellent discrimination for measuring blood flows of gray and white matter separately, it is not possible to measure SCBF sequentially in the same animal using this method. The microsphere technique or the hydrogen polarographic method is hence suggested where serial measurements are required. We used the latter method for our work because of the technical ease with which the measurement can be done.

8.3 Rationale and Design Objectives:

A Hydrogen Polarograph used for measuring the

concentration of the hydrogen in the spinal cord following an administration of the gas was purchased from Willis Medical Electronics. Washington D.C. The instrument indicates the concentration of hydrogen in millivolt units on an LED display. The blood flow in the tissue can be calculated from the rate of hydrogen clearance. The experimenter initially recorded these readings manually. Computation of the SCBF was carried out after the experiment. We found this method inconvenient and error prone during early recording of hydrogen concentration from multiple electrode locations. In addition, the probability of losing observations was high. Also, the computation of SCBF using the hydrogen polarography requires the fitting of a linear regression model to the logarithm of the hydrogen concentration. For efficient recording of the data and obtaining quick estimates of SCBF, an on-line data acquisition system was deemed essential. With these objectives, we developed a computerized SCBF measurement system which is described in this chapter.

8.4 Instrumentation and Hardware Configuration:

The concentration of hydrogen in spinal cord tissue depends on the amount of hydrogen administered, tissue/blood partition coefficient, the SCBF and time following

administration of hydrogen [Aukland et al.. 1964: Sandler and Tator. 1976a and 1976b]. A block diagram of the the computerized system for the measurement of SCBF is shown in figure 8.1 [Hansebout et al., 1987].

The polarograph measures the potential (in millivolt units) created by the hydrogen concentration using a platinum electrode and displays the reading on an LED seven segment display. The output of the polarograph produced a voltage in the range of 0-1 volt. A set of four d.c amplifiers were built with operational amplifiers to provide a gain of 5 for each channel. The ouptut voltages from the four channels were brought onto a suitable connector, for obtaining the desaturation curve on a physiograph. For our experiment, these output lines were sampled through an analog-to-digital converter. The output voltage on these lines thus ranged from 0 to 5 volts.

An APPLE-IIe computer with 64 Kbytes RAM was used for recording the data and performing the computations. An A/D converter (AI-02) manufactured by Interactive Structures (112 Bala Ave., Bala Cynwyd. Pa) was interfaced to the computer. The AI-02 has a resolution of 8 bits and can record up to 16 channels. The sampling aperture is 70 microseconds per channel. The eight bit resolution of the

A/D converter was found adequate for the purpose of obtaining the hydrogen concentration readings and would resolve SCBF measurements to within 0.4%. There were four electrodes which monitored the hydrogen concentration at four different locations in the spinal cord. Thus, only four of the sixteen channels of AI-02 were used. The polarizing voltage of the electrodes was set to 650 mV.

The animal was anesthetized and prepared for the study (described in the next chapter). Hydrogen gas was administered to the animal via an endotracheal tube connected to an anesthetic machine closed circuited with hydrogen, oxygen mixture. The electrode voltage rose and reached a plateau in roughly 10-15 minutes, indicating that a saturation of the tissue with hydrogen had been reached. Then the animal was removed from the anesthesia machine to breathe from atmosphere. The decaying electrode voltages were sampled and stored on a diskette.

8.5 Software Design:

A BASIC program was developed to digitize and store the output voltages of the hydrogen polarograph and compute the linear regression coefficients on-line. Initial experiments indicated that the higher SCBFs would need a

total sampling duration of 5-6 minutes and the slowest decay of hydrogen would last for a maximum of 20 minutes. The polarograph readings were sampled every 15 seconds to provide at least 20-24 points for computing the blood flow from the fastest decaying hydrogen concentrations. The computation of the linear regression and correlation coefficients took less than 15 seconds in BASIC, per channel, for a data of 20 minutes. This was an acceptable turn-around time for the experiment. The data were plotted off-line on a mainframe computer.

A provision was made to enter the experimental parameters such as animal identification, its body temperature and temperatures at the saddle and control sites, into the data file at the beginning of each recording of SCBF. The delay of 15 seconds between two samples of the hydrogen concentration was generated by a FOR..,NEXT loop. The duration of the loop was tuned to provide 15 seconds with an accuracy of 0.5% in 20 minutes. Figure 8.2 shows the flow chart of the software.

For an observed set of values of decaying hydrogen polarograph readings, natural logarithm was computed. A linear least squares line was fitted for these values, using the equation:

$$Y = MX + C \qquad (8.10)$$

where, Y = natural logarithm of the observed values from the hydrogen polarograph;

X = time in minutes;

M = slope of the line;

and C = intercept the line with the Y axis.

The slope, M, is estimated from the equation,

$$M = \frac{\sum_{i=1}^{n} (X_i - X_m)(Y_i - Y_m)}{\sum_{i=1}^{n} (X_i - X_m)^2} \qquad (8.11)$$

where Y_m and X_m are the mean values of the variables Y and X respectively. The X_i represent the observations 1,2,3..i...n . The intercept, C, is estimated from the equation,

$$C = Y_m - MX_m \qquad (8.12)$$

The correlation factor was estimated from the equation:

$$R = \frac{\sum_{i=1}^{n} (X_i - X_m)(Y_i - Y_m)}{\left[\sum_{i=1}^{n} (X_i - X_m)^2 \sum_{i=1}^{n} (Y_i - Y_m)^2\right]^{1/2}} \quad (8.13)$$

8.6 Electrode Fabrication:

The electrodes were made from Teflon coated platinum-iridium wire 150 microns in diameter (Medwire Corp., Vernon, NY). Two millimeter of exposed wire were etched to a 10 micron tip by passing 75-100 milliampere alternating current in a solution of 50% KCN and 30% KOH [Geddes, 1972].

8.7 Cooling Saddle:

A heat exchanger fabricated and tested earlier was used for the present study [Romero-Sierra et al., 1974]. It is made of silastic with multiple channels in the unit to permit circulation of the coolant, usually ice-water. The heat exchanger was shaped to conform to the posterior aspect of dura and was called a saddle.

8.8 Results:

The electrodes fabricated as well as the instrumentation developed for this study worked well and gave repeatable blood flow values. Typical hydrogen washout curves at a saddle site during normothermic (trace 1), cooled (trace 2) and rewarmed conditions (trace 3), are shown in Figure 8.3. The computed values of the SCBF are shown in the inset as the slope of the logarithm of the decaying curve, with units of ml./min./gm. of tissue. The SCBF during the above conditions are 10.1, 3.9 and 11.3 ml./min./100 gm. of tissue. The correlation coefficient for each washout curve was greater than 0.985.

Our measured values of SCBF agree with previously published values [De La Torre, 1981; Sandler and Tator, 1976a and 1976b].

8.9 Discussion:

The usefulness of hydrogen polarography in measuring the local blood flow in myocardium, renal cortex, skeletal muscle and spinal cord has been well established [Mathie, 1982: Woodcock, 1975; Aukland, 1964]. In the present work a portable computer has been used to perform

the data acquisition on-line and compute the values of blood flow soon after. There has been no reported use of an on-line computer system for the measurement of SCBF, to our knowledge. This significantly improved our experimental technique.

An inexpensive, stand-alone computer was needed for the application described herein and we chose the Apple IIe as the optimum host hardware. A compatible analog-to-digital converter was interfaced between the hydorgen polarograph and the computer. The driver software was written in BASIC. Our initial studies indicated that an 8-bit resolution was adequate and it provided sufficient accuracy in the SCBF measurement that permitted a comparison of the SCBF during normothermic and cooled states. The possible physiological mechanisms and its implications in clinical environment are discussed in the succeeding chapters.

The linear least-square estimates of the parameters involved in determining the SCBF were computed on-line and provided us with almost immediate estimates of SCBF. Thus, the quality of the data could be assessed by the correlation factor. A correlation factor less than 0.98 prompted us to repeat the SCBF measurement trial. Perhaps, the most

important factor for motivating the design of the system described in this chapter was its capability to monitor multiple channels simultaneously, an aspect which when done manually is fraught with observational errors and human fatigue.

8.10 Summary:

Several methods of measuring SCBF in animal experimental model were reviewed. Hydrogen polarographic method of measuring the blood flow was chosen, based on its unique capability to provide serial measurements of the flow at a site on the spinal cord. A microcomputerized measurement system for monitoring multichannel spinal cord blood flow using hydrogen polarography was described in this chapter. The instrumentation developed herein, improved the repeatability of the technique as the operator dependent observational errors were minimized. The instrument thus provided a strong vehicle for experimental studies, which are described in the next chapter.

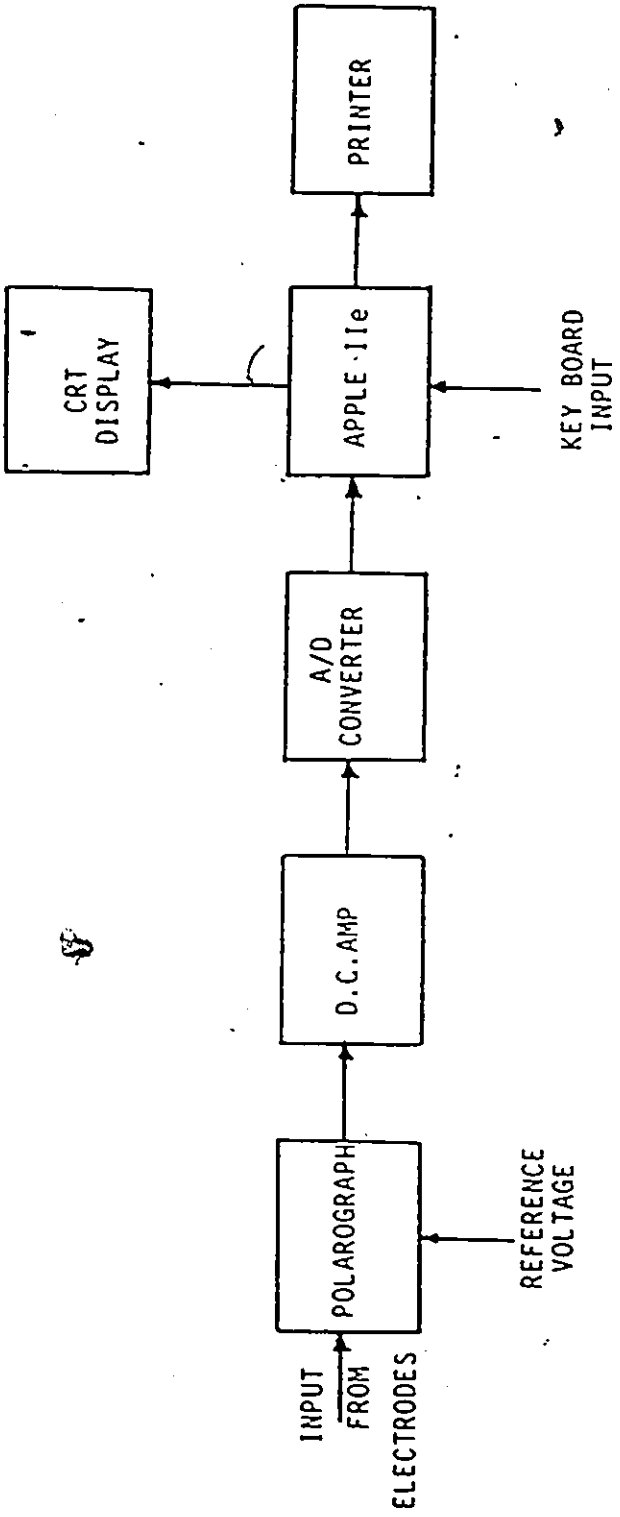

Figure 8.1 Computerized system for the measurement of spinal cord blood flow using hydrogen polarography.

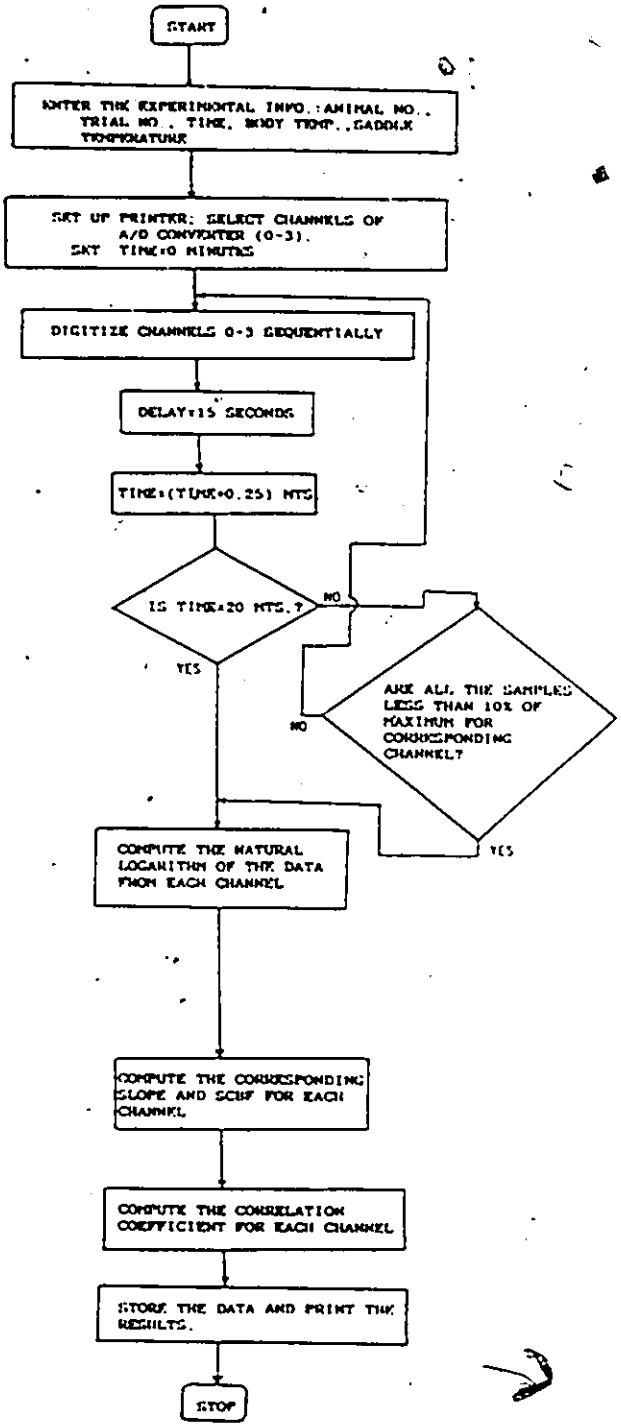

Figure 8.2 Flow chart of the software used for data acquisition and computation of the spinal cord blood flow.

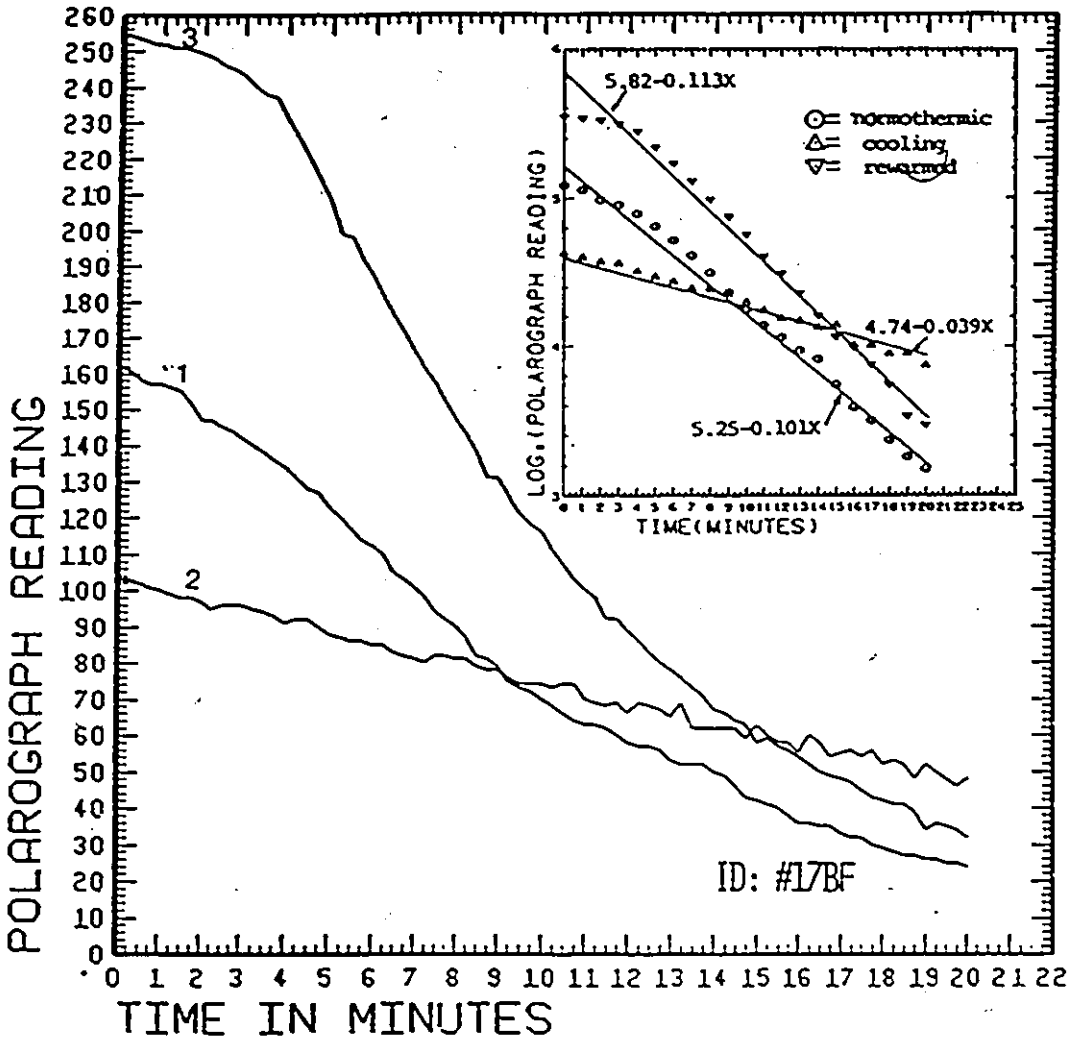

Figure 8.3 Hydrogen washout curves for a typical SCBF measurement and fitting of the linear regression.

CHAPTER 9

THE EFFECTS OF COOLING ON CANINE SPINAL CORD BLOOD FLOW

9.1 Introduction:

A study of the effect of localized cooling on canine spinal cord blood flow is desribed in this chapter. The details of animal preparation, experimental design and an evaluation of functional characteristics of the electrode are presented. Our studies reveal that blood flow in normal canine cord reduces by as much as 50%, as a result of localized cooling, at the site of cooling. It was also noted that the blood flow does not change at control sites, which remained at normothermic temperatures.

9.2 Materials and Methods:

To study the effect of cooling on spinal cord blood flow, the experiments were carried out on five mongrel dogs of either sex weighing 18-24 Kg. The dogs were anesthetized with pentobarbital (30 mg/kg) and maintained with pentobarbital. After an intravenous line was established

with normal saline. each dog was intubated. A central arterial line was inserted into the left femoral artery for monitoring of arterial blood pressure and sampling of blood for gases and pH determinations.

9.2.1 Animal Preparation:

Burr-hole laminectomies were performéd at T12, T13 and L-1 vertebral levels. The left pedicle of T-13 was exposed and partially removed to expose the lateral aspect of the dura for placement of hydrogen polarograph electrodes. The spinous processes at T-11 and L-2 were clamped in a frame to allow the suspension of the entire animal. This procedure reduced artifacts due to breathing movement [Senter et al., 1978]. A 5 mm. durotomy was performed to expose the lateral aspect of the spinal cord followed by a small pial puncture using a 26 gauge needle. Two teflon coated platinum electrodes with 2 mm exposed tip were guided into the puncture using a micromanipulator into an area judged to be gray matter.

A small cooling saddle of area 2 cms.sq. was positioned on the exposed portion of the cord and radially above the electrodes. These sites were termed as saddle sites. Two more platinum electrodes (controls) were attached

proximally and distally in the midline dorsal aspect of the cord at T-12 and L-1 following a pial puncture. Water at 6 degree Celsius was circulated through the saddle and the temperature in the cord at the saddle site (and beside the platinum electrodes) was measured by a thermocouple (dia 0.01 inch T-type. Copper/Constantan. High Temperature Instruments Corp. W.Conshohocken, Pa). The cooling saddle was sufficiently far away from the control electrodes and hence, the cooling of the cord did not produce any significant change in the temperature at these control sites as measured by two other thermocouples inserted at these sites. Figure 9.1 shows the arrangement of the cooling saddle, saddle and control electrodes and thermocouples etc. The wounds were filled with mineral oil to prevent tissue dessication and diffusion of hydrogen. These procedures took between 4 to 5 hours. The body temperature was monitored by a rectal probe.

9.2.2 Cord Cooling:

Local cord cooling was achieved by using a silastic saddle designed previously. [Romero-Sierra et al., 1974]. The saddle had been tested in several other canine cord cooling experiments. Cooled water at 6 degrees Celsius was circulated through the saddle. The electrode tips were

prepared as described earlier. The four platinum electrodes were connected to a hydrogen polarograph the details of which were given in the previous chapter. The reference voltage was set to 650 mV. The ground electrode was fixed to a muscle near the exposed portion of lumbar section.

Hydrogen gas was administered to the animal via an endotracheal tube connected to an anesthetic gas machine close circuited with a 50:50::H_2:O_2 mixture. The electrode voltage rose and reached a plateau. The animal was allowed to breathe freely via the endotracheal tube. Only occasional ventilatory assistance was needed to maintain blood gas values within normal range. This phase of the experiment took roughly 10-15 minutes.

At this time, the animal was disconnected from the anesthesia machine and was allowed to breathe room air. The level of the hydrogen in the tissue then decayed rapidly, and the electrode voltage fell exponentially. The electrode voltages were sampled for 20 minutes or until the polarographic reading reached less than 10% of the peak value. The data were stored on a diskette.

9.2.3 Experimental Procedure:

The blood flow was measured at room temperature, twice. If the reading did not agree with each other to within experimental error (10-12%), a third recording of the SCBF was made. The coolant was infused and circulated through the saddle through a roller pump at an uniform rate (0.5 ml/sec) for about 45 minutes. When the temperature in the cord reached a steady state, usually 15-18 degrees Celsius, SCBF was measured again.

After two trials of measuring SCBF, cooling was discontinued and the cord was permitted to reach normal temperature (34 deg. C). A third set of observations consisting of two trials of SCBF were obtained after rewarming the cord. For each SCBF measurement, the correlation was computed from the logarithm of the desaturation curve. If the correlation factor was less than 0.98, that trial was repeated. The whole experiment lasted about 18 hours after which time the dog was sacrificed.

The changes in spinal cord blood flow were evaluated by statistical 't' test at $p<0.01$.

9.2.4 Measurement of Functional Characteristics of the Platinum Electrode:

The electrode reaction is $H2 \rightarrow 2H+ + 2e-$. The electrode voltage is determined by the Nernst equation:

$$\text{electrode voltage} = \frac{RT}{ZnF} \ln \frac{aH+}{aH2} \qquad (9.1)$$

Since R, Z, n and F are all constants, in the above equation, the only variables are T (absolute temperature), aH+ (activity of hydrogen ion) and aH2 (activity of the hydrogen molecule) which are approximated by concentration of H+ and partial pressure of H2.

In order to evaluate the functional characteristics of platinum electrode, the following experiment was performed:

One dog was allowed to breathe a fixed amount of inhaled hydrogen and the polarograph was allowed to reach a plateau. The cord was cooled and rewarmed. The polarograph readings were noted during the course of this slow change in the temperature. This experiment lasted 15 minutes.

9.3 Results:

A linear regression was performed on the data from

the above experiment, conducted to evaluate the functional characteristics of the electrode. The relationship between cord temperature and electrode potential was found to be linear ($y=13.7+1.18x$), at a 99% confidence level (Fig. 9.2). The correlation coefficient was 0.99. The Nernst equation, (9.1), predicts that if temperature affects activities of H+ and H2, the voltage will vary logarithmically with temperature. If there is no effect on the activities and only the absolute temperature term (T) is changed, the voltage will vary linearly with temperature. Thus, the observed variations in the voltage are a result of decreased temperature rather than different lipid partitioning of hydrogen at lower temperature.

A baseline blood flow value for the cord at each electrode position in each dog was determined by averaging 2 or 3 consecutive trial values at normal temperature. These blood flow values are tabulated in Table 9.1. The observed values of the blood flow at a particular site were repeatable during successive trials and these observations strengthened our confidence in the technique.

At the body temperature, the mean blood flow was found to be dependent on the position of the electrode in the tissue due to differing flow in white or gray matter.

The electrodes inserted into the cord at the saddle sites resided deeper than at control sites. These electrodes at the saddle sites recorded 60-75% higher blood flows than at the control sites, suggesting that the measurement of the SCBF referred to gray matter, which has previously been shown to have higher SCBF at normal temperatures [Griffiths et al., 1975].

The SCBF values from Table 9.1 were used as 100% blood flow values for each electrode location in each animal. The average absolute blood flow values obtained during cooling and after rewarming were then expressed (in fig.9.3) as a percentage of the initial values in Table 9.1. The SCBF decreased by an average of 50% at the saddle sites during cooling and returned to the original blood flow levels on rewarming as the results demonstrate (Fig.9.3) The SCBF decrease during cooling was significant ($p<0.01$), while the average blood flow following rewarming was indistinguishable from the original average flow value. This decrease indicates a profound effect of cooling on local spinal cord blood flow alone [Hansebout et al., 1985]. The SCBF at proximal and distal control sites was not significantly affected during cooling or rewarming at the saddle sites. During the preliminary experiments the temperatures at these control sites were found to remain

normothermic.

The degree of cooling affected was an average of 18.5 degree Celsius lower than the initial temperature with rewarmed temperature returning to within 0.8 degree Celsius of original temperature. Actual temperatures achieved in the spinal cord were in the neighbourhood of 16 degree Celsius. The absolute value of the SCBF reported in Table 9.1 are comparable to those reported by several other groups [Griffiths et al.,1975; Kobrine et al.,1974; and Senter et al., 1978].

9.4 Summary:

The studies described in this chapter indicate that spinal cord cooling has a significant effect on the blood flow in the cord, in a canine experimental model. A decrease of 50% in the blood flow was observed at the site of cooling. Possible mechanisms which bring about this reduction in the observed blood flow in the cord as well as the implications of such reduction of SGBF in clinical setting are discussed in the next chapter.

TABLE- 9.1

Dog Number	Number of trials	SCBF (Mean±SD) ML/MIN/ 100 gm.of tissue Electrode Position			
		1	2	3	4
9	2	9.81 ± 0.79	-	12.91 ± 1.35	13.31 ± 0.70
11	2	-	-	9.10 ± 0.36	10.19 ± 0.45
12	3	7.65 ± 1.75	8.11 ± 0.81	12.89 ± 2.01	15.85 ± 4.09
14	2	6.32 ± 0.23	9.01 ± 0.89	13.82 ± 0.16	12.76 ± 0.07
17	2	7.88 ± 0.29	6.67 ± 0.05	10.63 ± 0.47	8.51 ± 0.09

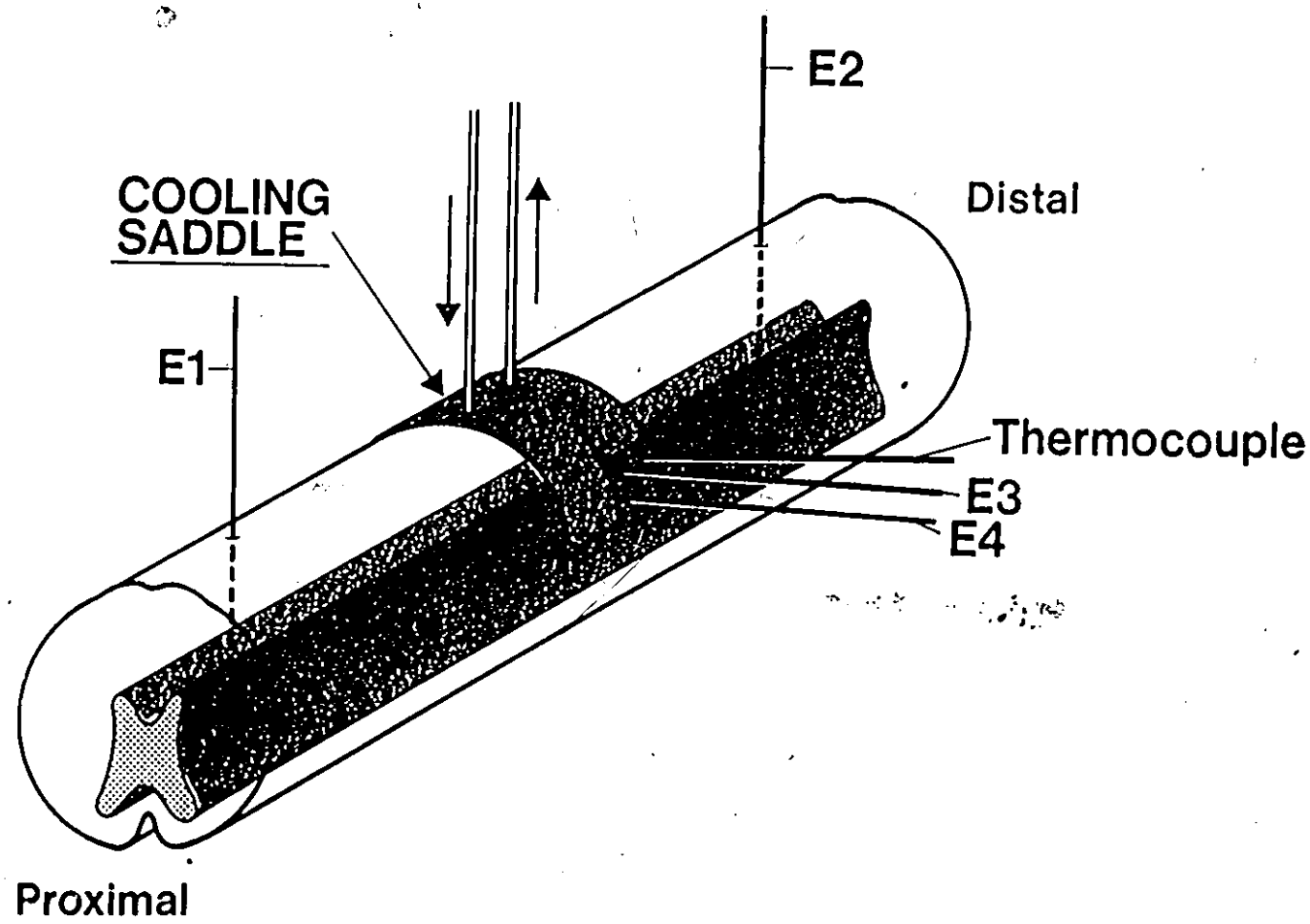

Figure 9.1 Location of electrodes and thermocouple. E1 and E2 were control electrodes and E3 and E4 were saddle electrodes.

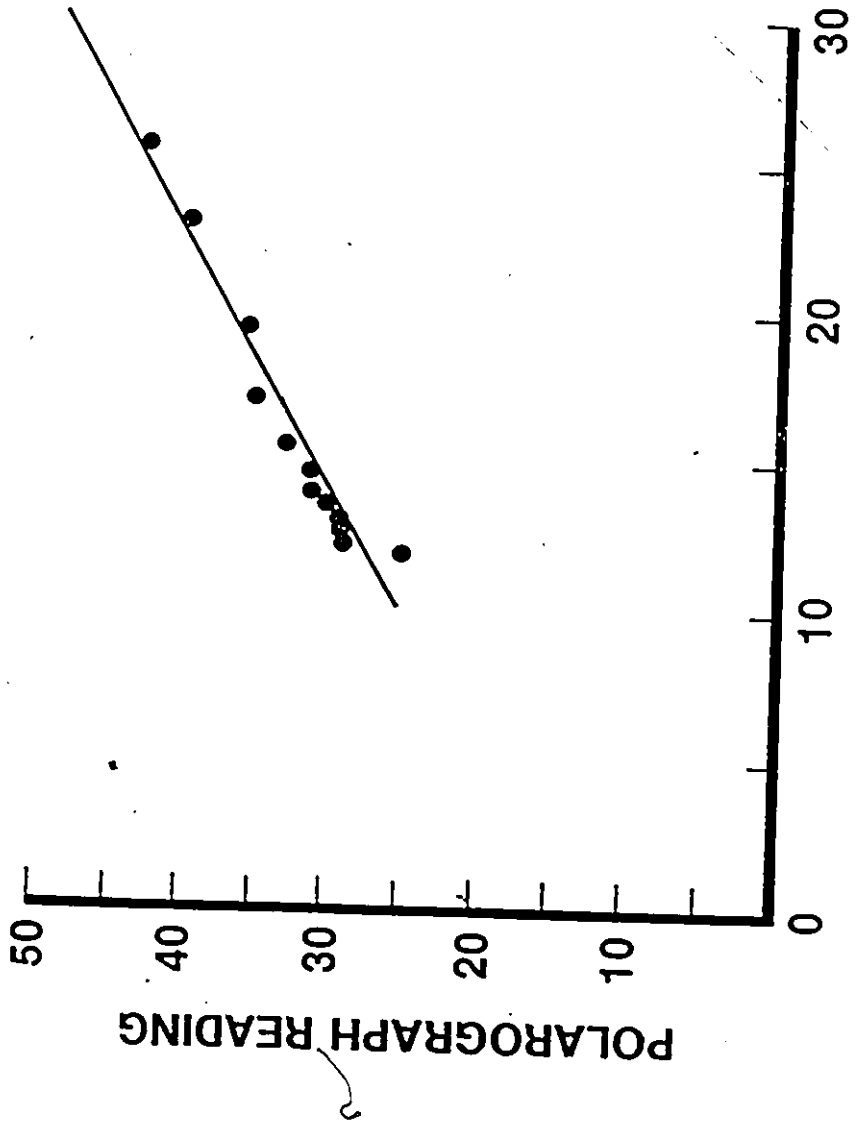

Figure 9.2 Measurement of electrode characteristic.

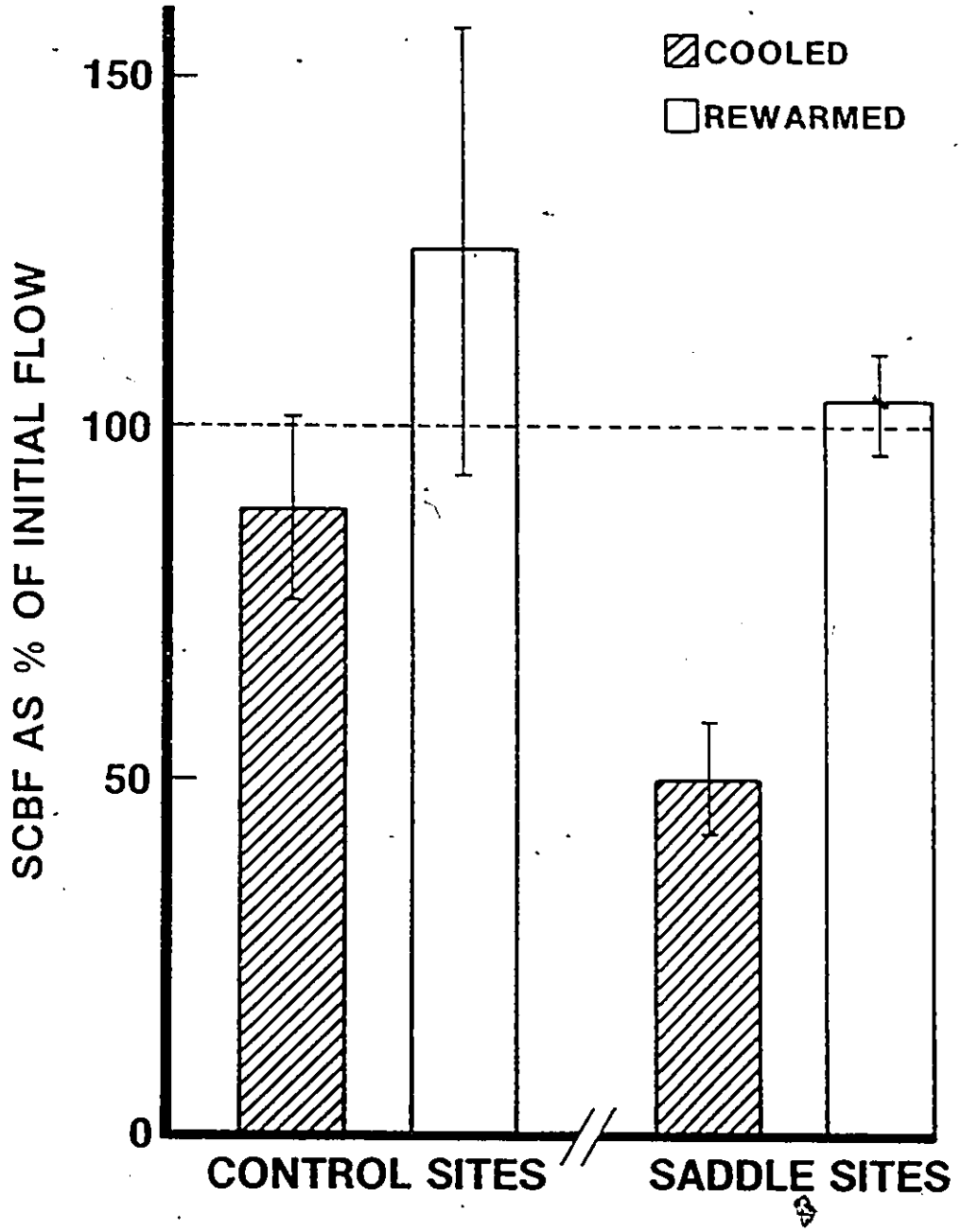

Figure 9.3 The summary of effects of cooling on spinal cord blood flow.

CHAPTER 10

POSSIBLE MECHANISMS FOR REDUCED BLOOD FLOW DURING COOLING, ITS CLINICAL IMPLICATIONS AND SUMMARY

10.1 Introduction:

In light of the observations reported in the last chapter, of a reduced blood flow during cooling in normal canine spinal cord, a number of possible mechanisms responsible for bringing about this change are proposed in section 10.2. Work done by other investigators in this area is compared to the present study. The clinical question, viz. in what way the cooling helps in preserving the functional integrity of the spinal cord, is addressed in section 10.3. Section 10.4 summarizes the work reported in the second part of this thesis.

10.2 Possible Mechanisms for Reduced SCBF During Cooling:

The polarograph voltage plateau following the administration of hydrogen, was found to be a function of the amount of hydrogen in the gas machine circuit and of

the temperature of the tissue around the electrode. Figure 10.1 shows a typical washout curve during normothermic, cooled and rewarmed conditions. The curves 'a' and 'c' in Figure 10.1 demonstrate the difference in plateau achieved in two trials at the same temperature. This difference can be accounted for by different amounts of hydrogen in the animal's ventilatory circuit during each trial. However, the half-times and therefore the blood flows of trials 'a' and 'c' are essentially same. However, curve 'b', obtained during cooling has a markedly lower plateau value as well as a longer half-time. The longer half-time indicates a lower blood flow value. The lower plateau is the result of electrode characteristics as explained earlier in chapter 9. Thus, the measured voltage changes at the site of cooling indicate an actual reduction in blood flow and not the effects of partitioning of dissolved gases in the tissues at lower temperatures. Similar results are reported by Meyer and Hunter [1957] for oxygen electrodes used under hypothermic conditions. Consequently, these results validate the measurement of blood flow during hypothermia using hydrogen polarography described in our study.

Our finding of a decreased SCBF during hypothermia corroborates reports by other investigators [Rosomoff, 1959; Meyer and Hunter, 1957] of a decrease in cerebral blood flow

during hypothermia. However, whole body hypothermia at 30 degree Celsius was used in those experiments rather than the low localized temperatures achieved in the present study. With whole body cooling, systemic effects can not be ruled out.

It is of interest to understand as to what happens to blood flow normally present in the region of the cord subjected to cooling as proximal and distal sites have a normal SCBF. At least two possibilities can be considered:

a) The hydrogen clearance method measures tissue perfusion within the cord rather than surface blood flow. It is possible that blood normally passing through the central part of the cord is shunted through the large surface vessels under the cooled area. Zielonka et al. [1974] have reported an increased flow in the intersegmental (surface) vessels of cooled segment of the spinal cord after 5 minutes of hypothermia. Their finding could be the result of increased shunting of blood past the cooled area avoiding deep capillary beds. Temperature can affect blood vessel calibre differently depending upon the location of the vessel [Janssens and Vanhoute, 1978]. Thus surface vessels of the cord could dilate, while the internal vessels constrict in response to hypothermia. This explanation

could reconcile our observed 50% SCBF decrease with Zielonka et al.'s [1974] noted increased blood flow in surface vessels.

A complete blockade through the cooled saddle site might be expected to decrease blood flow in at least one control site. Zielonka et al.,[1974] also noted an increased tissue perfusion after 60 minutes of hypothermia which they attribute to a loss of autoregulation. In the present study, the second SCBF measurement during cooling was made at least 60 minutes after hypothermia had been instituted. An identical 50% decrease was again noted. The discrepancy between these studies could be due to: difference in the method of blood flow measurement (Zielonka used Thioflavin S), the difference in cooling technique (Zielonka used cooled saline perfusion through durotomy), or more remotely, the difference in animal species (Zielonka used cats).

b) Meyer and Hunter [1957] have reported that the calibre of brain surface vessels reduced by as much as 50% when cooled below 30 degree Celsius. If the same constriction occurs in cord surface vessels then a more likely explanation for our findings is that all cord vessels constrict upon cooling. Thus extra blood may be shunted

away from the cooled segment by collateral flow as schematically represented in Figure 10.2 The hatched area represents the tissue perfusion or SCBF which is reduced in the cooled cord under the saddle. Proximally, blood is directed retrograde away from the cooled segment through the first available radicular arteries. Distally, blood is directed toward the cord via the radicular arteries to augment the blood flow to normal levels in the adjoining normothermic segment. Whether the blood normally flowing to the constricted central vessels is shunted past the cooled core by the surface vessels or radicular vessels as shown in Fig.10.2 is unknown. The present design of the experiment precludes observation of surface vessels and hence in the present work this hypothesis can not be confirmed.

Although this type of localized perfusion reduction could be mediated through an autonomic mechanism, it is possible that increased blood viscosity or a direct effect on vascular smooth muscle are more likely mechanisms for the decreased blood flow. If the cooling results into a membrane effect such as a decreased fluidity which in turn affects the ionic conductances or some other function, then one would expect the membrane effect to be generalized to all cells and subcellular organelles being cooled. Astrup [1982] notes that hypothermia reduces the consumption of

oxygen and glucose in the brain affording clinical protection but that a similar degree of metabolic reduction by barbiturates does not give protection. He concludes that hypothermia must be protecting the tissue by "membrane stabilization".

10.3 Clinical Significance of reduced SCBF during cooling:

Scutto et al. [1983] found that edema started within an hour after the impact of injury and then peaked between fourth and sixth hour after the injury, suggesting rapid onset of vasogenic edema. Kobrine et al. [1974] have reported that after a significant cord injury, blood flow in the gray matter was markedly reduced while flow in the white matter actually increased. If the cord is cooled for four hours during the first few hours after injury, this tends to preserve the cord function, an observation confirmed by Wells et al.[1978] in experimental canine cord trauma.

With these findings in mind, it is postulated that the decreased blood flow caused by cooling at the site of injury tends to prevent the outpouring of edema fluid and other toxic factors from the injured vessels thus preserving the cord function. However, if the injured cord is cooled for too long a time (18 hours) the beneficial effects of

cooling are obviated [Wells et al., 1978; Hansebout, 1984]. This may be result of an ischemic situation perpetrated by prolonged cooling. Thus, the finding of decreased SCBF in the locally cooled spinal cord is an observation which is clinically relevant.

To enhance the usefulness of the information obtained in this work, it is suggested that further studies in experimental injury models be carried out. Following, measurement of blood flow in normal cord, the SCBF may be measured following injury, cooling and after rewarming.

The next section presents a summary of the second part of the thesis.

10.4 Summary:

The spinal cord injury is an important clinical problem which results in permanent disability to the patient. Cooling of the cord during acute phase of injury has given some encouraging results. In this context, the role of spinal cord blood flow during injury and cooling has not been fully explained. The objective of this work was to examine the effects of cooling on spinal cord blood flow in

canine experimental model.

The instrumentation for the study consisted of a cooling apparatus with a saddle and a polarograph for measuring the SCBF as described in chapter 7. Of the different methods available for measuring SCBF, hydrogen polarography was chosen, the rationale for which was presented in chapter 6. A computer based instrumentation system was developed to monitor SCBF from cooled sites and control sites.

The experimental details and the results of effects of cooling are presented in chapter 9. It was observed that SCBF decreased by as much as 50% at the site of cooling in the normal canine cord. The significant reduction in normal spinal cord blood flow following cooling of the cord prompted us to examine the current literature for possible explanation of the phenomena. We believe that our results are compatible with research reported by others, in that, the observed reduction of SCBF at a specific site may be due to possible shunting of the blood from the site of cooling or increased blood flow at the surface vessels.

It is postulated that following SCI, decreased SCBF due to localized cooling tends to prevent the outpouring of

edema fluid and other toxic factors from the injured vessels, preserving the cord function. Thus, the finding of decreased SCBF during spinal cord cooling is clinically relevant.

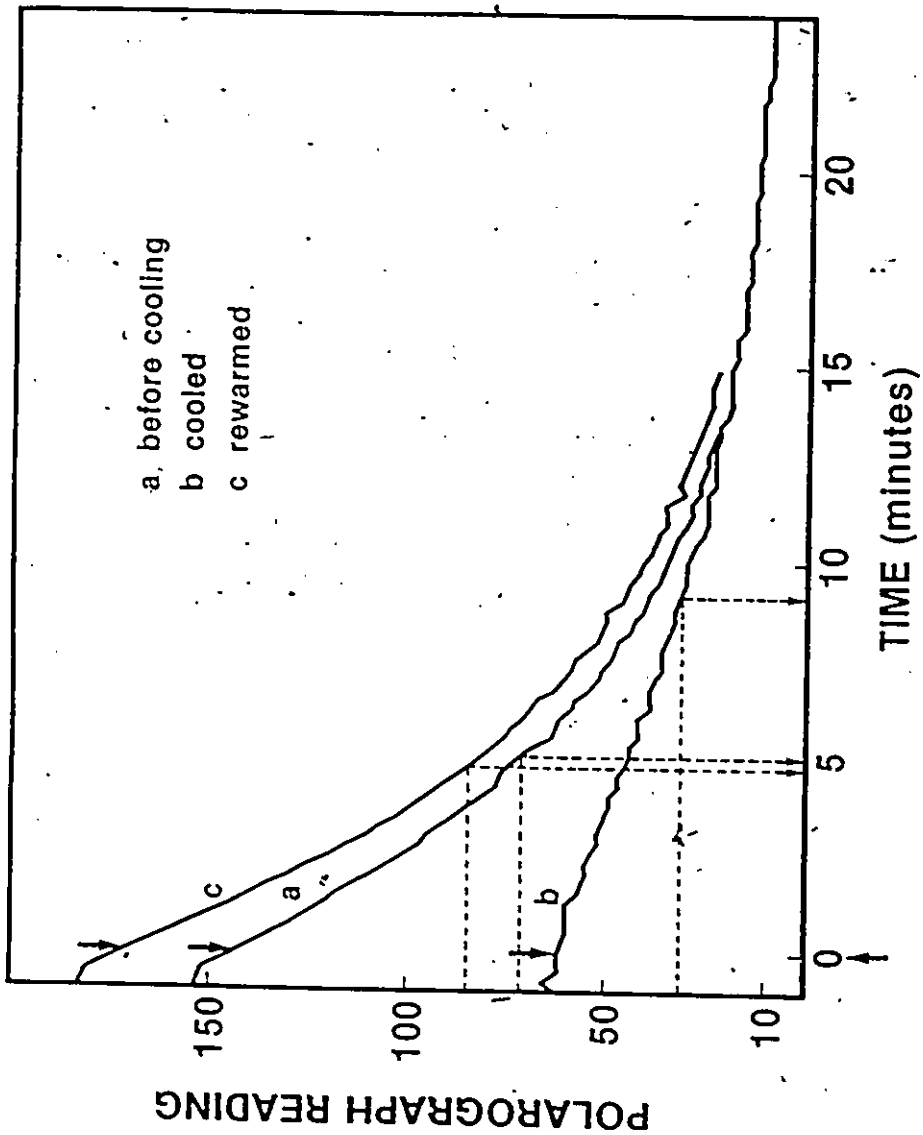

Figure 10.1 Typical hydrogen washout curves.

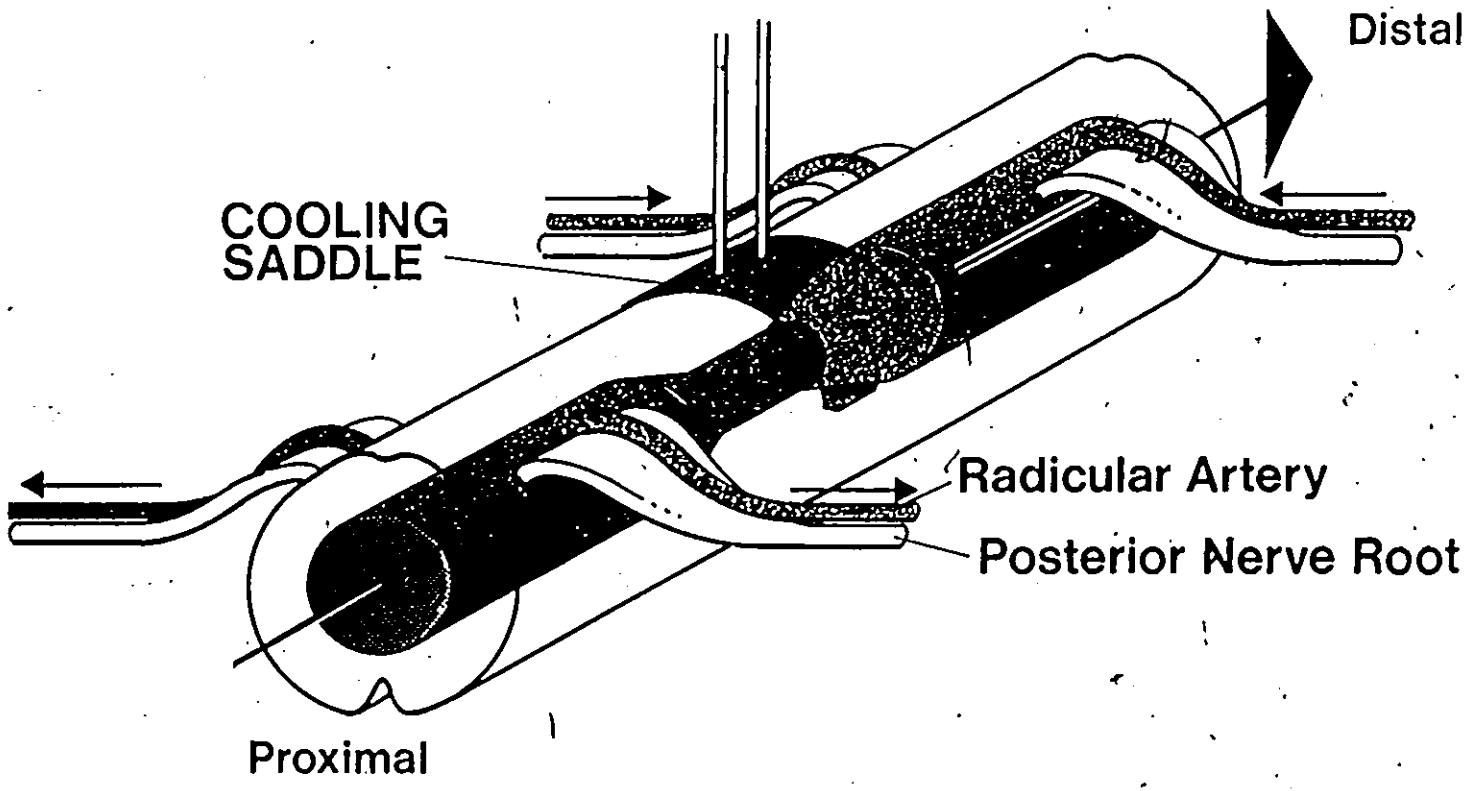

Figure 10.2 Schematic representation of changes in blood flow due to cooling.

APPENDIX A

This appendix outlines a set of sample computations on two BAEPs, to illustrate how classification is done in the FORTRAN program using time domain features.

1. Compute the mean vectors of each class. Latencies of the peaks V, IV and III are used as the features.

The number of training patterns, $n_A=73$, $n_B=97$.

Mean latencies of the pathological class:

$$M_A^T = [6.009\ 5.248\ 3.984] \qquad 1 \times 3$$

Mean latencies of the normal class:

$$M_B^T = [5.595\ 4.926\ 3.725] \qquad 1 \times 3$$

2. Compute for the labelled samples the covariance matrix for each class and their inverses.

Covariance matrix for the pathological class,

$$S_A = \begin{bmatrix} 0.127 & 0.090 & 0.066 \\ 0.090 & 0.123 & 0.073 \\ 0.066 & 0.073 & 0.092 \end{bmatrix}$$

Covariance matrix for the normal class.

$$S_B = \begin{bmatrix} 0.030 & 0.017 & 0.014 \\ 0.017 & 0.026 & 0.012 \\ 0.014 & 0.012 & 0.020 \end{bmatrix}$$

$$S_A^{-1} = \begin{bmatrix} 17.27 & -9.99 & -4.47 \\ -9.99 & 21.14 & -9.61 \\ -4.47 & -9.61 & 21.70 \end{bmatrix}$$

$$S_B^{-1} = \begin{bmatrix} 61.47 & -28.12 & -26.16 \\ -28.12 & 66.05 & -19.95 \\ -26.16 & -19.95 & 80.28 \end{bmatrix}$$

3. Compute the determinants of the covariance matrices:

$$|S_A| = 34.66 \text{ X } 10 \text{ E-5} \quad ; \quad |S_B| = 6.16 \text{ X } 10 \text{ E-7}$$

4. P(A) is estimated as the ratio of number of patients with abnormal BAEPs to the total number of patients whose BAEPs are recorded over a specific period of time, say one year. Then, P(B) = 1-P(A). At McMaster, based on 1000 consecutive BAEPs recorded in 1984. P(A) = 0.47 and P(B)=0.53.

5. Compute the threshold T=0.24 +4.038 =4.278 .

6. Given a test BAEP pattern, X, from figure 4.10 (lower trace),

X^T = [5.72 4.82 3.60] compute the distance measures from each class.

7. From equation, (3.7)

$$3.970 - 1.89 \begin{matrix} A \\ > \\ < \\ B \end{matrix} 4.278$$

Hence, pattern X^T = [5.72 4.82 3.60] belongs to class B.

For X^T = [6.3 5.32 4.04], from figure 4.11 (upper trace), substituting in equation 3.7 yields,

$$16.61 - 1.19 \begin{matrix} A \\ > \\ < \\ B \end{matrix} 4.278$$

Hence, X^T = [6.3 5.32 4.04] belongs to class A.

8. For Fisher's Linear Discriminant, compute the pooled

covariance matrix (eq.4.5). For $n_A = 73$ and $n_B = 97$,

$$S_P^{-1} = \begin{bmatrix} 28.79 & -15.57 & -8.87 \\ -15.57 & 33.76 & -14.21 \\ -8.87 & -14.21 & 36.39 \end{bmatrix}$$

9. Compute the midpoint between the classes from equation (3.11):

$$m = -39.98$$

10. For $X^T = [\,5.72\ 4.82\ 3.60]$, equation 3.12 yields,

$$Y0 = -38.82$$

From equations, 3.13 and 3.14, pattern X belongs to class B.

For $X^T = [6.3\ 5.32\ 4.04]$,

$$Y0 = -52.87$$

Hence, X^T belongs to class A.

APPENDIX B

This appendix outlines a set of sample computations for classifying two BAEPs using frequency domain features:

1. Compute the mean vectors of each class. Mean power in the three prinicpal bands are used as the features.

The number of training patterns, $n_A = 45$ and $n_B = 60$

Mean powers of the pathological class:

$$M_A^T = [17514.9 \quad 6815.4 \quad 1430.0] \qquad 1 \times 3$$

Mean latencies of the normal class:

$$M_B^T = [14121.1 \quad 8328.2 \quad 2915.5] \qquad 1 \times 3$$

2. Compute for the labelled samples the covariance matrix for each class and their inverses.

Covariance matrix for the pathological class,

$$S_A = 1.0\ E\ 07 \times \begin{bmatrix} 1.01 & -0.787 & -0.125 \\ -0.787 & 0.670 & 0.051 \\ -0.125 & 0.051 & 0.069 \end{bmatrix}$$

Covariance matrix for the normal class,

$$S_B = 1.0\ E\ 07\ X \begin{bmatrix} 1.08 & -0.643 & -0.289 \\ -0.643 & 0.497 & 0.088 \\ -0.289 & 0.088 & 0.150 \end{bmatrix}$$

The inverses are:

$$S_A^{-1} = 1.0\ E\ -05\ X \begin{bmatrix} 0.431 & 0.472 & 0.439 \\ 0.472 & 0.532 & 0.469 \\ 0.439 & 0.469 & 0.602 \end{bmatrix}$$

$$S_B^{-1} = 1.0\ E\ -05\ X \begin{bmatrix} 0.617 & 0.658 & 0.803 \\ 0.658 & 0.723 & 0.842 \\ 0.803 & 0.842 & 1.120 \end{bmatrix}$$

3. Compute the determinants of the covariance matrices:

$$|S_A| = 1.008\ E\ 19 \quad ; \quad |S_B| = 1.020\ E\ 19$$

4. P(A) and P(B) are estimated from patient population whose BAEPs are recorded over a specific period of time. As outlined in chapter 4,

P(A) = 0.47 and P(B)=0.53

5. Compute the threshold T=0.24 +0.016 =0.256

6. Given a test BAEP pattern, X, from figure 5.1 (upper trace), the power spectra yields the feature vector:

X^T = [14712.3 7819.9 2718.4].

Now, compute the distance measures from each class.

7. From equation, (3.7)

$$0.3386 \quad -3.07 \quad \begin{matrix} A \\ > \\ < \\ B \end{matrix} \quad 0.256$$

Hence, BAEP shown in Fig.5.1 (upper trace) belongs to class B.

For BAEP of figure 5.9 (upper trace) the power spectral analysis yields the feature vector,

X^T = [20228.1 4614.0 692.1].

Substituting these features in equation 3.7 yields,

$$8.12 - 2.20 \;\begin{matrix} A \\ > \\ < \\ B \end{matrix}\; 0.256$$

Hence, BAEP which generated the feature vector,

X^T = [20228.1 4614.0 690.1] belongs to class A.

8. For Fisher's Linear Discriminant, compute the pooled covariance matrix (eq.4.5). For n_A = 45 and n_B = 60

$$S_P^{-1} = 1.0\ E\text{-}06\ X \begin{bmatrix} 4.53 & 4.91 & 5.39 \\ 4.91 & 5.49 & 5.72 \\ 5.38 & 5.72 & 7.45 \end{bmatrix}$$

9. Compute the midpoint between the classes from equation (3.11):

$$m = 5.47$$

10. For X^T = [14712.3 7819.9 2718.4], equation 3.12 yields,

$$Y0 = 6.23$$

From equations, 3.13 and 3.14, pattern X belongs to class B.

11. For X^T = [20228.1 4614.0 692.1]

$$Y0 = 2.19$$

Hence, X^T belongs to class A.

REFERENCES

Albin, M.S., White, R.J. and Locke, G.E. 1965. Treatment of spinal cord trauma by selective hypothermic perfusion. Surg. Forum. 16:423-424.

Anderson, D.C., Bundlie, S. and Rockwold, G.L. 1984. Multimodality evoked potentials in closed head trauma. Arch. of Neurol. (Chicago). 41:369-374.

Astrup, J. 1982. Energy-requiring cell functions in the ischemic brain. J. Neurosurg. 56:482-497.

Aukland, K., Bower, B.F. and Berliner, R.W. 1964. Measurement of local blood flow with hydrogen gas. Circ. Res. 14:164-187.

Aunon, J.I. and McGillem, C.D. 1982. On the classification of single evoked potentials using a quadratic classifier. Comp. Prog. in Biomed. 14:29-40.

Beagley, H.A. and Sheldrake, J.B. 1978. Differences in brainstem response latency with age and sex. Br. J.

Audiol. 12:69-77.

Bingham, W.G., Goldman, H. and Friedman. (1975) Blood flow in normal and injured monkey spinal cord. J.Neurosurg.43:162-171.

Boston, J.R. and Ainslie, P.J. 1980. The effects of analog and digital filtering on brainstem evoked potentials. Electroenceph. Clin. Neurophysiol. 48:361-364.

Boston, J. 1985. Noise cancellation for brainstem auditory evoked potentials. IEEE Trans. Biomed. Engn. BME-32:1066-1070.

Callaway, E., Tueting, P. and Koslow, S.H. (Eds.). 1978. Event-Related Potentials in Man. Academic Press, New York.

Chiappa, K.H., Gladsotne, K.J. and Young, R.R. 1979. Brianstem auditory evoked responses: Studies of waveform variations in 50 normal human subjects. Arch. Neurol. (Chicago). 36:81-87.

Chiappa, K.H., Harrison, J.L., Brooks, E.B. and Young, R.R. 1980. Brainstem auditory evoked responses in 200 patients

with multiple sclerosis. Ann. Neurol., 7:135-143.

Chiappa, K.H. 1983. Evoked Potentials in Clinical Medicine. Raven Press, New York.

Chiappa, K.H. 1984. Brainstem auditory evoked potentials in multiple sclerosis. in The Diagnosis of Multiple Sclerosis. C.M.Poser, D.W.Paty, L.Scheinberg, W.I.Mcdonald, G.C.Ebers.(Eds.)Thieme-Stratton Inc., NY. pp.120-130.

Childers, D.G.,(Ed.) Modern Spectal Analysis. 1978. IEEE Press, N.Y.

Courjon, J., Mauguiere, F. and Revol, M. (eds.). 1982. Clinical Applications of Evoked Potentials in Neurology. Adv. Neurol. Vol. 32. pp.157-256. Raven Press, New York.

Dawson, G.D. 1947. Cerebral responses to electrical stimulation of peripheral nerve in man. J.Neurol. Neurosurg. Psychiatr., 10: 134-140.

De La Torre, J.C. 1981. Spinal cord injury: Review of basic and applied research. Spine, 6:315-335.

Desmedt, J.E. (Ed.). 1977. Auditory Evoked Potentials in

Man. Psychopharmacological Correlates of EPs. Progress in Clinical Neurophysiology, Vol.2, Karger, Basel.

Desmedt, J.E. (Ed.). 1980. Clinical Uses of Cerebral, Brainstem and Spinal Somatosensory Evoked Potentials. Progress in Clinical Neurophysiology Vol.7. Karger, Basel.

Duda, R.O. and Hart, P.E. 1973. Pattern Classification and Scene Analysis. John Wiley and Sons, New York.

Ducker, T.B. and Perot Jr.P.L. 1971. Spinal cord oxygen and blood flow intrauma. Surg. Forum. 22:413-415.

Facco, E., Martin, A., Zuccarello, M., Agnoletto, M and Giron, G.P. 1985. Is the auditory brainstem response effective in the assessment of the post-traumatic coma? Electroenceph. Clin. Neurophysiol. 62:332-337.

Fridman, J., John, E.R., Bergelson, M., Kaiser, J.B., Baird, B.H. 1982. Applications of digital filtering and automatic peak detection to brainstem auditory evoked potentials. Electroenceph. Clin. Neurophysiol. 53:405-416.

Fu, K.S. 1982.Syntactic Pattern Recognition and Applications. Prentice-Hall Inc., Englewood Cliffs, N.J.

Fukunaga, K. 1972.Introduction to Statistical Pattern Recognition. Academic Press Inc., N.Y.

Geddes, L.A. 1972. Electrodes and the Measurement of Bioelectric Events. John Wiley and Sons, Toronto.

Green, J.B. and Walcoff, M.R. 1982. Evoked potentials in multiple sclerosis. Arch. of Neurol. 39:696-697.

Greenberg, R.P, Ducker, T.B. 1982. Evoked potentials in clinical neurosciences. J. Neurosurg. 56:1-18.

Griffiths, I.R., Rowan, J.O. and Crawford, R.A. 1975. Spinal cord blood flow by a hydrogen clearance technique. J. Neurol. Sci. 26:529-544.

Grundy, B.L., Jannetta, P.J, Procopio, P.T., Lina, A, Boston, J.R. and Doyle, E. 1982. Intraoperative monitoring of brainstem auditory evoked potentials. J. Neurosurg. 57:674-681.

Hales, J.R.S. 1974. Radioactive microsphere techniques for

studies of the circulation. Clin. Exp. Pharmcol. Physiol. suppl. 1:31-46.

Hall, E.D., Braughler, J.M. 1982. Glucocorticoid mechanisms in acute spinal cord injury: a review and therapeutic rationale. Surg. Neurol. 18:320-327.

Halliday, A.M. (Ed.). 1982. Evoked Potentials in Clinical Testing. Churchill Livingstone, Edinburgh.

Hand, D.J. 1981. Discrimination and Classification.John Wiley and Sons, London.

Hansebout, R.R. 1982. A comprehensive review of methods of improving cord recovery after acute spinal cord injury. in Tator, C.H. (ed.). Early Management of Acute Spinal Cord Injury. Semin. Neurol. Surg. Raven Press, N.Y.

Hansebout, R.R. 1983 Spinal Injuries. Can. J. Surg.26:440.

Hansebout, R.R., Tanner, A., Romero-Sierra, C. 1984 Current status of spinal cord cooling in the treatment of acute SCI. Spine 9:508-511.

Hansebout, R.R., Lamont, R.N. and Kamath, M.V. 1985. The

effects of local cooling on canine spinal cord blood flow. Can. J. Neurol. Sci. 12:83-87.

Hansebout, R.R. 1986. The neurosurgical management of cord injuries. in R.F.Bloch and M.Basbaum (eds.) Management of spinal cord injuries. Williams and Wilkins, Baltimore.

Hansebout, R.R., Kamath, M.V. and Lamont, R.N. 1987. Monitoring spinal cord blood flow using hydrogen polarography. Accepted for publication. To appear in Comp. Biol. Med.

Haykin, S.(ed). 1979. Nonlinear Methods of Spectral Analysis. Springer-Verlag, Berlin.

Heymann, M.A., Payne, B.D., Hoffman, J. and Rudolph, A.M. 1977. Blood flow measurements with radionuclide-labeled particles. Prgr. Cardiovas. Dis. 20:55-79.

Jansen, B.H., Hasman, A., Lenten, R. 1981. Piecewise analysis of EEGs using AR modelling and clustering. Comp. and Biomed. Res. 14:168-178.

Janssens, W.J. and Vanhoutte, P.M. 1978. Instantaneous

changes of alpha-adrenoceptor affinity caused by moderate cooling in canine cutaneous veins. Am. J. Physiol. 234: H330-H337.

Jewett, D.L. 1970a Volume conducted potentials in response to auditory stimuli as detected by averaging in the cat. Electroenceph. Clin. Neurophysiol. 28:609-618.

Jewett, D.L., Romano, M.N. and Williston, J.S. 1970b. Human auditory evoked potentials: Possible brainstem components detected on the scalp. Science, 167:1517-1518.

Jewett, D.L. and Williston, J.S. 1971. Auditory far fields averaged from the scalp of humans. Brain. 94:681-696.

Johnson, R.A. and Wichern, R.M. 1982. Applied Multivariate Statistical Analysis. Prentice Hall Inc., Englewood Cliffs, N.J.

Kamath, M.V., Reddy S.N., Ghista D.N. and Upton A.R.M. 1984. The nature of power spectra of clinical brainstem auditory evoked potentials. Proc. of X Can. Med. and Biol. Engn. Conf. Ottawa.

Kamath, M.V., Upton, A.R.M., Ghista, D.N., Reddy, S.N. and Jernigan, M.E. 1986a. A statistical distance measure for objective quantification of brainstem auditory evoked potentials of normals and patients. Proc. of Fifth Int. Conf. Mech. in Med. and Biol. Bologna, Italy.

Kamath, M.V., Reddy, S.N., Upton, A.R.M., Ghista, D.N. and Jernigan, M.E. 1986b. Pattern classification of brainstem auditory evoked potentials of normals and patients. Proc. of 12 Can. Med. and Biol. Engn. Conf., Vancouver.

Kamath, M.V., Reddy, S.N., Ghista, D.N., and Upton, A.R.M. 1987a. Power spectral analysis of brainstem auditory evoked potentials. Int. J. Bio-med. Comput. 21:33-54.

Kamath, M.V., Reddy, S.N., Upton, A.R.M. and Jernigan, M.E. 1987b. Statistical pattern classificaiton of clinical brainstem auditory evoked potentials. Accepted for publication. To appear in Int.J. Bio-med. Comput.

Kamath, M.V., Ghista, D.N., Fallen, E.L., Fitchett, D., Miller, D.N. and McKelvie. 1987c. Heart rate variability power spectrogram as a potential noninvasive signature of cardiac regulatory system response, mechanisms and

disorders. Accepted for publication in Heart and Vessels. vol3.

Karnaze, D.S., Marshall, L.F., McCarthy, C.S., Klauber, M.R., Bickford, R.G. 1982. Localizing and prognostic value of auditory evoked responses in coma after closed head injury. Neurology. 32:299-302.

Kay, S. and Marple, S.L. 1981. Spectrum Analysis- A modern perspective. Proc. of IEEE 69:1380-1419.

Kelly,D., Lassiter,K., Calegro. 1970. Effects of local hypothermia and tissue oxygen studies in experimental paraplegia. J. Neurosurg. 33:554-563.

Kety, S.S. 1951. The theory and applications of the exchange of inert gas at the lungs and tissues. Pharmacol. Rev. 3:1-41.

Kety, S.S. 1960. Measurement of local blood flow by the exchange of inert,diffusible substance. Method. Med. Res. 8:228-236.

Kiloh, L.G, McComas, A.J., Osselton, J.W. and Upton, A.R.M. 1981. Clinical Electroencephalography, London,

Butterworths.

Kjaer, M. 1980a. Brainstem auditory and visual evoked potentials in multiple sclerosis. Acta Neurol. Scandinav. 62:14-19.

Kjaer, M. 1980b. The value of brainstem auditory, visual and somatosensory evoked potentials and blink reflexes in the diagnosis of multiple sclerosis. Acta Neurol. Scandinav. 62:220-236.

Kling, T.F., Wilton, N., Hensinger, R.N.and Knight, P.R. 1986. The influence of Trimethaphan (Arfonad)-induced Hypotension with and without spine distraction on canine spinal cord blood flow. Spine 11:219-224.

Kobrine, A.I., Doyle T.F., and Martins, A.N. 1974. Spinal cord blood flow in the rhesus monkeys by the hydrogen clearance method. Surg. Neurol. 2:197-200.

Madhavan, G.P., de Bruin, H. and Upton, A.R.M. 1984. Evoked potential processing and pattern recognition. Proc. VI Ann. Conf. IEEE Eng. Med. Biol. Soc. pp.29.10.1-29.10.4. Los Angeles.

Madhavan, G.P. 1985. Adaptive Filtering and Pattern Recognition of evoked potentials. Ph.D. Thesis. McMaster University, Hamilton, Ontario, Canada.

Madhavan, G.P., de Bruin, H., Upton, A.R.M. and Jernigan, M.E. 1986. Classification of brainstm auditory evoked potentials by syntactic methods. Electroenceph. Clin. Neurophysiol. 65:289-296.

McGillem, C.D., Aunon, J.I. and Childers, D.G. 1981. Signal processing in evoked potential research: Applications of filtering and pattern recognition. Crit. Rev. Bioengineer. 6:225-265.

McGillem, C.D., Aunon, J.I. and Yu, K. 1985. Signals and noise in evoked brain potentials. IEEE Trans. Biomed. Engn. BME-12:1012-1017.

Makhoul, J. 1975. Linear Prediction: A tutorial Review. Proc. IEEE. 63:561-580.

Mathie, R.T. (Ed.). 1982. Blood flow measurement in man. Castle House Publications Ltd. Kent,England.

Meyer, J.D. and Hunter, J. 1957. Effects of hypothermia on

local blood flow and metabolism during cerebral ischemia and hypoxia. J. neurosurg. 14: 210-227.

Morley, G.K. and Liedtke, K.E. 1977. Automated evoked potential analysis using peak and latency discrimination. Ed. J.I. Martin. Proc. San Diego Biomed. Sympos. 16:291-298, Academic Press, N.Y.

Newlon, P.G., Greenberg, R.P., Hyatt, M.S., Enas, G.G. and Becker, D.P. 1982. The dyanmics of neuronal dysfunction and recovery following severe head injury assessed with serial multimodality evoked potentials. J.Neurosurg. 57:168-177.

Nodar, R.H., Lonsdale, D and Orlowski, J.P. 1980. Abnormal brainstem potentials in infants threatened with sudden infant death syndrome. Otolarngol. Head Neck Surg., 88:619-621.

Phillips, K.R., Potvin, A.R., Syndulko, K., Cohen, S.N., Tourtellote, W.W. 1983. Multimodality evoked potentials and neurophysiological tests in multiple sclerosis: effects of hyperthermia on test results. Arch. Neurol., 40:159-164.

Raudzens, P.A. and Shetter, A.G. 1982. Intraoperative monitoring of brainstem auditory evoked potentials. J. Neurosurg., 57:341-348.

Reddy, S.N and Kirlin, L. 1979. Spectral analysis of auditory evoked potentials with psuedo random noise excitation. IEEE Trans. Biomed. Engn. BME-26:479-487.

Reivich, M., Jehle, J. and Sokoloff, L., Kety, S.S. 1969. Measurement of regional cerebral blood flow with ^{14}C-antipyrine in awake cats. J. Appl. Physiol: 27:296-300.

Rivlin, A.S. and Tator,C. 1978. Regional spinal cord blood flow in rats after severe cord trauma. J.Neurosurg. 49:844-853.

Robinson, K. and Rudge, P. 1977. Abnormalities of the auditory evoked potentials in patients with mulitple sclerosis. Brain, 100:19-40.

Robinson, K. and Rudge, P. 1982a. Centrally generated auditory potentials. in Halliday, A.M. (Ed.). Evoked Potentials in Clinical Testing. pp.345-372. Churchill Livingstone, Edinburgh.

Robinson, K. and Rudge, P. 1982b. The use of auditory potenitals in nuerology. in Halliday, A.M. (Ed.). Evoked Potentials in Clinical Testing. pp. 373-392. Churchill Livingstone, Edinburgh.

Romero-Sierra, C., Hansebout, R.R., Sierhuis, A. and Lewin,M. 1974. A new method for localized spinal cord cooling. Med. Biol. Engn. 12:188-193.

Rosomoff, H.L. 1959. Protective effects of hypothermia against pathological processes of the nervous system. Ann. Ny. Acad. Sci. 80:475-486.

Rowe, M.J. III. 1978. Normal variability of the brainstem auditory evoked response in young and old adult subjects. Electroenceph. Clin. Neurphysiol. 44:459-470.

Sackett, D.L , Haynes, R. and Tugwell, P. 1985. Clinical Epidemiology: A Basic Science for Clinical Medicine. Little Brown and Co., Boston.

Samii, M. 1986. Surgery in and around the Brain Stem and the Third Ventricle. pp. 147-175. Springer-Verlag. Berlin.

Salamy, A., Mendelson, T., Tooley, W.H. and Chaplain, E.R.

1980. Contrasts in brainstem function between normal and high-risk infants in early postnatal life. Early human development. 4:179-185.

Sandler, A.N. and Tator, C.H. 1976a. Review of the measurement of normal spinal cord blood flow. Br. Res., 118:181-198.

Sandler, A.N. and Tator, C.H. 1976b. Regional spinal cord blood flow in primates. J. Neurosurg. 45:647-659.

Scherg, M. and Speulda, E.W. 1982. Brainstem auditory evoked potentials in the neurology clinic: Improved stimulation and analysis methods. in J. Courjon, F. Mauguiere and M.Revol (eds.) Clinical Applications of evoked potentials in Neurology. pp. 211-218. Raven Press, New York.

Schwartz, M. and Shaw, L. 1975. Signal Processing: Discrete Spectral Analaysis, Detection and Estimation. McGraw-Hill Book Co., N.Y.

Scutto, A., Borriello, R., Paggio, G. 1983. Evalauation of some biological parameters in acute spinal cord trauma: experimental study. (Ab). Seminar on Spinal Cord

Reconstruction, Auditorium Museo di Capodimonte, Naples, Italy.

Seales, M., Rossiter, V.S., Weinstein, M.E. and Spencer, J.D. 1979. Brainstem auditory evoked responses in patients comatose as a result of blunt head trauma. J. Trauma. 19:347-353.

Selters, W.A. and Brackmann, D.E. 1977. Acoustic tumor detection with brainstem electric response audiometry. Arch. of Otolaryngol. 103:181-187.

Senter, H.J. and Venes, J.L. 1978. Altered blood flow and secondary injury in experimental spinal cord trauma. J. Neurosurg. 49:569-5 .

Senter, H.J., Burgess, D.H. and Metzler, J. 1978. An improved technique for measurement of spinal cord blood flow. Brain Res. 149:197-203.

Shangkai, G. and Loew, M.H. 1986. An autoregressive model of the BAEP signal for hearing threshold testing. IEEE Trans. on Biomed. Engn. BME-33: 560-565.

Shapiro, S.M., Moller, A.R. and Shiu, G.K. 1984. Brainstem

auditory evoked potentials in rats with high dose pentobarbital. Electroenceph. Clin. Neurophysiol. 58:266-276.

Sharpless, S.K. 1970. Hypnotics and sedatives. I. The barbiturates, in Goodman L.S. and Gilman, A. (Eds.): The Pharmacological Baisis of the Therapeutics. ed.4,pp 98-120. MacMillan, New York.

Sklar, B. 1971. A computer classification of normal dyslexic children using spectral estimates of their EEGs. Doctoral Dissertation, Univ. of California, Los Angeles.

Smith, A.L., Pender, J.W. and Alexander, S.C. 1969. Effects of pCO_2 on spinal cord blood flow. Amer. J. Physiol., 216:1158-1163.

Starr, A. and Achor, L.J. 1975. Auditory brainstem responses in neurological diseas. Arch. of Neurol. (Chicago). 32:761-768.

Starr, A. 1976 Auditory brainstem responses in brain death. Brain. 99:543-554.

Stockard, J.J., Stockard, J.E. and Sharbrough, F.W. 1977a.

Detection and localization of occult lesions with brainstem auditory responses. Mayo Clin.Proc., 32:761-769.

Stockard, J.J. and Rossiter, V.S., 1977b, Clinical and pathological correlates of brainstem auditory response abnormalities. Neurol. 27:316-325.

Stockard, J.J., Stockar, J.E. and Sharbrough, F.W. 1978. Nonpathologic factores influencing brainstem auditory evoked potentials. Amer. J. EEG Technol., 18:177-209.

Sutton, L.N., Frewen, T., Marsh, R., Jaggi, J. and Bruce, D.A. 1982. The effect of deep barbiturate coma on multimodality evoked potentials. J. Neurosurg. 57:178-185.

Thakor, N.V. 1986. Monitoring brain electrical and magnetic activity. IEEE Engn. in Med. and Biol.11-15.

Thakor, N.V. 1987. Adaptive filtering of evoked potentials. IEEE Trans. Biomed. Engn. BME-34:6-13

Thickbroom, G.W., Carroll, W.M., Mastaglia, F.L. 1985. Dipole source derivation. Application to the

half-field pattern evoked potential. Int. J. Bio-med.Comput.16:17-28.

Tou, J.T. and Gonzalez, R. 1974. Pattern Recognition Principles. Addison-Wesley Publ. Co., Inc. Reading, Mass.

Ulrych, T.J. and Bishop, T.N. 1975. Maximum entropy spectral analysis and autoregressive spectral decomposition. Rev. Geophysics. 13:183-200.

Ulrych, T.J. and Ooe, M. 1979. Autoregressive and mixed autoregressive-moving average models and spectra. In Nonlinear Methods of Spectral Analaysis. S.Haykin (Ed) Springer-Verlag, N.Y.

Uziel, A. and Benezech, J. 1978. Auditory Brainstem response in comatose patients: relationship with brainstem reflexes and levels of coma. Electroenceph. Clin. Neurophysiol. 45:515-524.

Vitrai, J., Czobor, P., Simon, G. and Marfosi, S. 1984. Beyond principal component analysis: Canonical component analysis for reduction in classification of EPs. Int. J. Bio-med. Comput. 15:93-111.

Wada, S. and Starr, A. 1983. Generation of auditory brainstem responses (ABRs): I. Effects of injection of a local anaesthetic (Procaine HCl) into the trapezoid body of guinea pigs and cats. Electroenceph. Clin. Neurophysiol., 56:326-339.

Welch, P.D. 1967. The use of fast Fourier transform for the estimation of power spectra: A method based on time averaging over short modified periodograms. IEEE Trans. Audio and Electroacoust. AV-15, 70-73.

Wells, J.D. and Hansebout, R.R. 1978. Local hypothermia in experimental spinal cord trauma. Surg.Neurol., 10:200-204.

Woodcock, J.P., 1975. Theory and Practice of Blood flow Measurement. Butterworths, London, England.

Yoo, J.H., Herring, J.M. and Yu, J. 1979. Power spectral changes of the vastus medalis electromyogram for graded isometric torques. Electromyogr. and Clin. Neurophysiol. 19:183-197.

Zielonka, J.S., Wagner, F.C., Dohrmann, G.J. 1974.

Alterations in spinal cord blood flow during local hypothermia. Surg. Forum. 25:434-435.